AD

USAAVLABS TECHNICAL REPORT 70-28

CONVERTIBLE FAN/SHAFT ENGINE VARIABLE FAN GEOMETRY INVESTIGATION

By

David L. Wright
Burton A. Jones

April 1970

U. S. ARMY AVIATION MATERIEL LABORATORIES
FORT EUSTIS, VIRGINIA

CONTRACT DAAJ02-69-C-0002
PRATT & WHITNEY AIRCRAFT DIVISION
UNITED AIRCRAFT CORPORATION
FLORIDA RESEARCH AND DEVELOPMENT CENTER
WEST PALM BEACH, FLORIDA

121

DISCLAIMERS

The findings in this report are not to be construed as an official Department of the Army position unless so designated by other authorized documents.

When Government drawings, specifications, or other data are used for any purpose other than in connection with a definitely related Government procurement operation, the United States Government thereby incurs no responsibility nor any obligation whatsoever; and the fact that the Government may have formulated, furnished, or in any way supplied the said drawings, specifications, or other data is not to be regarded by implication or otherwise as in any manner licensing the holder or any other person or corporation, or conveying any rights or permission, to manufacture, use, or sell any patented invention that may in any way be related thereto.

Trade names cited in this report do not constitute an official endorsement or approval of the use of such commercial hardware or software.

DISPOSITION INSTRUCTIONS

Destroy this report when no longer needed. Do not return it to the originator.

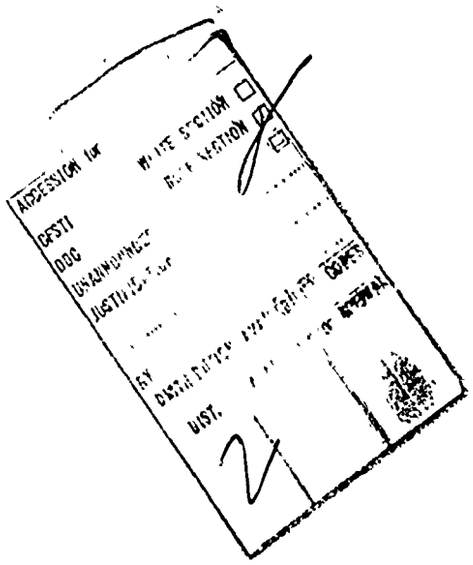

DEPARTMENT OF THE ARMY
HEADQUARTERS US ARMY AVIATION MATERIEL LABORATORIES
FORT EUSTIS, VIRGINIA 23604

The research described herein was conducted by the Pratt and Whitney Aircraft Division, United Aircraft Corporation, under Contract DAAJ02-69-C-0002. This contract was carried out under the technical management of the U. S. Army Aviation Materiel Laboratories, Propulsion Division.

The report presents an evaluation of the convertible fan/shaft engine incorporating variable fan geometry as it may relate to future V/STOL propulsion systems.

This command concurs with the conclusions and recommendations herein.

Task 1G162203D14415
Contract DAAJ02-69-C-0002
USAAVLABS Technical Report 70-28
April 1970

CONVERTIBLE FAN/SHAFT ENGINE VARIABLE FAN GEOMETRY INVESTIGATION

Final Report

By

David L. Wright
Burton A. Jones

Prepared By

Pratt & Whitney Aircraft Division
United Aircraft Corporation
Florida Research and Development Center
West Palm Beach, Florida

for

U. S. Army Aviation Materiel Laboratories
Fort Eustis, Virginia

SUMMARY

Preliminary design studies have shown that advanced VTOL aircraft performance can be enhanced when the aircraft are coupled with a turbofan engine having the ability to provide shaft power to the vertical lift rotor (convertible fan/shaft engine). The program reported herein was conducted to determine the feasibility of using variable fan inlet and duct exit guide vanes to effectively reduce fan horsepower and eliminate thrust during periods of vertical lift and hover. An exploratory test program was conducted in an existing 0.5 hub-tip ratio compressor research rig modified to simulate a high-bypass-ratio fan configuration. This fan configuration consisted of variable inlet and exit guide vanes, a fan rotor, and a simulated gas generator flowpath providing a 4.2:1 bypass ratio. The fan rotor was an existing moderate-speed rotor blade with a tip diameter of 43 inches, tip speed of 1150 fps, and design pressure ratio and flow of 1.35 and 285 lb/sec, respectively.

Results from the test program established the feasibility of using varible-geometry inlet and duct exit guide vanes to effectively reduce fan horsepower and thrust. Fan horsepower was reduced to 16 percent of the maximum (cruise) power absorbed by the fan, and fan thrust was reduced by 100 percent. The test results indicate that the potential exists for reducing fan horsepower to values of less than 10 percent of the cruise power. Inlet guide vane, rotor blade, and duct exit guide vane stresses were within safe operating limits over the test range of guide vane positions.

TABLE OF CONTENTS

LIST OF ILLUSTRATIONS

LIST OF ILLUSTRATIONS (Continued)

LIST OF ILLUSTRATIONS (Continued)

LIST OF TABLES

LIST OF SYMBOLS

A_D	duct exit area, $in.^2$
C_p	specific heat at constant pressure, $Btu/lb_m-°R$
F	thrust, lb
HP	horsepower
K_n	horsepower correction factor
p	static pressure, psi
P	total pressure, psi
SHP	shaft horsepower
T	total temperature, °R
V_Z	axial velocity, ft/sec
W_D	duct weight flow, lb/sec
W	weight flow (orifice), lb/sec
γ	ratio of specific heats
δ	pressure ratio, average plenum pressure/14.7 psi
θ	temperature ratio, plenum temperature/518.7°R

SUBSCRIPTS

act	actual inlet conditions
cal	calculated
corr	corrected inlet conditions
pr	predicted
ptp	predicted turbine power
0	stage inlet
1	instrumentation station 1
2	instrumentation station 2
4	instrumentation station 4

INTRODUCTION

Advanced VTOL aircraft preliminary design studies have confirmed the promising potential of combining the excellent hover characteristics of rotory-wing aircraft with the high-speed characteristics of fixed-wing aircraft. These studies have also indicated that the capabilities of these aircraft are enhanced when the aircraft are coupled with a turbofan engine that has the ability to provide shaft power to the vertical lift rotor during hover (convertible fan/shaft engine). Because no such engines are available today, a conceptual study was conducted by the U. S. Army Aviation Materiel Laboratories (USAAVLABS)(Reference 1) to compare various means of reducing the power required by the fan during periods of vertical lift rotor operation. One of the promising concepts that resulted from this study used variable fan inlet and duct exit guide vanes for modulating fan power and thrust, as illustrated in Figure 1.

In the variable-geometry guide vane concept, the inlet and duct exit guide vanes are actuated toward the closed position during hover to reduce flow through the fan, thereby reducing the power absorbed by the fan and eliminating thrust. Analytical methods were not heretofore available to accurately predict either the lower limit of fan thrust or the minimum parasitic power conditions that could be achieved. Consequently, a 12-month exploratory test program was initiated to establish the overall feasibility of this concept and to define the possible limitations. An existing 0.5 hub-tip ratio compressor research rig was modified to simulate a high-bypass-ratio fan stage configuration. This configuration consisted of variable inlet and duct exit guide vanes, a fan rotor, and a simulated gas generator flowpath that provided a 4.2:1 bypass ratio. The fan rotor used existing moderate-speed rotor blading having a tip diameter of 43 inches and a tip velocity of 1150 fps; the cruise design pressure ratio and mass flowrate were 1.35 and 285 lb/sec, respectively. Tests were conducted at design-corrected rotor speed and at 70-percent design-corrected rotor speed with the inlet and duct exit guide vanes varying from their fully open to fully closed positions, with several selected combinations in between. Additionally, one test was conducted at inlet and exit guide vane positions selected for minimum fan horsepower with the gas generator flowpath exit closed.

This report presents a description of the aerodynamic and mechanical design; a description of the test equipment; the procedures for test, data reduction and analysis; a discussion of the test results; the conclusions reached on the basis of these results; and the recommendations for future work.

STAGE DESIGN

AERODYNAMIC DESIGN

The aerodynamic design included a cruise design point analysis and an off-design (intermediate between cruise and hover) analysis. Selection of the flowpath for these analyses was based on the use of an existing 0.5 hub-tip ratio compressor research rig. A flow splitter was designed for this rig to provide simulated fan duct and gas generator flowpaths. Design velocity diagrams were selected for the inlet guide vanes, rotor blades, duct exit guide vanes, and flow-straightening vanes in the gas generator flowpath. Computer programs that were used for the selection of velocity diagrams are described in Appendix I. These velocity diagrams were used in conjunction with airfoil design data to select the metal geometry for the inlet and exit guide vanes and the flow-straightening vanes.

Cruise Design Point Analysis

The rotor speed, weight flow, and pressure ratio characteristics of the existing rotor blading used in the fan stage were known. Thus, it was possible to establish tentative cruise design point parameter values, with an inlet guide vane loss distribution and zero rotor prewhirl assumed. A summary of the design parameters thus established is given in Table I.

TABLE I. CRUISE DESIGN POINT PARAMETER VALUES

Rotor Tip Diameter, in.	43
Fan Hub-Tip Ratio	0.5
Tip Speed, fps	1150
Weight Flow, lb_m/sec	285
Bypass Ratio	4.2
Fan Pressure Ratio	1.35
Stage Pressure Ratio	
Duct Side	1.35
Gas Generator Side	1.28

Flowpath Definition

The flowpath consisted of fan inlet, rotor, fan exit, fan duct, and gas generator duct sections, as shown in Figure 2. Although this flowpath was somewhat unconventional for a fan engine, it permitted the use of existing hardware and was suitable for meeting the program objectives.

A major concern in the final selection of the fan inlet section was the interaction between the inlet guide vane wakes and the rotor blades that might occur as a result of the close axial spacing between these

blade rows provided by the existing hardware. At high turning angles the inlet guide vane wakes could be large, and their interaction with the rotor blades could adversely affect the stability of the rotor. Data presented in References 2, 3, and 4 were reviewed. These data implied (in terms of noise-level measurements) that for the ratio of the number of rotor blades to the number of inlet guide vanes for the existing rig, the advantage of spacings larger than one chord length was negligible. The average (hub-to-tip) spacing for the existing rig was one chord length. Therefore, no adjustment was made for wake interference.

The fan duct and gas generator flowpaths were formed by adding a flow splitter to the diffuser section of the existing rig flowpath. The leading edge of the flow splitter was located a distance of approximately one rotor blade span downstream of the rotor to provide a region in which radial flow shifts could be accommodated as the inlet and exit guide vanes were closed. The flow splitter leading edge was positioned radially to provide a 4.2:1 bypass ratio at cruise design rotor speed and flow conditions. The leading edge cross section was elliptical, as shown in Figure 3, to maintain attached flow over a wide range of incidence angles. The trailing edge of the flow splitter was positioned radially to provide equal static pressures at the fan duct and gas generator flowpath exit at cruise design point conditions. Diffusion in the fan duct and gas generator flowpath, as well as losses across the exit guide vanes and flow-straightening vanes, was accounted for. The axial location of the flow-splitter trailing edge was positioned such that the existing rig throttle vane actuation mechanism could be used for varying the duct exit guide vane chord angle.

The existing outer wall geometry of the rig diffuser section required modification to reduce the diffusion in the fan duct and thereby to reduce the turning required by the exit guide vanes to return the flow to the near-axial direction. On the basis of constant angular momentum, reducing the duct flow area increased the axial velocity and reduced the swirl angle into the exit guide vane. The proper incidence angle was then achieved at an acceptable level of camber angle.

Inlet Guide Vanes

Several inlet guide vane cruise design point swirl distributions were analyzed to determine if any benefit in off-design performance resulted due to improved flow matching at the rotor inlet. The influence of cruise design point swirl on off-design performance was found to be negligible; therefore, the guide vanes were designed to produce an axial flow distribution at cruise design conditions and thus to provide maximum flow and thrust.

The NACA 4-digit-series airfoil (NACA M400) was selected for the inlet guide vanes because the relatively large leading-edge radius permits unstalled operation over a wide range of incidence angles. This feature was desirable from the standpoint of maintaining high rotor efficiency over as wide a range of inlet guide vane chord angles as possible.

The final inlet guide vane geometry was selected to provide an acceptable seal in the closed position. The variables included in this evaluation were camber angle, chord length distribution, twist, and chordal overlap in the closed position. The number of vanes was set by the existing synchronous ring actuation system for positioning the guide vanes. Although the cruise design zero swirl condition could be satisfied with a symmetrical airfoil, it was noted that surface contact and sealing were improved as camber angle was increased; however, it was necessary to limit camber angle to avoid a high choke incidence condition in the cruise design configuration. As a result of this study, a constant camber angle of 20 degrees was selected in conjunction with the chord length and chord angle (twist) distributions shown in Figure 4 to provide line-on-line contact of the vane surfaces in the closed position. The chordal overlap was 20 percent (of the chord length) at midspan. The inlet guide vanes are shown in their closed position in Figure 5.

Rotor

An existing rotor disk and existing rotor blading were used in this program. This rotor has 34 blades comprised of circular arc airfoil sections and a design tip velocity of approximately 1150 feet per second. The rotor blades have part-span shrouds at 50-percent chord for flutter damping. Spanwise distributions of blade camber, chord length, chord angle, and thickness ratio are presented in Figure 6.

From the known blade element loss and deviation angle characteristics for this blading, it was possible to calculate the rotor exit velocity diagrams using the Axial Flow Compressor Calculation computer program described in Appendix I. These exit velocity diagrams were subsequently used in conjunction with the fan duct and gas generator flowpath geometry to calculate the velocity diagrams at the duct exit guide vane and flow-straightening vane inlets.

Flow-Straightening Vanes

Existing 65-series airfoil vanes were selected for the gas generator flowpath flow-straightening vanes. The chord angle for these vanes was selected such that it provided axial exit flow with near minimum loss incidence at cruise design point conditions. This chord angle selection resulted in an average (spanwise) air turning of 29 degrees. Airfoil geometry variables for the flow-straightening vanes are given in Table II.

Duct Exit Guide Vanes

The duct exit guide vanes were located near the exit of the diffusing section of the existing compressor rig (Figure 2) because a synchronous guide vane positioning mechanism, normally used to control rig throttle vane setting, was available at this location. The number of vanes (24) matched the existing mechanism.

TABLE II. AIRFOIL GEOMETRY VARIABLES FOR FLOW-STRAIGHTENING VANES	
Camber, deg	53.18
Chord Angle, deg	79.9
Chord, in.	2.18
Thickness Ratio	0.09
Number of Vanes	40
Solidity (Hub)	1.072
Solidity (Tip)	0.927
Aspect Ratio	0.93

The exit guide vanes were comprised of NACA 65-series airfoil sections. Pratt & Whitney Aircraft cascade loss data and the deviation angle calculation method of Reference 5 for the 65-series airfoil were used in the selection of exit velocity diagrams. Selection of the spanwise distributions of airfoil geometry variables required an iteration between the design point requirements of minimum loss incidence and axial exit flow, and the need to seal the duct when the vanes were in the closed position. This iteration resulted in an exit vane with a constant chord angle, a varying spanwise chord length, and a 9-degree hub-to-tip variation in camber, as shown in Figure 7. It was necessary to modify the duct exit guide vane exit air angle from the axial direction to 10 degrees off the axial direction in order to match the vane leading edge at minimum loss incidence angle and to maintain camber angles within limits consistent with current design practice.

In the closed position, the duct exit guide vanes overlapped approximately 25 percent of the chord, and their design provided a line-on-line contact. The hub and tip sections were contoured to match the flowpath wall. The duct exit guide vanes are shown in the closed position in Figure 8.

Off-Design Analysis

An off-design analysis was conducted to predict fan performance, shaft horsepower, and fan thrust at cruise design rotor speed for various inlet and exit guide vane settings. Performance predictions were obtained for inlet guide vane exit flow angles of 0, 15, 30, and 45 degrees (measured from the rig centerline) with the duct exit guide vane setting varied in 10-degree increments from the fully open position. During this analysis it was found that as the inlet guide vane exit swirl increased, the predicted tip-to-hub flow shift increased; and for a swirl angle of 45 degrees the rotor blades had either high choke incidence at the hub or high stall incidence at the tip, depending on the flowrate. Similar results were noted in the analyses presented in References 6 and 7. This flow shift necessitated extrapolation of existing cascade performance data (Pratt & Whitney Aircraft) to accommodate the large range of incidence angles. No analysis was attempted for exit swirl angles larger than 45 degrees since any further extension of the cascade data would have been questionable.

The results of the off-design analysis are presented in Figures 9 through 11. Figure 9 shows the predicted rotor pressure ratio as a function of corrected weight flow for several inlet and exit guide vane settings. The estimated surge line in Figure 9 was determined from a correlation of surge point rotor diffusion factor with aspect ratio.

The estimated rig operating limit points in Figure 9 correspond to conditions where the combination of calculated rotor pressure ratio and system losses results in a stage exit pressure equal to ambient pressure, since the rig exhausts to ambient pressure. The indicated duct exit guide vane positions for these points refer to closure angles below which the exit guide vane loss would increase above a limiting value consistent with ambient exit pressure conditions. Thus, it might be expected that some reverse flow could occur in the rotor hub region for inlet guide vane closure angles greater than 30 degrees and exit guide vane closure angles less than the limiting values indicated in the figure. For zero degrees of inlet guide vane closure, the lower limit of pressure ratio (combined with system losses) required to match ambient exit pressure is substantially higher than the lower limit of pressure ratio for the other inlet guide vane closure angles shown. This result is due to an anticipated requirement for operating the compressor stage at reduced inlet pressure (by throttling the inlet) in order for the compressor to achieve its cruise design point flow and pressure ratio with the inlet and exit guide vanes in their cruise design positions.

Predicted shaft horsepower and fan thrust for the inlet and exit guide vane settings analyzed are shown in Figures 10 and 11, respectively. The cruise design point shaft horsepower and thrust are 5350 and 6000 pounds, respectively. At an inlet guide vane closure angle of 45 degrees and an exit guide vane closure angle of 35 degrees, the predicted horsepower and thrust are 2450 and 1350 pounds, respectively.

As part of the off-design evaluation, the percent of increase in rotor exit temperature was evaluated as a function of the percent of design weight flow to estimate the rotor exit temperature that can be expected when the inlet and exit guide vanes are in the fully closed configuration. On the basis of this evaluation, the anticipated rotor exit temperature for zero weight flow is 250°F. This temperature was used to define material strength properties in the guide vane and rotor blade stress analyses.

MECHANICAL DESIGN

The mechanical design consisted of the stress analysis and preparation of drawings for the inlet guide vanes, duct exit guide vanes, and gas generator flowpath flow-straightening vanes. Steady-state stresses were also calculated for the existing rotor configuration, and drawings were prepared for the gas generator flowpath cover plate, the fan duct-gas generator flowpath splitter, an outer wall filler piece to modify the fan duct flowpath, and diffuser case support rods to replace the stator vane row that was normally located behind the rotor in the existing rig.

Analysis of the inlet guide vane hub and tip spindle design indicated that a large interface area between the airfoil section and the spindle would be required at the hub to sustain the predicted airloads. The interface area was therefore increased to the full area of the spindle with the overhang blended into the suction and pressure surfaces, as shown in Figure 12. A maximum stress of 22,000 psi was calculated and occurred at the tip spindle. The vanes were fabricated from AMS 5613 stainless steel, which has a 0.2-percent yield strength of approximately 98,000 psi at 250°F, which provided an adequate strength margin.

The stress and vibration characteristics of the existing rotor blades used in this program are well documented, and no problems concerning their use were anticipated. A maximum steady-state stress of 38,000 psi was calculated for the rotor blades at 100 percent of cruise design rotor speed. The titanium alloy rotor blades had a 0.2-percent yield strength of 99,000 psi at 250°F. A rotor blade, with the dovetail blade attachment design, is shown in Figure 13.

The duct exit guide vane is shown in Figure 14. A maximum stress of 48,000 psi occurred at the hub spindle section which provided an approximately 100-percent stress margin for the AMS 5613 stainless steel material selected for the exit vanes. The hub spindle was elongated to pass through the gas generator flowpath and to make use of the existing holes in the rig wall (Figure 15). The tip spindle was designed to fit the existing synchronous ring levers for guide vane positioning.

The gas generator flowpath flow-straightening vanes are shown in Figure 16. These were existing vanes that were trimmed to fit the gas generator flowpath span. The tip spindles were welded to the flow splitter, and the vanes were cantilevered. A maximum stress of 18,000 psi was calculated at the tip spindle. These existing vanes were fabricated from AMS 5613 stainless steel, and no stress problems were anticipated with them.

The gas generator flowpath cover plate was a flat annular plate which was attached with rivets to the rig inner wall and to the flow splitter. The cover plate was cut in angular segments to allow installation over the exit of the gas generator flowpath while the rig was on the test stand (Figure 15).

The flow splitter was designed as a cone and was fabricated from rolled, welded, and machined sheet stock. The flow splitter was supported by two sets of four airfoil-shaped struts located near the leading and trailing edges, respectively. The outer wall filler piece was cylindrically-shaped, was fastened directly to the existing wall at one end and was supported by four struts at the opposite end (Figure 15).

Four 0.5-inch diameter support rods and a short outer wall spacer ring were provided behind the rotor at the front end of the rig diffuser case. These support rods replaced the stator vane row that was normally located behind the rotor in the existing rig (Figure 15).

TEST EQUIPMENT

FACILITY

The compressor test facility is shown in Figure 17. The compressor rotor is driven by a single-stage free turbine that is powered by exhaust gases from a J75 slave engine. Drive turbine speed is controlled by means of the engine throttle. Air entered the compressor test section through a 103-foot combined inlet duct, plenum, and bellmouth inlet and exhausted through an exit diffuser to the atmosphere. A 7-degree diffuser at the plenum inlet and a 10:1 bellmouth contraction ratio ensured uniform flow conditions at the compressor inlet.

COMPRESSOR TEST RIG

An existing compressor rig was modified as shown in Figure 15 to provide the required fan stage simulation. The rotor assembly and shaft are supported on two bearings that transmit loads to the outer case through four struts in the inlet case and the struts in the exhaust case. The rig exhaust is divided into two paths: one through the facility exhaust case and a second radially outward through the outer case at the exit of the diffuser section (see Figure 15). The radial overboard dump was provided in the existing rig to accommodate high-volume flowrates. The overboard dump resulted in ambient pressure conditions at the simulated fan stage exit.

INSTRUMENTATION

Fan Stage Performance Instrumentation

A summary of the instrumentation used in this investigation, together with estimates of the measuring system accuracy for each instrument, is presented in Table III.

Weight flow was measured by means of a 38.4-inch-diameter thin plate orifice fabricated and installed in accordance with ASME standards. Two upstream static pressures, two differential static pressures, and one upstream temperature were recorded. The 3-sigma repeatability for flow measurement through an orifice is a function of the flow, as shown in Figure 18. For this orifice the 3-sigma repeatability varied from ±1.0 percent at the cruise design flow of 285 lb/sec to ±3.0 percent at 110 lb/sec (40-percent design flow).

Fan stage inlet total pressure and total temperature were measured, respectively, by means of two Kiel-head probes and one half-shielded thermocouple probe located in the inlet plenum.

Rotor speed was measured with an electromagnetic sensor mounted adjacent to a 60-tooth gear on the rotor shaft. Gear-tooth-passing frequency was displayed as rpm on an anadex digital counter.

TABLE III. INSTRUMENTATION SUMMARY

Station	Flow Variable	Instrumentation Type	Quantity	Range	System Accuracy
Plenum	Total pressure	Kiel-head probe	2	5.0 psid	±0.034 psi
	Total temperature	Half-shielded thermocouple	1	CC	±1.0°R
	Speed	Fan rotational speed	1	0-7000 rpm	±0.1%
1	Total pressure	Kiel-head rake (ports at 10, 30, 50, 70, and 90% spans)	2	5.0 psid	±0.034 psi
	Total temperature	Kiel-head rake (ports at 10, 30, 50, 70, and 90% spans)	1	CC	±1.0°R
	Flow angle	20-deg wedge traverse probe - radially fixed at 50% span	1	0-180 deg	±1.06 deg
2	Total pressure	Individual Kiel-head sensors positioned at 10, 30, 50, 70, and 90% spans	2	10.0 psid*	±0.102 psi
	Total temperature	Kiel-head rake (ports at 10, 30, 50 70, and 90% spans)	1	CC	±1.0°R
3	Total pressure	Kiel-head rake (ports at 10, 50, and 90% spans)	2	5.0 psid	±0.034 psi
	Static pressure	Inner wall tap	2	5.0 psid	±0.034 psi
		Outer wall tap	2	5.0 psid	±0.034 psi
	Total temperature	Kiel-head rake (ports at 10, 50, and 90% spans)	1	CC	±1.0°R
	Flow angle	20-deg wedge traverse probe - radially fixed at 50% span	1	0-180 deg	±1.06 deg
4	Total pressure	Individual Kiel-head sensors fixed to exit vane at 10, 30, 50 70, and 90% spans	2	7.5 psid	±0.055 psi.
	Total temperature	Individual Kiel-head sensors fixed to exit vane at 10, 30, 50, 70, and 90% spans	1	CA	±1.0°R
	Flow angle	20-deg wedge traverse probe - radially fixed at 50% span	1	0-180 deg	±1.06 deg

TABLE III - CONTINUED

Station	Flow Variable	Instrumentation Type	Quantity	Range	System Accuracy
6	Total pressure	Individual Kiel-head sensors positioned at 10, 50, and 90% of duct width	1	15.0 psid	±0.153 psi
	Static pressure	Individual Pitot-static tubes positioned at 5 and 95% of duct width	1	15.0 psid	±0.153 psi
6A	Total Temperature	Kiel-head rake (ports at 10, 50, and 90% spans)	2	CA	±1.0°R
7	Delta temperature	Kiel-head rake (ports at 10, 50, and 90% spans) Delta to Station 6A sensor	2	CA	±1.0°R

*One set of sensors at 30, 50, 70% spans used 15.0 psid with a system accuracy of ±0.153 psi.

Axial locations of rotor inlet, rotor exit, gas generator flowpath, and fan duct exit instrumentation stations are shown in Figure 2.

Rotor inlet total pressure was measured by two Kiel-head rakes with pressure sensors at 10-, 30-, 50-, 70-, and 90-percent span. One Kiel-head thermocouple rake with sensors at the same span locations was provided for rotor inlet temperature measurement. Rotor inlet absolute air angle was measured at midspan by means of a self-balancing 20-degree wedge probe. Circumferential locations of this instrumentation are shown in Figure 19.

Rotor exit total pressure and total temperature were measured with individual Kiel-head probes and/or Kiel-head rakes located radially and circumferentially, as shown in Figure 19.

Two Kiel-head total pressure rakes, one Kiel-head total temperature rake, one midspan 20-degree wedge air angle probe, and two inner and two outer wall static pressure taps were provided in the gas generator flowpath to measure gas-generator-side weight flow. The radial and circumferential locations of this instrumentation are shown in Figure 19.

Two sets of Kiel-head total pressure probes, one set of Kiel-head total temperature probes, and one midspan 20-degree wedge air angle probe were located at the fan duct exit, as shown in Figure 19. The total pressure and total temperature probes were mounted on duct exit guide vanes because the acceptance angle of these probes was less than the anticipated change in exit air angle over the test range.

A typical total pressure and total temperature rake is shown in Figure 20. A 20-degree wedge probe is shown in Figure 21, and a set of vane-mounted total pressure probes is shown in Figure 22.

Drive Turbine Instrumentation

A summary of the drive turbine instrumentation is given in Table III; measuring stations are shown schematically in Figure 23, and circumferential locations at each station are shown in Figure 24. Instrumentation was provided for turbine weight flow and temperature drop, from which turbine output horsepower was to be calculated. Turbine inlet total and static pressure used for the weight flow calculation were obtained by individual Kiel-head sensors and Pitot-static probes. These probes were located in the inlet duct at Station 6 upstream of the turbine inlet collector manifold (Figure 23), where flow gradients and swirl are at a minimum. Effective flow area for calculating turbine inlet flow was obtained from the geometry of the duct at Station 6. Turbine inlet temperature was measured by two Kiel-head thermocouple rakes positioned immediately upstream of the turbine at Station 6A to minimize the error in the turbine temperature drop measurement. Any error introduced into the weight flow calculation by the small temperature drop between Stations 6 and 6A due to radiation losses would be negligible because of the high absolute level of the inlet temperature. To improve accuracy, turbine temperature drop was measured as a delta temperature instead of calculated as the difference

between two absolute readings. This was accomplished by electrically linking two Kiel-head thermocouple rakes at Station 7 downstream of the turbine to the rakes at Station 6A, as shown schematically in Figure 25. Figure 25 also shows that the Kiel-head sensors were combined to provide two individual and one average absolute temperature and two average temperature difference readings. This consolidation was necessary because of capacity limitations of the data recording system.

Strain Gage Instrumentation

Strain gages were installed on the inlet guide vanes, fan blades, and exit guide vanes at locations where maximum stresses were expected to occur during test. For the inlet guide vanes, the maximum stress locations were determined from stress coat patterns that formed as a result of vibration stresses when selected vanes were vibrated in the first bending and first torsional modes. Two vanes were instrumented at the locations shown in Figure 26. Stress patterns had been previously documented for the rotor blades that were used in this program, and bench vibration tests were therefore not required. Six fan blades were instrumented with three strain gages each at the locations shown in Figure 27. Because of the large chord and thickness of the duct exit guide vane airfoil sections, bench vibration tests were not considered to be necessary. Maximum stresses on these vanes were expected to occur in the vicinity of the spindles; accordingly, strain gages were located near the hub and tip on the pressure surface in line with the spindle centerline, and a third gage was located at midspan in line with the other two gages (see Figure 28). Two vanes were instrumented.

Test Stand Instrumentation

Instrumentation was provided to monitor rig operation, such as lubricant pressures, bearing temperatures, chip detection system, etc. In addition, the rig external case and test facility mounts were instrumented with self-generated accelerometers to detect test rig case and drive shaft vibrations. A vibration monitor electrically integrated the transducer signal and displayed vibration loads and amplitudes for observation by the test engineer.

Instrumentation Accuracy

Accuracy estimates for the fan stage and drive turbine instrumentation are given in Table III. System accuracy consists of the combined estimated accuracies of the individual sensor, associated transducer, and recording system.

Pressure measurement accuracy was improved by referencing pressure transducers to ambient pressure, which permitted the use of low-range transducers. The pressure measurements were converted to absolute values using a barometer reading that is obtained every hour by the Florida Research and Development Center Instrumentation Laboratory and input to the pressure recording system.

Kiel-head total pressure probes did not require calibration because of their relative insensitivity to pitch and yaw. The Kiel-head total temperature probes, designed with relatively long exposed wires between the thermocouple junction and insulating material, did not require correction. A typical calibration curve for these total temperature probes is shown in Figure 29.

Flags are installed on 20-degree wedge (air angle) probes, using an airflow facility in the Instrumentation Laboratory, to permit alignment of these probes with the compressor rig centerline.

Data Acquisition

The data acquisition system used in this test program consists of an 88-channel Consolidated Systems Corporation Model 1 Microsadic digital magnetic tape recorder. Data from each of the 88 channels may be recorded at a rate of up to 100 cycles per second. The output of this recording system is compatible with an IBM system 360 computer that is used for data processing.

PROCEDURES

TEST PROCEDURE

The test program consisted of a checkout test, a contingency test with inlet and duct exit guide vanes closed, the tests with various guide vane chord angle settings, and a test with a cover plate over the gas generator flowpath exit. These tests were subject to limitations of rig vibration and blade stresses that have been established as safe margins in previous test programs. The limiting rig vibration was 3.0-mil displacement, and the limiting blade stress was 10,000 psi.

Checkout Test

The purposes of the checkout test were to evaluate the stress and vibration characteristics of the compressor rig and to evaluate the instrumentation under actual compressor operating conditions. Inlet and exit vanes were set in the fully open position, and data were recorded continuously as the fan was accelerated from idle to 110-percent design speed and returned to idle.

Contingency Test

The contingency test was run to ensure that minimum program objectives were attained in the event of hardware damage while operating in the stall conditions that would be encountered during actuation of the exit guide vanes. For this test, Station 1 instrumentation was removed, inlet and duct exit guide vanes were set in the fully closed position, and data were recorded continuously as the fan was accelerated from zero to 110-percent design rotor speed and returned to idle. Station 1 instrumentation was then installed in the test rig for the remainder of the test program.

Variable Chord-Angle Tests

The variable chord-angle tests constituted the main body of the test program and were conducted as follows. With the inlet guide vanes fixed in their fully open position (zero swirl), the rotor speed was set at the design value and data were recorded continuously as the duct exit guide vanes were slowly closed from the fully open (0-degree) position to the fully closed (80-degree) position and returned to the open position. The rate of closure of the exit guide vane was sufficiently slow to ensure quasi-equilibrium operation. The fan speed was then set at 70-percent design rotor speed and the test was repeated. This procedure was repeated with the inlet guide vane set at 45, 60, 70, and 80 degrees from the fully open position.

During the off-design analysis discussion, it was mentioned that it would be necessary to reduce inlet pressure to achieve design pressure ratio and flow with the inlet and duct exit guide vanes in their fully open position because the duct exit guide vanes were the only means of increasing the rotor exit pressure. This procedure was omitted during the test because the

resulting horsepower-guide vane relationship with reduced inlet pressure would have been incompatible with data obtained at ambient inlet conditions. Demonstration of the cruise design point performance was considered of secondary importance relative to having compatible data. Consequently, all of the tests were performed with ambient inlet conditions.

Test With Gas Generator Flowpath Cover Plate

The last phase of the test program required that the fan be run with the inlet and exit guide vanes set at near minimum parasitic power positions and that an annular cover plate be installed over the exit of the gas generator flowpath to simulate the use of variable geometry vanes to seal the gas generator inlet. Based on data from the variable chord-angle tests, two inlet guide vane positions, 70 and 80 degrees, were selected to ensure that the minimum parasitic power setting (within an acceptable temperature limit) was obtained. The duct exit guide vane was set at 68 degrees because the variable chord-angle test data indicated a sharp increase in rotor exit temperature at higher exit guide vane closures. Data were continuously recorded as the rotor was accelerated from idle to design rotor speed and returned to idle.

Test Program Summary

A summary of the test program is given in Table IV. No stress or vibration problems were encountered during the checkout test, but some of the instrumentation malfunctioned and required correction before continuing the test program. The contingency test (with inlet and duct exit guide vanes fully closed) was successfully completed without exceeding stress or vibration limits but resulted in rotor exit temperatures in excess of 540°F (uncorrected).

During the variable chord-angle tests, the exit guide vane closures for the fully open inlet guide vane test were rotor blade stress limited at 41 and 50 degrees at 100- and 70-percent design rotor speed, respectively. In addition, there was a stress-limited region between 5 and 18 degrees of exit guide vane closure at design rotor speed when the inlet guide vane was set at 45 degrees. The 5 degree boundary of this stress-limited region was reached as the exit guide vane was being closed from the fully open position. The 18 degree boundary was determined by reducing the rotor speed with the exit guide vane set at 0 degrees, closing the exit guide vane 40 degrees at the reduced rotor speed, increasing the speed to design speed, and opening the exit vane until the stress limit was reached. The remaining combinations of inlet guide vane settings and rotor speeds were successfully run over the full range of exit guide vane closure without exceeding vibration or stress limitations.

The 80 degree inlet guide vane setting for the annular cover plate test was successfully completed, but the 70 degree setting was tested to only 69-percent design rotor speed because of erratic rotor blade strain gage readings.

TABLE IV. TEST PROGRAM SUMMARY

IGV Closure (deg)	DEGV Closure (deg)	Design Speed (%)	Comments
0	0	Idle - 110	Checkout test; IGV and DEGV fully open; no serious problems encountered
90	80	0 - 110	IGV and DEGV fully closed; fan environmental temperatures exceeded 540°F
0	0 - 41	100	Rotor blade stress limited at 41-deg closure
	0 - 50	70	Rotor blade stress limited at 50-deg closure
45	0 - 5, 18 - 75	100	Rotor blade stress limited between 5- to 18-deg closure
	0 - 80	70	No problems encountered
60	0 - 80	70, 100	No problems encountered
70	0 - 80	70, 100	No problems encountered
80	0 - 80	70, 100	No problems encountered
80	68	Idle - 100	Estimated minimum parasitic power setting with annular cover plate installed; no problems encountered
70	68	Idle - 69	Estimated minimum parasitic power setting with annular cover plate installed; limited to 69% speed by erratic rotor blade strain gage signals

Zyglo inspection of the inlet guide vanes, exit guide vanes, and rotor blades, and visual inspection of the remainder of the test hardware during rig disassembly revealed that the tests had no effect on the structural integrity of the hardware.

DATA-REDUCTION PROCEDURE

Fan stage and drive turbine measurements were recorded in electrical units on a magnetic tape that was processed through a computer program to provide tabulated data in engineering units. This computer program also corrected the pressure and temperature data to standard-day inlet conditions; these corrected data were subsequently used to calculate the performance variables, except as noted. Pressure and temperature data were corrected by the following relationships:

$$\text{Pressure (Standard Day)} = \frac{\text{Pressure (measured)}}{\delta}$$

$$\text{Temperature (Standard Day)} = \frac{\text{Temperature (measured)}}{\theta}$$

where $$\delta = \frac{\text{Average Plenum Pressure}}{14.7 \text{ psi}}$$

$$\theta = \frac{\text{Plenum Temperature}}{518.7^{\circ}\text{R}}$$

CALCULATION OF PERFORMANCE VARIABLES

Rotor Speed

Actual rotor speed was a directly measured quantity. Corrected rotor speed and percent design corrected speed were calculated from the actual speed as follows:

$$\text{Correct Speed} = \frac{\text{Actual Speed}}{\sqrt{\theta}}$$

$$\text{Percent Design Speed} = \frac{\text{Corrected Speed}}{\text{Design Speed}} \times 100$$

Orifice Weight Flow

Orifice weight flow was calculated from measured differential static pressure, total pressure, and total temperature data using an ASME standard orifice equation with known coefficients. Corrected inlet weight flow was computed as follows:

$$\text{Corrected Flow} = \frac{\text{Actual Flow} \sqrt{\theta}}{\delta}$$

Fan Horsepower

Fan horsepower was calculated from drive turbine measurements instead of fan weight flow and enthalpy rise because of the inaccuracy of the orifice weight flow measurement at the low flows associated with high inlet and duct exit guide vane closure angles. These flows were frequently less than 20 percent of the design flow, resulting in a flow measurement uncertainty greater than 10 percent (see Figure 18). Additional error was introduced by the flow recirculation effects encountered at the high inlet and exit vane closures. Two methods for calculating fan horsepower, based on drive turbine measurements, were available from the test data.

The first method for calculating the power absorbed by the fan accounts for the energy transfer between the drive turbine and the fan. This method, based on the first law of thermodynamics, requires correcting the turbine thermodynamic power for mechanical losses due to heat transfer, windage, and bearing friction. Turbine power is obtained from the turbine flowrate calculated from the pressure and temperature measurements in the turbine inlet duct and the inlet duct effective flow area, and the measured turbine temperature drop. The mechanical losses are empirically evaluated at each rotor speed by calculating the difference between the turbine power and the shaft horsepower calculated from the fan enthalpy rise and weight flow. The best estimate of the mechanical losses is obtained with the inlet guide vanes in their design open position to avoid the problems of orifice weight flow measurement inaccuracy and recirculation effects at low flowrates.

Use of turbine weight flow, however, proved to be unsatisfactory because of the extreme sensitivity of the calculated turbine weight flow to the total-to-static pressure ratio in the turbine inlet duct. As an example of this sensitivity, a 20-percent change in calculated turbine horsepower resulted from a 0.3-percent change in either total or static pressure when the fan stage was in its maximum power configuration (design rotor speed and fully open inlet guide vanes). This sensitivity was increased at the lower power settings. The random fluctuation of the pressure transducers in the data acquisition system was 0.3 to 0.5 percent, allowing a wide range of turbine horsepower values.

The alternative method for calculating fan horsepower was based on the relationship between the J75 slave engine exhaust and drive turbine power. The turbine power was varied by controlling the fuel flowrate to the J75 slave engine and thereby controlling the turbine inlet temperature uniquely. Thus, the turbine inlet temperature is related to the shaft horsepower at

each rotor speed, and a unique relationship can be established for given combinations of rotor speed and turbine inlet temperature. The correlation shown in Figure 30 was established from the power equivalent of the fan enthalpy rise (shaft horsepower), turbine inlet total temperature, and rotor speed based on test data from this program and from a NASA contract program, NAS3-7604, that used the same compressor rig. The need to determine the mechanical losses is avoided in this method since the correlation is based on calculated adiabatic shaft horsepower. The NAS3-7604 test stage used in this correlation consisted of variable geometry inlet guide vanes, a 0.5 hub-tip ratio rotor, and a variable geometry stator. The rotor blade tip diameter was 43 inches, the design speed was 6050 rpm, and the design weight flow was 265 lb/sec. The close similarities in the design point values between the NAS3-7604 stage and the stage tested in this program provided a sound foundation for this correlation. Actual shaft horsepower (not corrected to standard-day inlet conditions) was calculated as

$$SHP_{act} = \frac{778\ W_{act}\ C_p\ (T_2 - T_0)}{550}$$

where W_{act} = Actual fan weight flow, lb/sec

C_p = Specific heat of air

T_2 = Actual average rotor exit temperature, °R

T_0 = Actual stage inlet temperature, °R

Fan horsepower calculations were performed for the NAS3-7604 program results at 50-, 70-, and 100-percent design rotor speed. Data at 50-percent speed were included in the correlation to define the initial curvature of the speed lines in the low horsepower region. Fan horsepower values were determined for the USAAVLABS program at 70- and 100-percent design rotor speeds with an inlet guide vane angle of 0 degrees and at 100-percent design rotor speed with an inlet guide vane angle of 45 degrees. Data from the 45-degree inlet guide vane setting were restricted to inlet weight flows greater than 100 lb/sec to minimize the error introduced by orifice weight flow inaccuracy and recirculation effects.

An analytical turbine performance computer program was used to calculate shaft horsepower as an independent verification of the turbine inlet temperature/shaft horsepower correlation. The program predicted turbine power from input consisting of turbine inlet total pressure (taken from the Station 6 data), inlet total temperature (Station 6A), exit static pressure (assumed to be ambient), turbine speed, and turbine blade geometry. Predicted shaft horsepower values for comparison with the correlation were calculated by subtracting a factor, K_n, from the turbine power computed by the turbine performance program. The factor, K_n, accounts for the drive

system mechanical losses and for the fact that zero total pressure loss was assumed by using Station 6 total pressure data as the turbine inlet conditions. K_n was empirically evaluated at each speed as the difference between the predicted turbine power and the shaft horsepower calculated from the fan test data with the inlet guide vanes at 0 degrees (fully open). Calculation of the shaft horsepower predicted by the analytical computer program can be expressed by the following relationships:

$$SHP_{pr} = HP_{ptp} - K_n$$

$$K_n = HP_{ptp} - SHP_{cal}$$

where SHP_{pr} = Predicted shaft horsepower

HP_{ptp} = Predicted turbine power

K_n = Correction factor

SHP_{cal} = Shaft horsepower calculated from fan test data

Predicted shaft horsepower values were calculated for several exit guide vane settings for inlet guide vane positions of 0, 45, and 80 degrees at 100- and 70-percent design rotor speed for comparison with the correlation. Figure 31 shows that the predicted shaft horsepower as defined above agrees closely with the turbine inlet temperature correlation developed in Figure 30. The values of shaft horsepower obtained from Figure 30 as a function of turbine inlet temperature and rotor speed were corrected to standard-day inlet conditions using the following relationship:

$$SHP_{corr} = \frac{SHP_{act}}{\delta\sqrt{\theta}}$$

Thrust

Fan thrust was determined from measurement of the duct exit flow conditions. The thrust equation is of the form

$$F = (W_D)\ (V_Z) + (p_4 - P_0)\ A_D$$

where W_D = Duct weight flow

V_Z = Duct exit axial velocity

p_4 = Duct exit static pressure

P_0 = Corrected plenum pressure (14.7 psia)

A_D = Duct exit area

Duct weight flow was obtained as the difference between the orifice weight flow and the gas generator weight flow. Gas generator weight flow was calculated from the data measured at Station 3. Duct exit axial velocity was calculated from the Station 4 measurements of total pressure, total temperature, and air angle. Ambient static pressure, corrected to standard-day inlet conditions, was assumed at Station 4.

Fan Stage Performance

Pressure ratio, temperature ratio, and adiabatic efficiency were calculated to describe fan stage performance. These performance variables are defined as follows:

$$\text{Pressure ratio} = \frac{\bar{P}_4}{P_0}$$

$$\text{Temperature ratio} = \frac{\bar{T}_2}{\bar{T}_1}$$

$$\text{Adiabatic efficiency} = \frac{(\bar{P}_4/P_0)^{\frac{\gamma - 1}{\gamma}} - 1}{(\bar{T}_2/T_0) - 1}$$

where $\bar{P}_4$ = Duct exit (Station 4) total pressure

T_0 = Stage inlet total temperature

$\bar{T}_1$ = Rotor inlet (Station 1) total temperature

$\bar{T}_2$ = Rotor exit (Station 2) total temperature

γ = Ratio of specific heats

The bar notation refers to arithmetic averages of the pressures and temperatures at the indicated measuring stations.

Blade Row Performance

Calculated blade row performance variables consisted of inlet guide vane pressure ratio, inlet guide vane - rotor pressure ratio, and inlet guide vane - rotor adiabatic efficiency. These variables were calculated according to the following relationship:

$$\text{Inlet guide vane pressure ratio} = \frac{\bar{P}_1}{P_0}$$

$$\text{Inlet guide vane - rotor pressure ratio} = \frac{\bar{P}_2}{P_0}$$

$$\text{Inlet guide vane - rotor adiabatic efficiency} = \frac{(\bar{P}_2/P_0)^{\frac{\gamma - 1}{\gamma}} - 1}{(\bar{T}_2/T_0) - 1}$$

where $\bar{P}_1$ = Rotor inlet (Station 1) total pressure

$\bar{P}_2$ = Rotor exit (Station 2) total pressure.

RESULTS AND DISCUSSION

INFLUENCE OF GUIDE VANE POSITION ON SHAFT HORSEPOWER AND ENVIRONMENTAL TEMPERATURE

The residual fan (shaft) horsepower measured in the contingency test with both the inlet and duct exit guide vanes fully closed is shown as a function of rotor speed in Figure 32. This test demonstrated that the stage could operate without high vibration at design rotor speed with the vanes closed. The residual horsepower at design rotor speed was 720, or approximately 14 percent of the cruise design point horsepower.

It was observed during this test that the temperatures recorded behind the rotor at design speed were on the order of 500°F, as shown in Figure 33. Furthermore, it was noted that the temperature at a given speed increased with time, as shown in Figure 34. Thus, it is possible that equilibrium temperature conditions at design rotor speed would be reached at an even higher temperature than 500°F. This high envrionmental temperature is considered to be above the limit for compressor mechanical design without recourse to exotic materials; the resulting temperature in a gas generator compressor would be unacceptably high if the fan was a supercharging stage.

The reduction of shaft horsepower as a function of inlet guide vane closure for various exit guide vane settings is shown in Figure 35. Data for both 70- and 100-percent design rotor speed are included. For both rotor speeds, the shaft horsepower was reduced to approximately 30 percent of the respective maximum values by closing the inlet guide vane 45 degrees. The exit guide vane position does not appreciably influence the horsepower between inlet guide vane settings of 45 and 80 degrees. Beyond 80 degrees the horsepower drops as the inlet and exit guide vanes approach the fully closed position.

The sensitivity of rotor exit temperature to inlet and exit guide vane position is shown in Figure 36. A rapid increase in temperature can be seen for inlet guide vane closures above 60 degrees when the exit guide vane is closed. The temperature rise was not as pronounced when the exit guide vanes were partially or fully open.

The data in Figures 35 and 36 indicate that low fan parasitic power was achieved with the inlet and exit guide vanes closed or nearly closed, but that caution must be exercised to avoid the unacceptably high temperatures associated with high guide vane closure angles. Consequently, the test data obtained at design speed were extrapolated and cross-plotted to define the relationship between shaft horsepower and rotor exit temperature for high inlet and exit guide vane closure angles. The cross plots were accomplished as follows. First, the horsepower and temperature data for each inlet guide position were plotted as a function of exit guide vane closure angle. Data selected from these curves at exit guide vane settings of 60, 65, 70, 72, 74, 76, 78, and 80 degrees were then replotted as a function of inlet guide vane position. Finally,

horsepower was plotted as a function of temperature for the constant values of inlet and exit guide vane closure angles indicated in Figure 37. These results are repeated in Figure 38 with horsepower represented as a percent of the maximum (cruise design point) horsepower.

The results in Figures 37 and 38 clearly indicate the sensitivity of rotor exit temperature to exit guide vane closure. For example, when the inlet guide vane is varied from the 70-degree closed to the fully closed (90-degree) position with the exit guide vane at 72 degrees, the horsepower drops from 1500 to 1190 and the rotor exit temperature increases from about 180° to 205°F; but, for the same inlet guide vane closure with the exit guide vane fully closed (80 degrees), the horsepower drops from 1385 to 715 and the temperature increases to nearly 500°F. Since the inlet guide vanes in their closed position cut off the flow into the fan, the residual horsepower, and the high temperatures associated with high exit guide vane closure angles, must be a result of flow recirculation through the rotor. The amount of recirculating flow apparently diminishes as the exit guide vane is moved toward the fully closed position; hence, the decrease in horsepower. The level of recirculation in the rotor apparently increases as the exit vanes are closed; hence, the increase in temperature. Recirculation is discussed further on page 29.

The results in Figure 38 indicate that it is possible to reduce the shaft horsepower to about 16 percent of the maximum value without exceeding a temperature of 370°F. This is considered to be a safe upper limit of temperature for a supercharging fan stage.

It is possible that the residual horsepower, as a percent of maximum, could be less for a higher work fan stage than the one used in this investigation. For example, a fan having a lower hub-tip ratio, higher blade tip velocity, and higher pressure ratio with the same amount of flow recirculation in the rotor at reduced flow may have the same absolute level of residual horsepower but a greater maximum (cruise) horsepower. Residual horsepower might be further reduced by means of improvements to the flowpath geometry and flow conditions in the gas generator flowpath to reduce flow recirculation since a large portion of the residual horsepower and temperature rise was due to reverse flow in the gas generator flowpath.

INFLUENCE OF GAS GENERATOR FLOWPATH COVER PLATE ON SHAFT HORSEPOWER AND ENVIRONMENTAL TEMPERATURE

Data were obtained with a cover plate over the gas generator flowpath exit for the following guide vane settings:

Inlet Guide Vane Closure, deg	Duct Exit Guide Vane Closure, deg
70	68
80	68

These settings were selected on the basis of preliminary data analysis and were thought to encompass the minimum residual shaft horsepower condition within an acceptable rotor exit temperature limit. Horsepower as a function of rotor speed for these configurations is shown in Figure 39. Data obtained at the same guide vane settings without the cover plate are shown for comparison. Closing the gas generator flowpath exit reduced the shaft horsepower by approximately 50 percent at the two rotor speed conditions (70 and 100 percent of design) indicated. At design speed, the residual horsepower with the cover plate was the same as that obtained without the cover plate but with both the inlet and duct exit guide vanes fully closed (Figure 35).

Rotor exit temperature as a function of rotor speed is presented in Figure 40. The temperatures with the cover plate installed are slightly lower than the temperatures without the cover plate. A maximum temperature of 160°F was observed at design rotor speed. This temperature is substantially lower than the temperature obtained without the cover plate and with the guide vanes fully closed (Figure 33). Examination of the gas generator flowpath (Station 3) data revealed that, without the cover plate, the total pressure and static pressure were below ambient pressure, which indicated reverse flow in the gas generator flowpath. At design rotor speed and with the inlet guide vanes at 80 degrees, the reverse flow was calculated to be 14.8 lb/sec, assuming that the total pressure at Station 3 was equal to ambient pressure. The total and static pressure measurements at Station 3 further indicated that the reverse flow was eliminated when the cover plate was installed. This reverse-flow condition is possibly responsible for the shaft horsepower and temperature differences indicated in Figures 39 and 40 for operation with and without the cover plate. The path of the reverse flow after it left the gas generator flow path or the mechanism that caused the differences in power and temperature cannot be established from the data available.

INFLUENCE OF GUIDE VANE POSITION ON FAN THRUST

Fan thrust is shown as a function of inlet guide vane position for various exit guide vane settings in Figure 41 (design rotor speed) and Figure 42 (70-percent design rotor speed). The data in these figures indicate that essentially 100-percent fan axial thrust reduction is possible with the variable geometry inlet and duct exit guide vanes. Closing the inlet guide vane 80 degrees results in zero thrust for any exit guide vane position. Closing the exit guide vane with the inlet guide vane closed 60 degrees also results in zero thrust.

The relationship between fan thrust and fan horsepower during transition of a convertible fan/shaft engine from a cruise mode to a hover mode is of primary concern in propulsion system studies for VTOL (composite) aircraft. The operating envelope of horsepower available to a vertical lift rotor and fan thrust as defined by the data obtained in this investigation is presented in Figure 43. This operating envelope indicates the possibility of substantial thrust increases at constant fan power levels, as well as linear changes of thrust and power.

GUIDE VANE AND ROTOR BLADE STRESSES

Vibratory stresses observed during the test program for the inlet and duct exit guide vanes were less than 1000 psi. This level of stress is small compared to the 50,000- to 60,000-psi allowable vibratory stress limits for common vane materials.

Rotor blade vibratory stresses recorded during the test program are summarized in Table V. At 0-degree inlet guide vane setting and 100-percent design rotor speed, the blade stresses were constant at 3000 psi with a sudden increase to 10,000 psi at the stall point, which was induced by closing the exit guide vanes. This same increase in stress from a constant low value also occurred when the inlet guide vane was closed 45 degrees, but it was not observed at higher closure angles. The peak rotor stress for the 0-degree inlet guide vane position at 70-percent design rotor speed is only 7000 psi in Table V, whereas the test summary in Table IV implies that the 10,000-psi allowable stress limit (for the test program) was reached. This discrepancy occurred because the exact level of stress is difficult to ascertain on an oscilloscope during transient operating conditions; analysis of the recorded stress data was required to determine the exact stress limit reached. Even though this test was ended prematurely at the 7000-psi stress level, the fact that this is a stress-limited configuration is not compromised since the oscillograph analysis revealed that the exit guide vane could not have been closed more than a few degrees further before the 10,000-psi stress limit would have been reached. Rotor stresses for inlet guide vane closure angles greater than 45 degrees were constant, independent of the exit guide vane setting, and were well below the maximum allowable stress of 10,000 psi. A rapid increase in stress did not occur because the low flows associated with the high inlet guide vane closure angles minimized the aerodynamic forces which affect vibratory stress level.

The inlet and exit guide vane and rotor blade vibratory stress data indicate that zero fan thrust and low horsepower operating conditions can be achieved within acceptable stress limits.

TABLE V. FAN BLADE VIBRATORY STRESS SUMMARY			
Design Speed (%)	IGV Closure (deg)	DEGV Closure (deg)	Blade Stress* (psi)
100	0	0-41	3000 (10,000)
	45	0-5, 18-75	5000 (10,000)
	60	0-80	5000
	70	0-80	7500
	80	0-80	3000
70	0	0-50	2000 (7000)
	45	0-80	1000
	60	0-80	1000
	70	0-80	1000
	80	0-80	1000

*Maximum stresses are given in parentheses

FAN STAGE PERFORMANCE

Stage Pressure Ratio and Efficiency

Fan stage performance results in terms of pressure ratio and adiabatic efficiency are presented in Figures 44 and 45 for design rotor speed conditions and in Figures 46 and 47 for 70-percent design rotor speed conditions.

The peak pressure ratio at design rotor speed was 1.302 with the inlet and exit guide vanes in their fully open position (Figure 44). The corresponding weight flow was 284 lb/sec. Closing the inlet guide vane 45 degrees reduced the pressure ratio and flow to 1.082 and approximately 100 lb/sec, respectively. Further closure of the inlet guide vane reduced the pressure ratio to values between 1.0 and 1.06, depending on the exit guide vane position. The indicated weight flow for the 80-degree closure angle was about 10 lb/sec. These reductions in pressure ratio and flow are generally consistent with the reductions in shaft horsepower determined from the drive turbine measurements.

Two pressure ratio/weight flow data points are indicated in Figures 44 and 46 for inlet and exit guide vane settings of 45 and 40 degrees. Analysis of the data showed that this apparent flow discontinuity actually occurred and was a result of flow reversal in the gas generator flowpath.

A maximum fan stage efficiency of 80 percent was achieved at design rotor speed with the inlet guide vane fully open (Figure 45). Closing the inlet guide vane 45 degrees dropped the efficiency to 25 percent. Further closure of the inlet vanes resulted in further decreases in efficiency, which reflects the high rotor exit temperatures at minimum residual horsepower values shown earlier.

Flow Reversal in Gas Generator Flowpath

Analysis of the fan stage performance data revealed instantaneous changes in inlet weight flow for the 45-, 60-, 70-, and 80-degree inlet guide vane positions. The variation in inlet weight flow as a function of exit guide vane position for the 45-degree inlet vane setting (shown in Figure 48) indicated that the inlet flow increased 25 lb/sec at 52 degrees as the exit guide vanes were closing and decreased 16 lb/sec at 33 degrees as the exit guide vanes were opening. These weight flow changes occurred within 1 second (one scan of the data system). Flow measurements in the gas generator flowpath indicated similar discontinuities, as shown in Figure 49.

These weight flow discontinuities were apparently caused by the changing back pressure in the fan duct, resulting from movement of the exit guide vanes, which in turn affected the flow field at the gas generator flowpath inlet. When the exit vanes were closed 52 degrees, the pressure at the gas generator flowpath inlet was sufficient to overcome the gas generator flowpath losses and to cause flow through the gas generator flowpath. As the exit vanes were opened, the pressure at the gas generator flowpath inlet decreased until a flow reversal occurred when the exit guide vanes reached a 33-degree closure angle. This variation of weight flow at the gas generator inlet implies a wide variation of axial velocity and, hence, incidence angle, on the gas generator flowpath flow-straightening vanes. Incidence angles as high as 40 degrees beyond the stable operating range for these airfoil sections were calculated in a one-dimensional flow analysis. Operation at these high incidence angles causes high overall gas generator flowpath loss. Variable geometry guide vanes at the gas generator flowpath inlet would permit a smooth transition from cruise to VTOL modes of operation. In an engine configuration, flow reversal will also be affected by the pressure field in the gas generator flowpath induced by a compressor. A more comprehensive evaluation of this phenomenon should therefore include the effect of gas generator flowpath back pressure variation.

Blade Row Performance

Inlet guide vane pressure ratio as a function of weight flow for various inlet and exit guide vane settings is given in Figures 50 and 51 for 100- and 70-percent speeds, respectively. These data show that the pressure ratio is approximately 1.0 at the cruise inlet guide vane setting, indicating a low-loss blade row, and increases as the inlet vane is closed due to the recirculation of flow in the rotor tip region.

Attempts to rationalize the inconsistencies between the design rotor speed data in Figure 50 and the 70-percent design rotor speed data in Figure 51 are precluded by the unknown specific nature of the flow recirculation in the rotor. The variation of inlet guide vane pressure ratio with exit guide vane settings for 70-percent design rotor speed data is more systematic than the variation of pressure ratio for the 100-percent design rotor speed data. Part of the difference in the pressure ratio/weight flow trends in the two figures is attributed to overscaling of the Station 1

pressure transducers at 70- and 90-percent span due to recirculation at design rotor speed conditions. No explanation was found for the low pressure ratios at the 60-degree inlet guide vane setting (see Figure 50); however, this apparent data anomaly is not considered to be of any consequence relative to the program objectives. The systematic variation of pressure ratio, shown in Figure 51, reflects the influence of back pressure, induced by closing the exit guide vanes, on recirculation in the rotor. This back pressure effect becomes more pronounced at the lower weight flows (high inlet guide vane closure angles).

Inlet guide vane-rotor pressure ratio is presented as a function of corrected weight flow for 100- and 70-percent design rotor speed in Figures 52 and 53, respectively. These two figures further illustrate the influence of exit guide vane closure angle on flow recirculation in the rotor for high inlet guide vane closure angles. The dashed curves in Figure 52 are the predicted inlet guide vane-rotor pressure ratios that were calculated as part of the off-design analysis. The difference between predicted and measured pressure ratios for the cruise (0-degree) setting of the inlet guide vane is due to the fact that the inlet pressure was not reduced, as originally planned, to achieve the design pressure ratio and corrected weight flow conditions (see TEST PROCEDURE, page 14). The disagreement between the predicted and measured inlet guide vane-rotor pressure ratios for the 45-degree inlet guide vane closure angle is due primarily to the flow recirculation in the vicinity of the rotor. Since part of this recirculation is due to reverse flow in the gas generator flowpath, it is difficult to determine how accurately present design techniques might be expected to predict off-design performance (for relatively high inlet guide vane closure angles) when flow recirculation is not present.

Efficiency for the inlet guide vane rotor combination is shown in Figures 54 and 55 for 100- and 70-percent design rotor speed, respectively. The trend of efficiency with inlet guide vane closure angle is generally consistent with the stage efficiency data presented in Figures 45 and 47. The inlet guide vane rotor efficiencies are higher than the stage efficiencies because they do not include the fan duct and exit guide vane losses.

Rotor Flow Recirculation

Rotor temperature ratio is presented as a function of corrected weight flow in Figures 56 and 57 for 100- and 70-percent design rotor speed, respectively. Temperature ratios of less than one are the result of flow recirculation in the fan tip region, which substantially increased the fan inlet temperature. Flow recirculation also accounts for the high temperature ratios for the 80-degree inlet guide vane data, since little adiabatic flow work was done by the rotor in this configuration to cause a temperature rise. Figure 58 shows the spanwise total temperature distribution at the rotor inlet for design rotor speed conditions as the inlet guide vane closure angle is varied from 0 to 80 degrees with the exit guide vane set in the cruise (open) position. Corresponding total temperature data at

the rotor exit are presented in Figure 59. At 0-degree inlet vane setting, no flow recirculation is indicated because the rotor inlet temperature is equal to ambient temperature across the span. At 45-degree inlet guide vane closure, the rotor inlet temperature is equal to or greater than the exit temperature at 50-, 70-, and 90-percent span, indicating that flow recirculation is present over the outer 50-percent span upstream of the rotor. These same conditions exist at the 60-degree setting of the inlet guide vane except that the rotor inlet temperature at 70-percent span has increased significantly. As the inlet guide vane setting is increased to 80 degrees, the rotor inlet temperature becomes less than the exit temperature at 50- and 70-percent span, suggesting a reduction in the size of the recirculation zone; however, the inlet temperature at 90-percent span remains above the exit temperature, indicating that recirculation still exists in the tip region. Concurrent with these changes is a sharp increase in inlet temperature at 10- and 30-percent span, which indicates an increase in the spanwise influence of the recirculating flow field upstream of the rotor. Similar increases in rotor inlet temperature were noted in a program that investigated the effect of downstream annular flow blockage on rotor performance (Reference 8).

Total temperature data in Figures 60 and 61 show the change in the recirculation as the exit guide vane is closed from 0 to 80 degrees at a constant inlet guide vane setting of 70 degrees. The recirculation flow pattern appears to remain constant as the exit vane is closed from 0 to 60 degrees. At closures above 60 degrees, the spanwise influence of the recirculation spreads until it encompasses the entire span. Similar recirculating flow field development with exit guide vane angle change was also noted for the other inlet guide vane settings.

Insufficient blade element data were obtained to permit a rigorous analysis of the flow recirculation phenomena. However, the data shown in Figures 58 through 61 provide a qualitative evaluation of the basic flow mechanism and its characteristics. The apparent flow mechanism is a recirculating "pocket" of secondary flow which is circumvented by the primary fan flow and has three phases of development that depend on inlet and exit guide vane settings. The first two phases of development are shown schematically in Figure 62. In Phase I, the flow passes smoothly through the rotor blades at all spanwise positions without flow recirculation. This phase corresponds to the cruise inlet guide vane setting. Phase II develops as the fan inlet flow is restricted by the inlet guide vane closure, causing the rotor tip region to become stalled and flow to separate from the blade suction surface. The primary flow is displaced radially inward away from this separated region, and a secondary flow field is established in the tip region. Fluid particles in this secondary flow field pass over the rotor leading edge but are prevented from leaving at the fan blade exit by the primary flow stream. Consequently, the fluid particles move radially outward along the blade, reverse in direction, and return to the rotor leading edge where the process is repeated. When the inlet guide vane is closed to the 60-degree setting, the recirculation zone apparently increases in size and intensity, as indicated by the increased temperature upstream of the rotor at 70-percent span (Figure 58).

The recirculation zone is greatly reduced in size as the inlet guide vane is closed toward the 80-degree setting, but in the process some fluid particles leave the recirculating flow field and enter the primary flow stream upstream of the rotor. This is supported in Figures 58 and 59 by the decrease in rotor inlet temperature at 70-percent span and the sharp increases in both inlet and exit temperatures over the inner 50-percent span. No schematic representation of this latter phase of recirculation was attempted because the flow angle is only a few degrees from the plane of the rotor, and convection and eddy currents are probably of the same magnitude as the primary flow.

CONCLUDING DISCUSSION

A 0.5 hub-tip ratio fan stage having variable chord-angle inlet and duct exit guide vanes was tested to determine the reduction in fan horsepower and thrust that could be obtained over a range of guide vane settings between fully open (cruise) and fully closed.

The fan horsepower was reduced to a minimum residual horsepower equal to 14 percent of the maximum horsepower with the inlet and exit guide vanes fully closed. Rotor exit temperature for this guide vane configuration was on the order of 500°F. This level of temperature is considered to be above the upper temperature limit for practical compressor design.

With the inlet and exit guide vanes partially open, a residual horsepower equal to 16 percent of the maximum value was achieved within an acceptable upper limit of rotor exit temperature (370°F).

Installation of a cover plate over the gas generator flowpath with the guide vanes partially open reduced the residual horsepower to 14 percent of the maximum value at a rotor exit temperature of only 160°F. This result was attributed to the influence of flow conditions in the gas generator flowpath on flow recirculation in the rotor. The flow measurements obtained during the test program were not in sufficient detail to permit a detailed analysis of the recirculation. However, control of the gas generator flowpath pressure and variable geometry vanes in the gas generator flowpath could lead to further reductions in residual horsepower within safe temperature limits.

Fan thrust was reduced to essentially zero axial thrust within safe temperature limits.

Rotor blade and guide vane stresses were within acceptable limits throughout the test range of guide vane settings and rotor speed. Maximum stresses during stage stall did not exceed 10,000 psi. For high values of guide vane closure angles, the stresses were below 10,000 psi.

CONCLUSIONS

It is concluded that:

1. The use of variable chord-angle fan inlet and duct exit guide vanes to modulate fan horsepower and thrust for convertible aircraft application is feasible.

2. Methods for effective control of flow recirculation in the rotor are required to minimize the fan environmental temperature at the minimum achievable residual horsepower levels.

RECOMMENDATIONS

Recommendations for further investigation of the concept of variable chord-angle inlet and duct exit guide vanes for fan horsepower and thrust modulation for convertible aircraft application are as follows:

1. Perform mission analyses for selected convertible aircraft configurations using the experimental results obtained in this program.

2. Evaluate methods, such as a porous rotor shroud, to reduce flow recirculation in the rotor at high guide vane closure angles.

3. Investigate the influence of gas generator flowpath back pressure on residual horsepower and envrionmental temperature (recirculation).

4. Investigate variable chord-angle vanes in the gas generator inlet.

5. Evaluate fan configuration having split flowpath through the rotor to separate fan duct and gas generator flow.

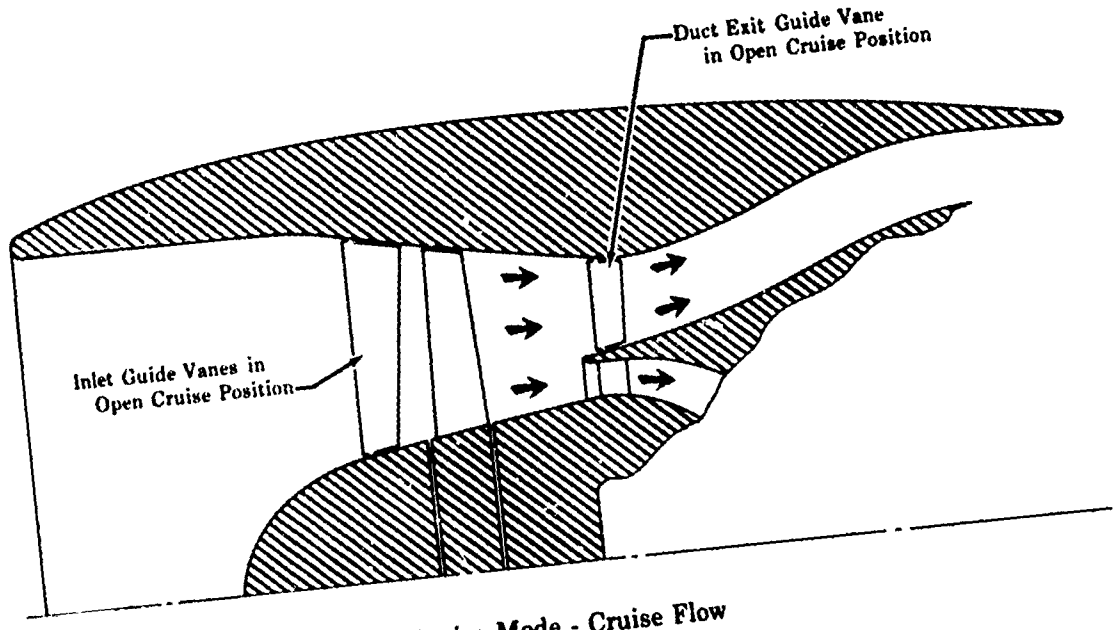

Cruise Mode - Cruise Flow

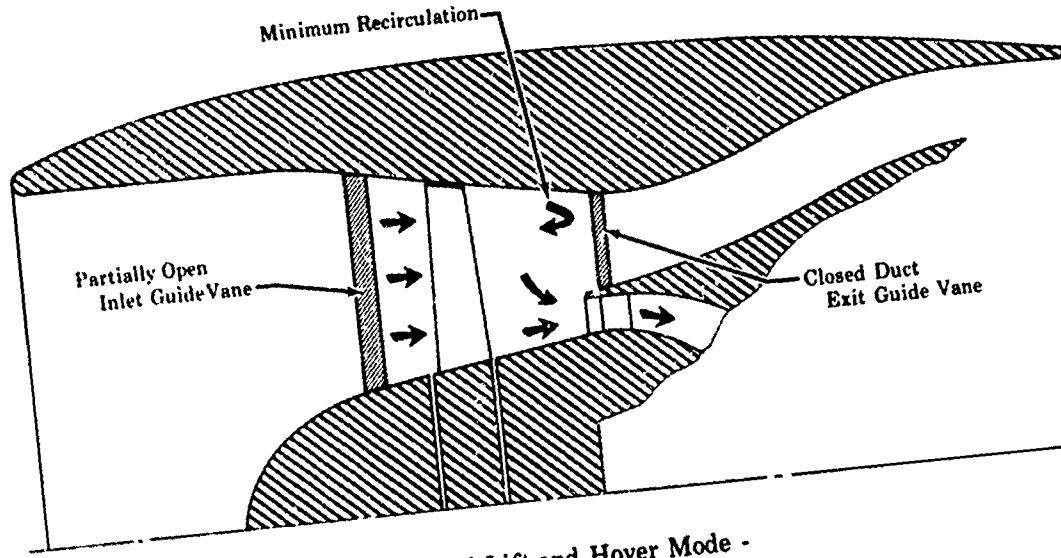

Vertical Lift and Hover Mode -
Approximately One-Fifth Cruise Flow

Figure 1. Variable Geometry Fan for Efficient Fan-to-Shaft Power Transfer.

Plane	ID	Flow Splitter	OD
①	18.65	- -	43.23
②	18.65	- -	43.19
③	18.65	- -	43.18
④	20.78	- -	43.13
⑤	20.91	- -	43.12
⑥	21.30	- -	43.10
⑦	23.40	- -	43.10
⑧	23.69	- -	43.10
⑨	24.63	- -	43.10
⑩	25.44	- -	43.10
⑪	25.90	- -	42.16
⑫	25.90	30.03	41.87
⑬	25.90	29.77	41.88
⑭	25.90	29.72	41.88
⑮	25.90	29.61	41.95
⑯	24.30	29.16	43.14
⑰	20.40	28.18	43.85
⑱	20.40	28.30	43.85
⑲	20.35	27.81	- -

Note: Flow-Splitter Diameters to Gas Generator Flowpath Side

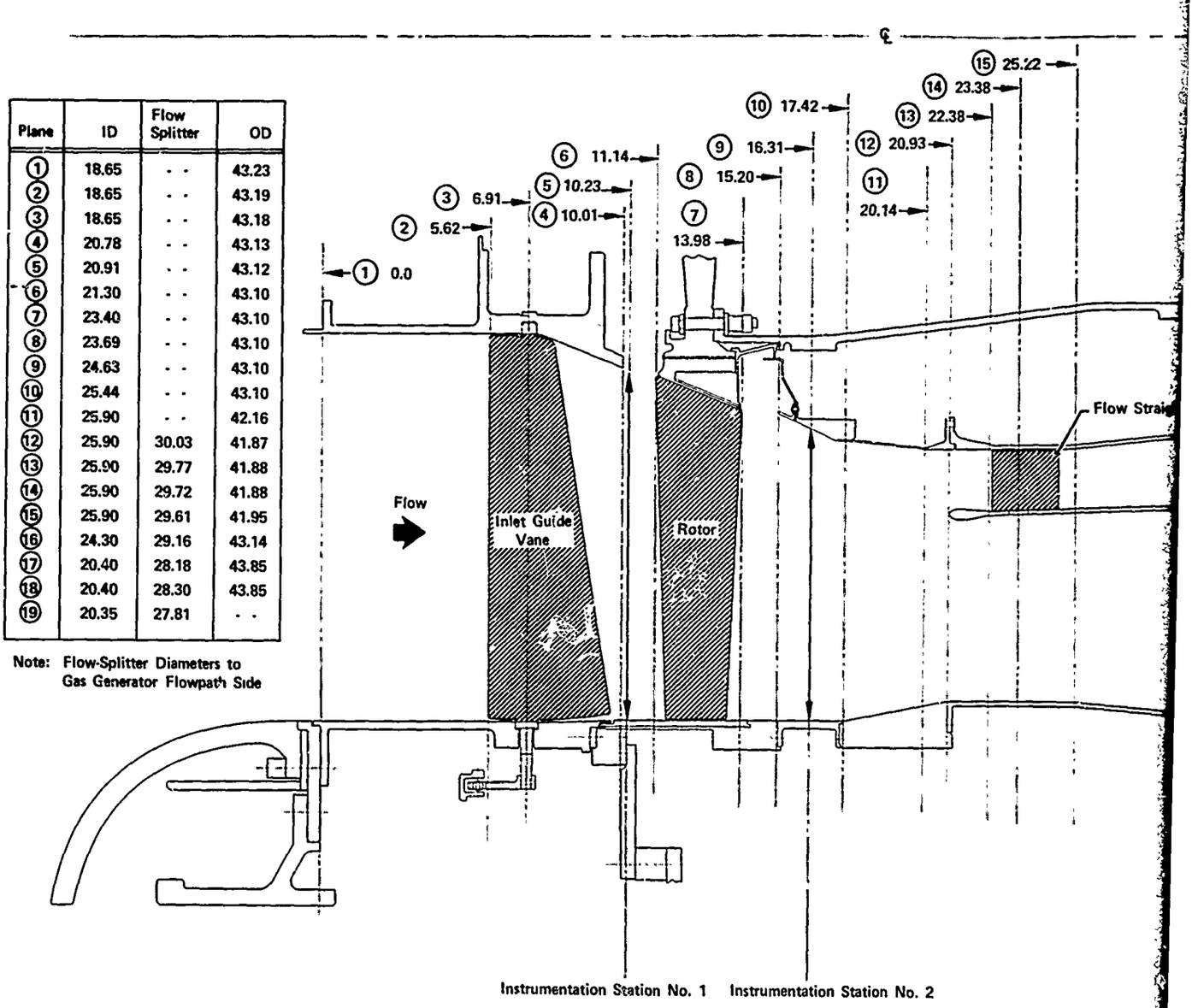

Figure 2. Flowpath Definition.

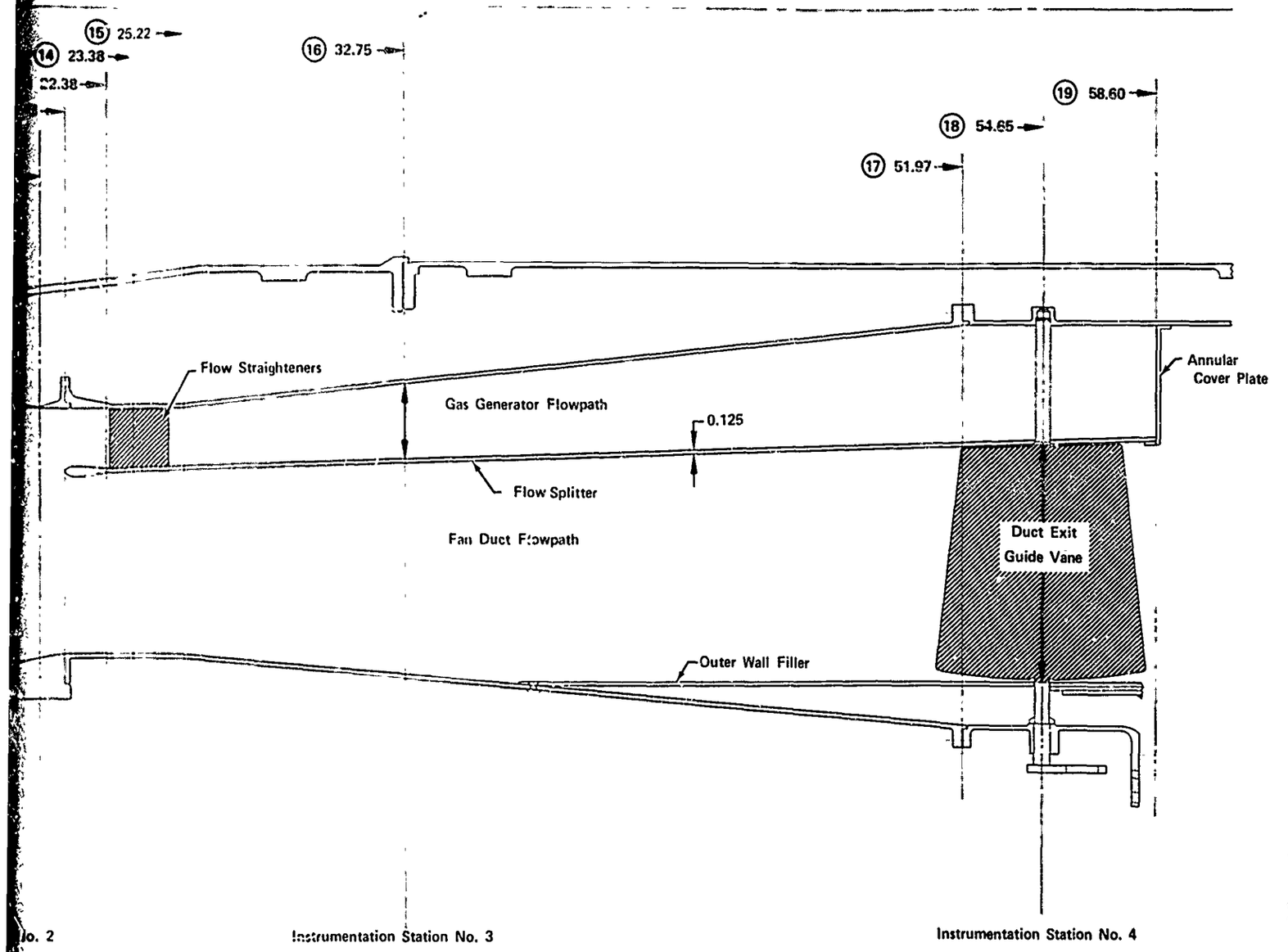
15 25.22
14 23.38
22.38
16 32.75
19 58.60
18 54.65
17 51.97
Flow Straighteners
Gas Generator Flowpath
0.125
Annular
Cover Plate
Flow Splitter
Fan Duct Flowpath
Duct Exit
Guide Vane
Outer Wall Filler
lo. 2
Instrumentation Station No. 3
Instrumentation Station No. 4

B

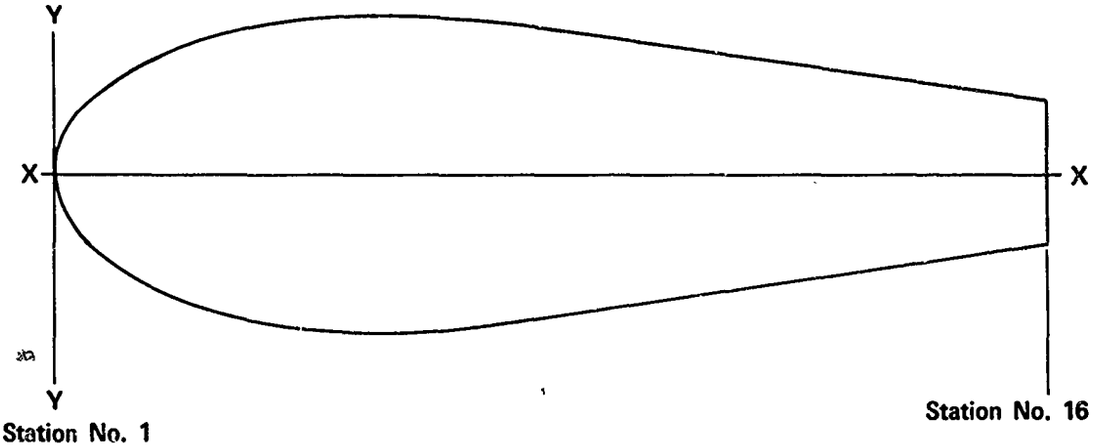

Section Coordinates, in.		
Station	X	Y
1	0.000	0.000
2	0.002	±0.016
3	0.006	±0.032
4	0.012	±0.045
5	0.020	±0.058
6	0.030	±0.070
7	0.058	±0.096
8	0.094	±0.120
9	0.136	±0.140
10	0.193	±0.160
11	0.285	±0.180
12	0.420	±0.190
13	0.555	±0.180
14	0.698	±0.160
15	1.000	±0.118
16	1.400	±0.063

Figure 3. Flow-Splitter Leading-Edge Geometry.

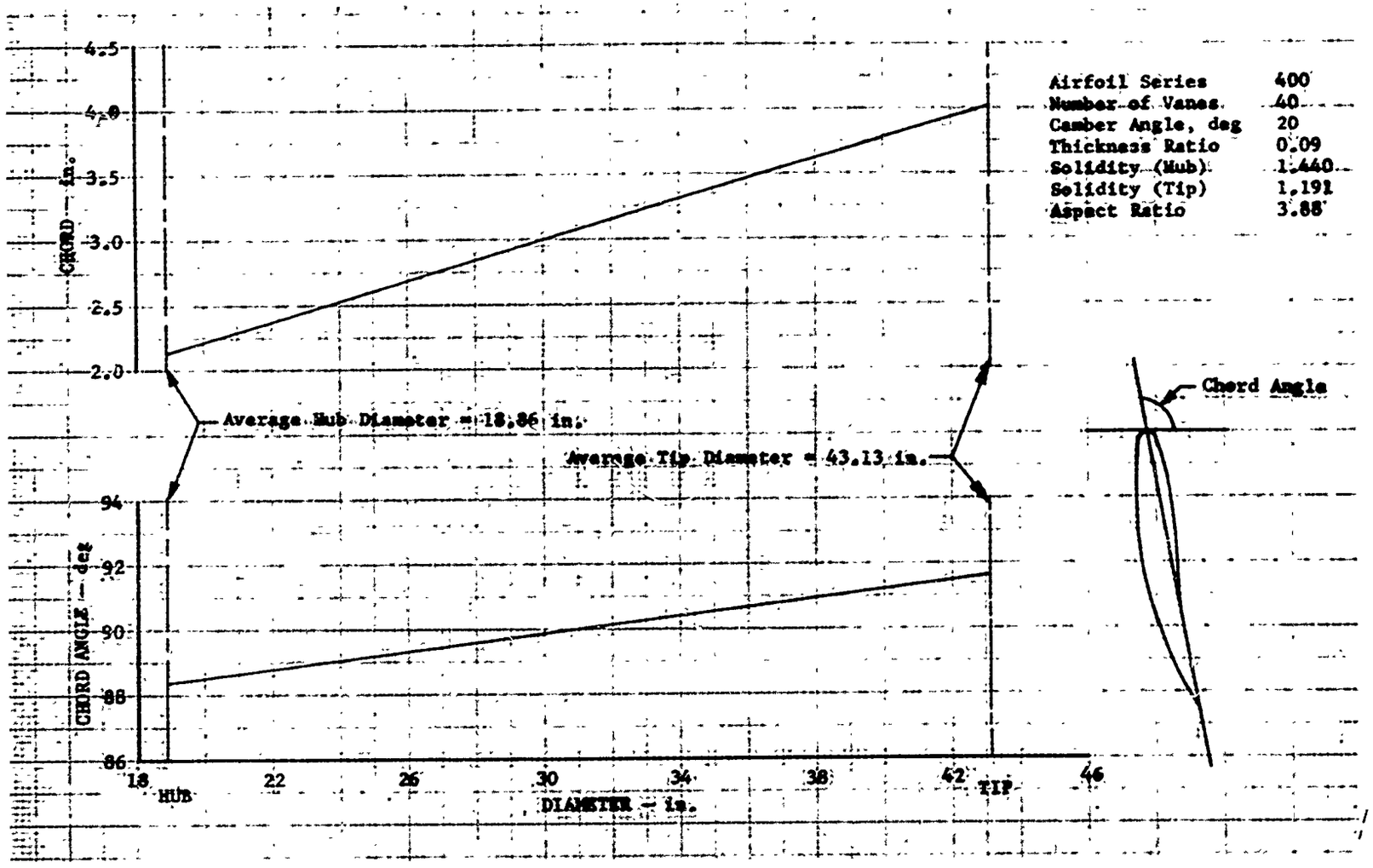

Figure 4. Inlet Guide Vane Geometry Details.

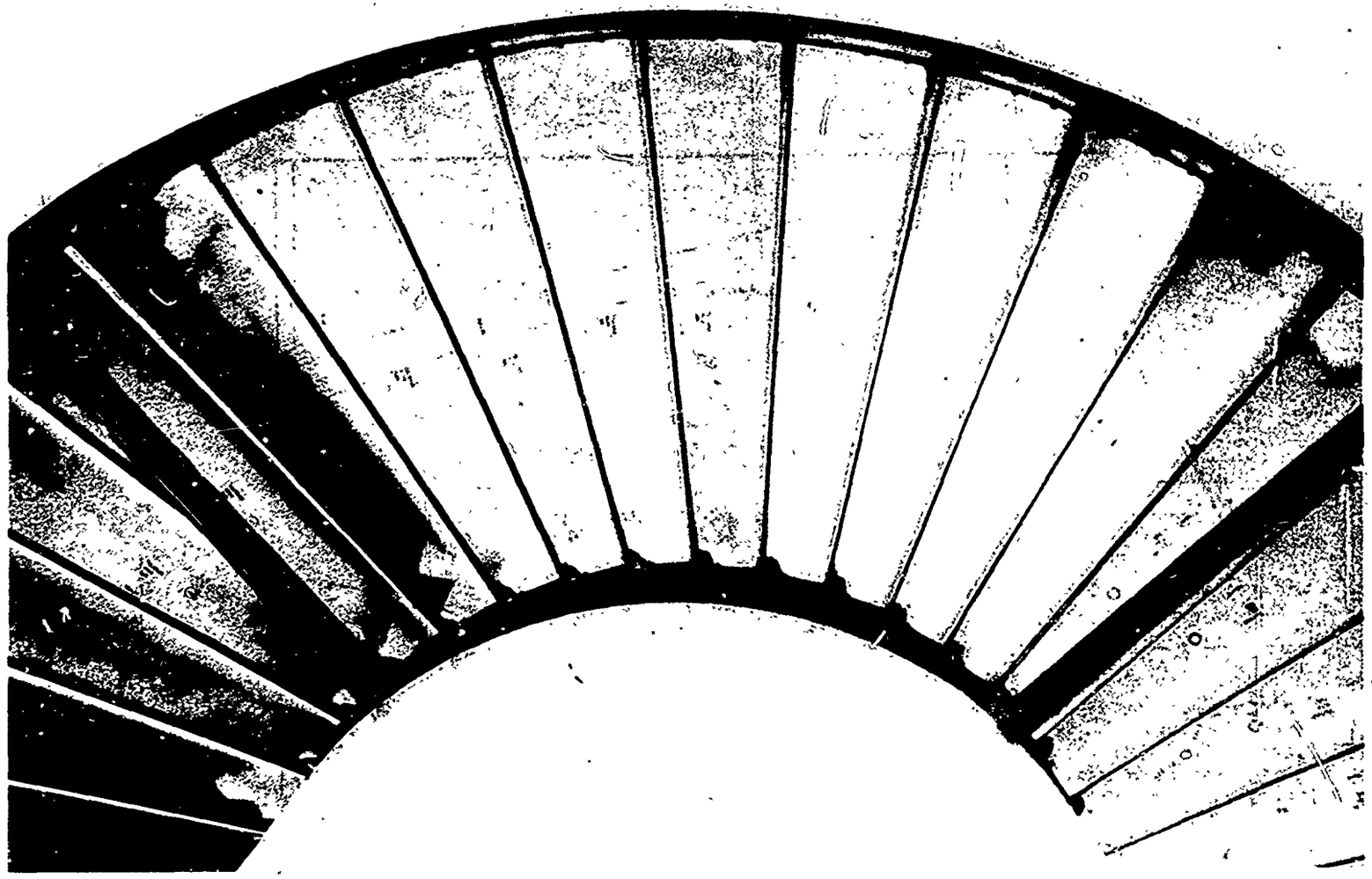

Figure 5. Inlet Guide Vanes in Closed Position.

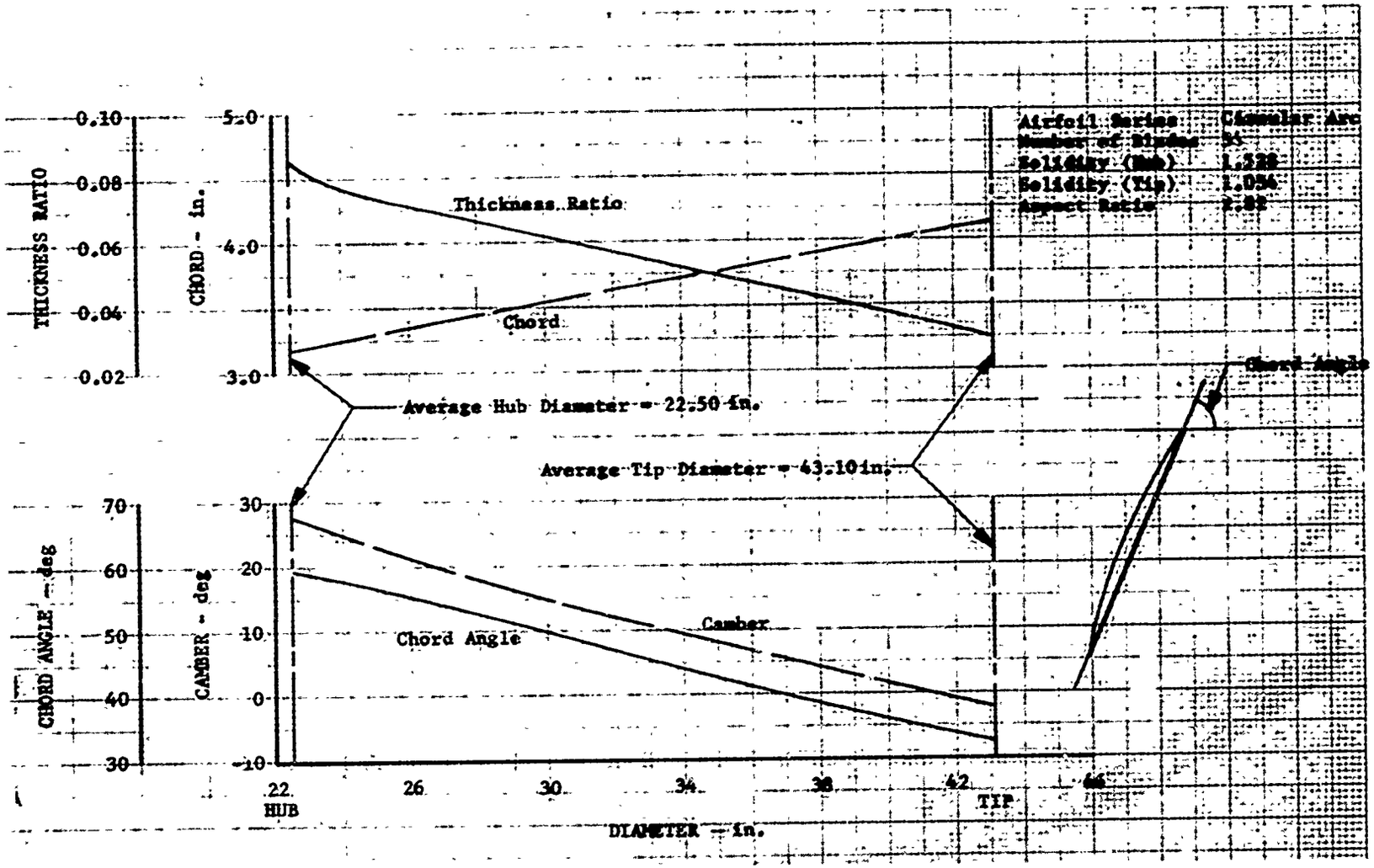

Figure 6. Rotor Geometry Detail .

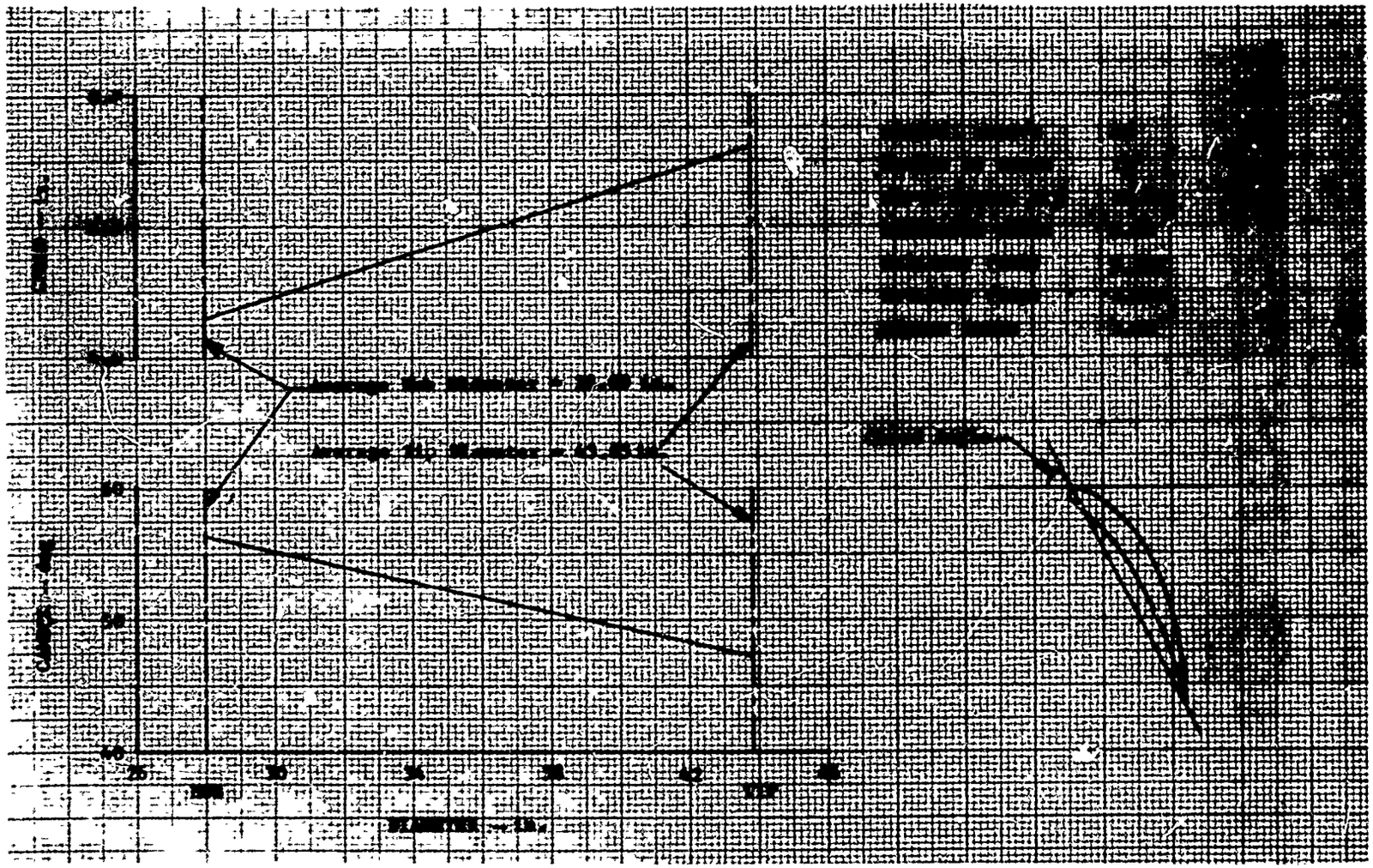

Figure 7. Duct Exit Guide Vane Geometry Details.

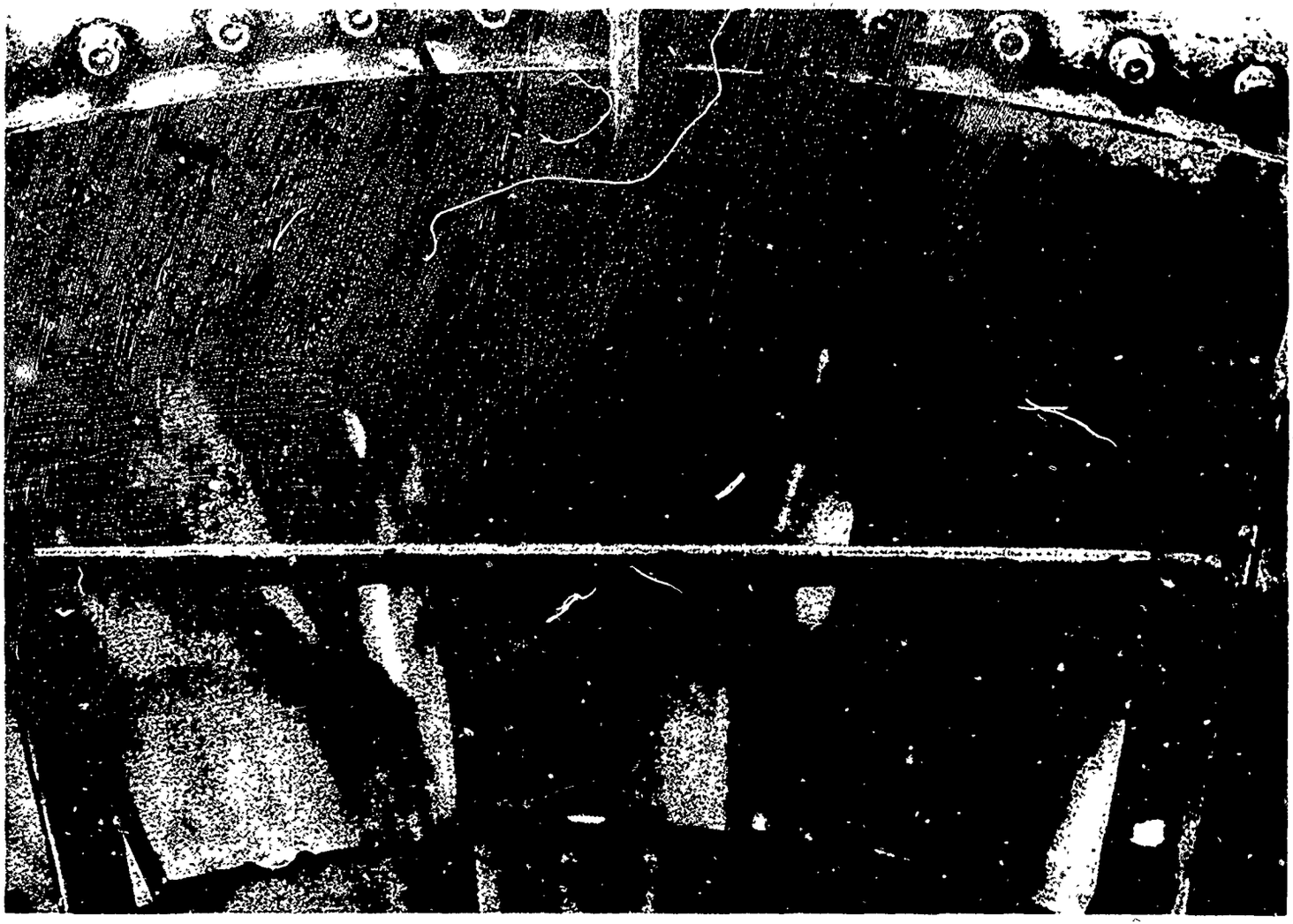

Figure 8. Duct Exit Guide Vanes in Closed Position.

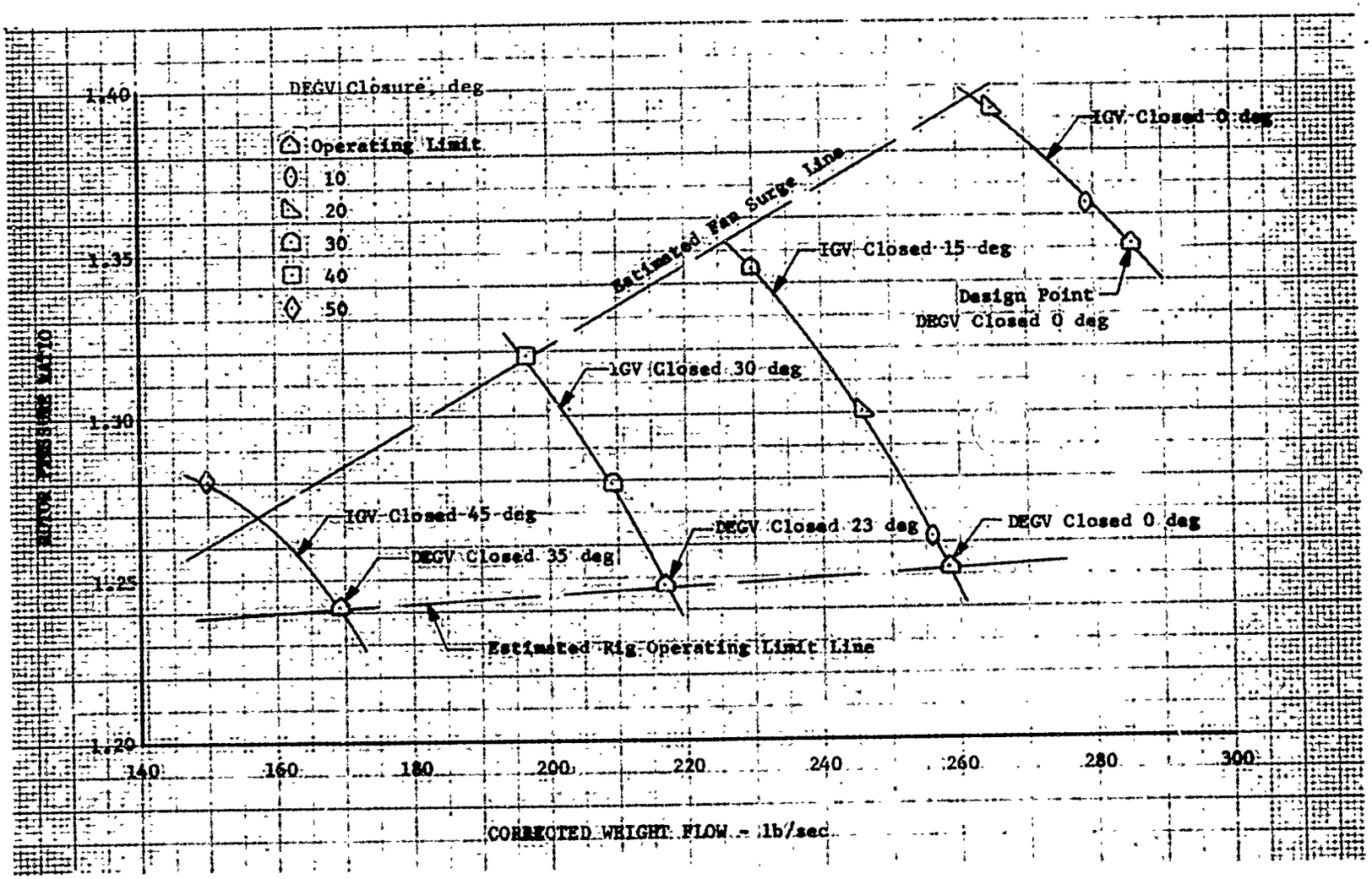

Figure 9. Predicted Rotor Pressure Ratio and Corrected Weight Flow at Off-Design Guide Vane Settings; Design Rotor Speed.

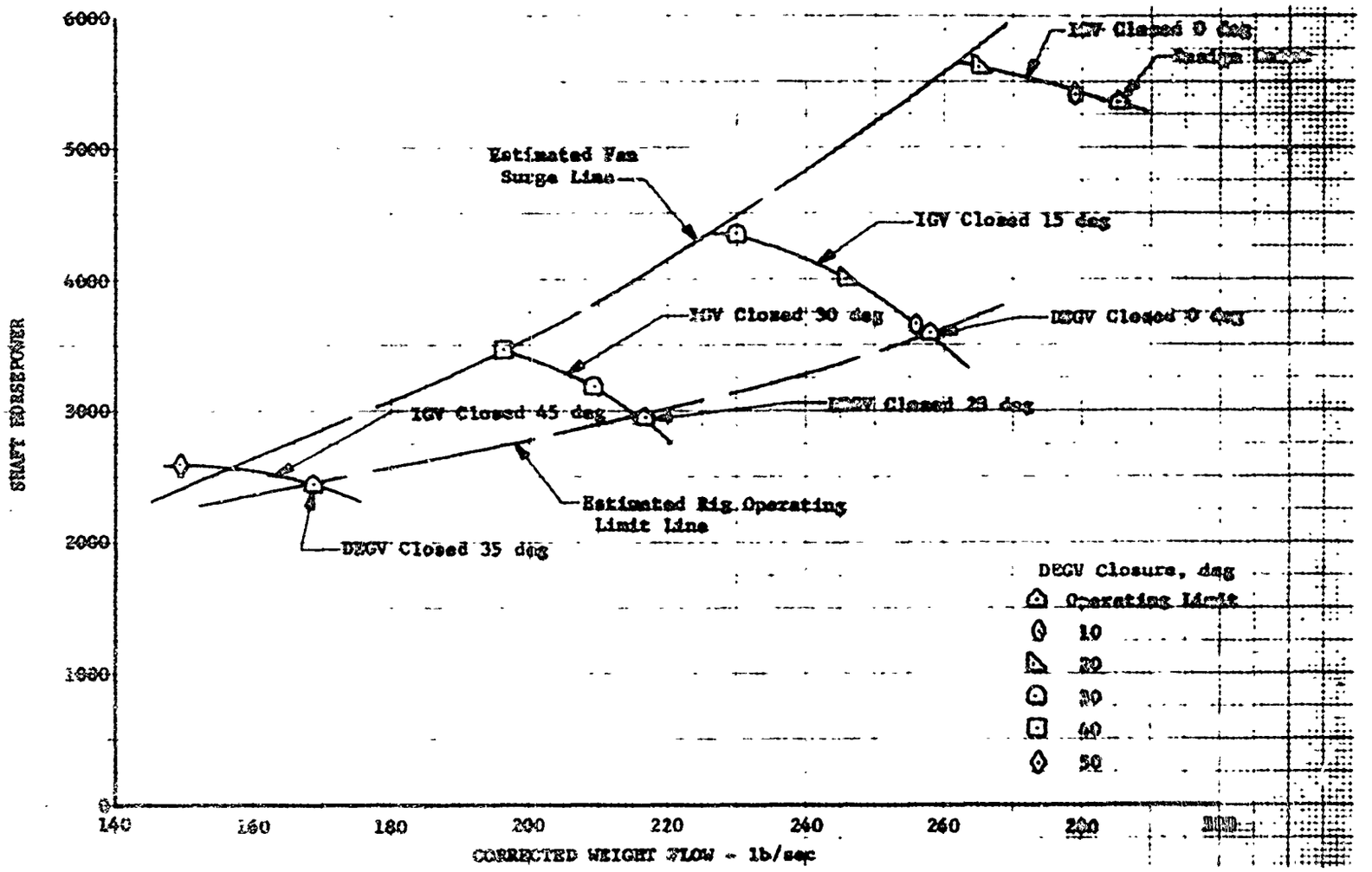

Figure 10. Predicted Influence of Guide Vane Setting on Shaft Horsepower; Design Rotor Speed.

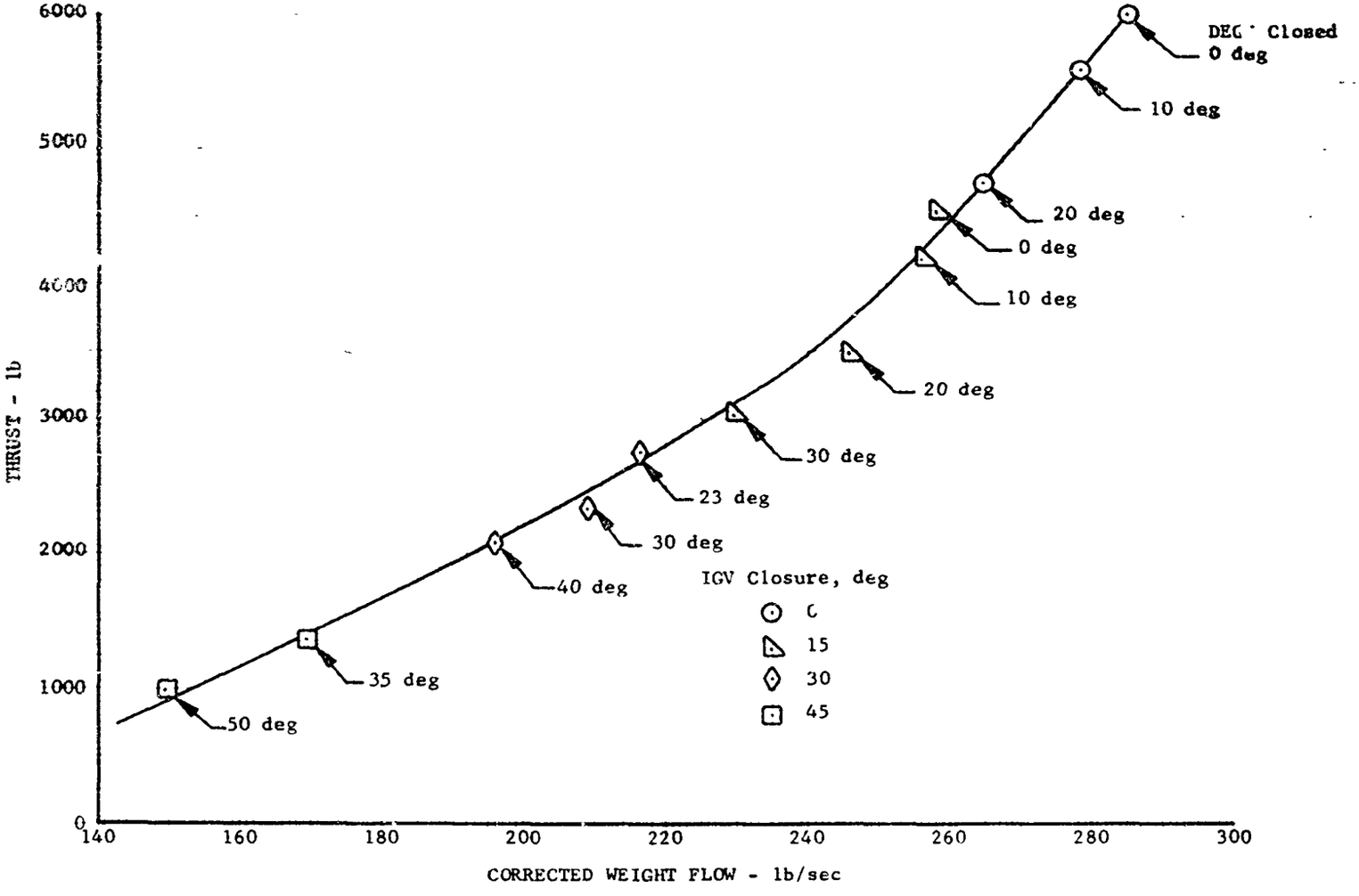

Figure 11. Predicted Influence of Guide Vane Setting on Thrust; Design Rotor Speed.

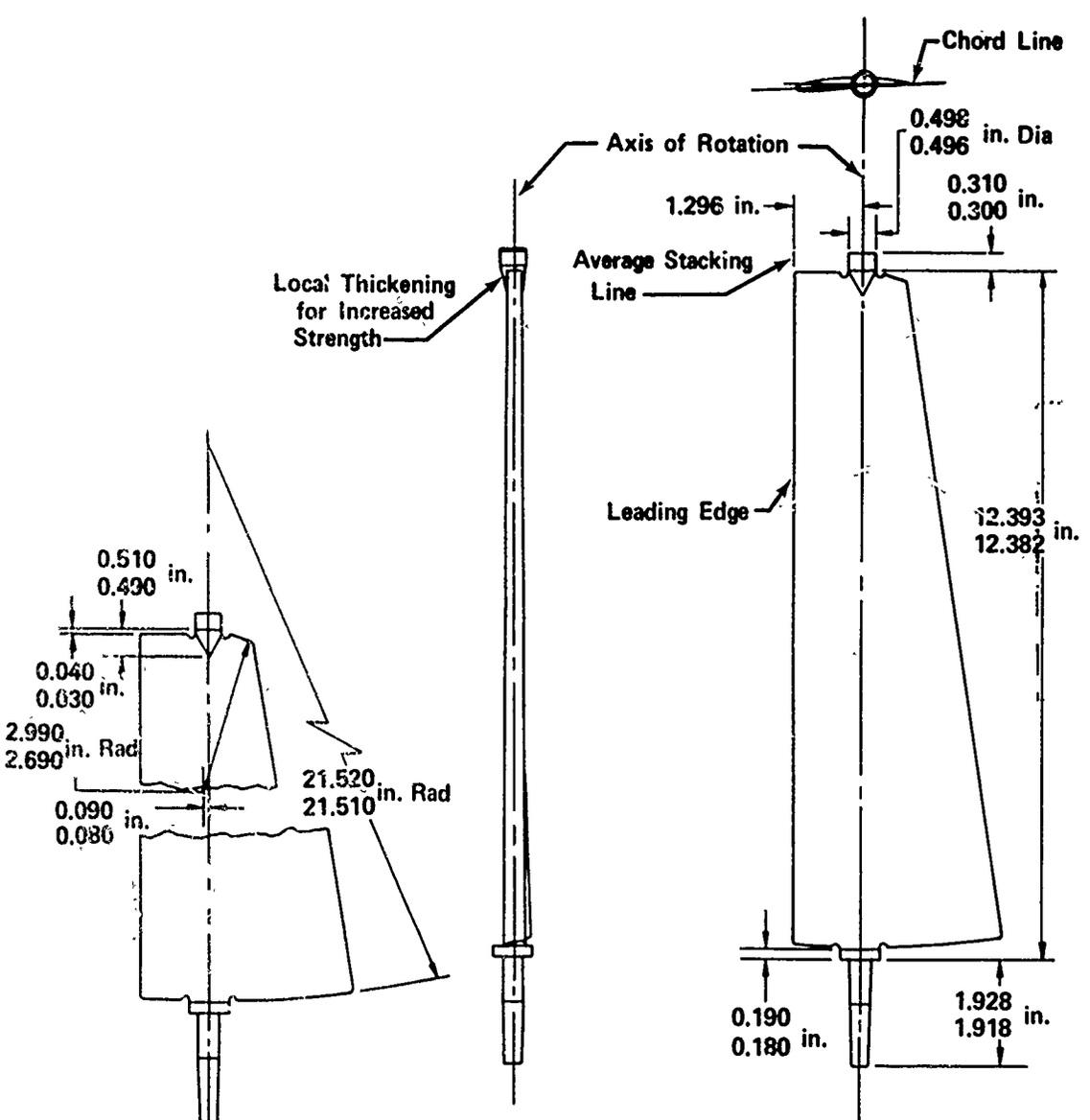

Figure 12. Inlet Guide Vane Design.

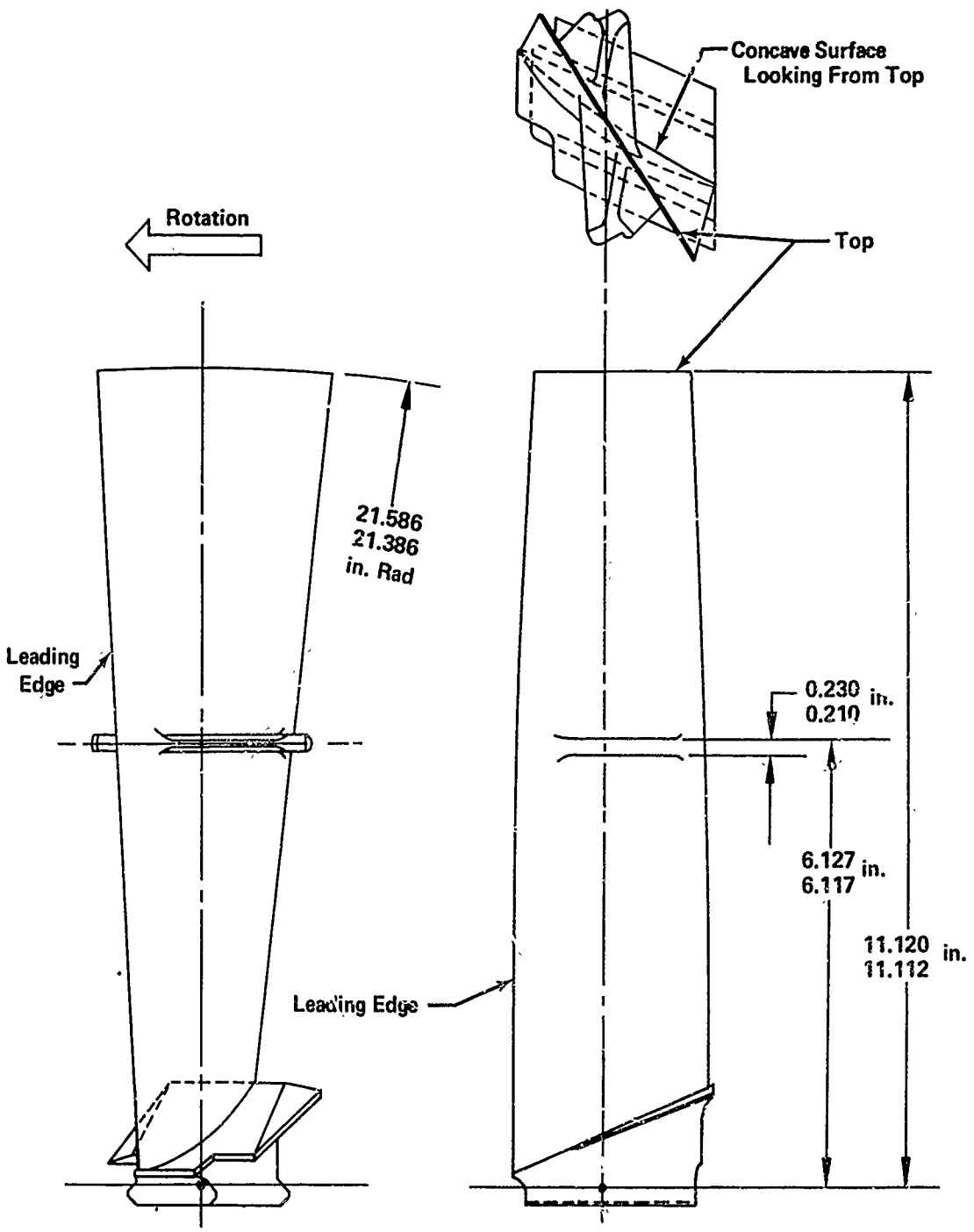

Figure 13. Rotor Blade and Attachment Design.

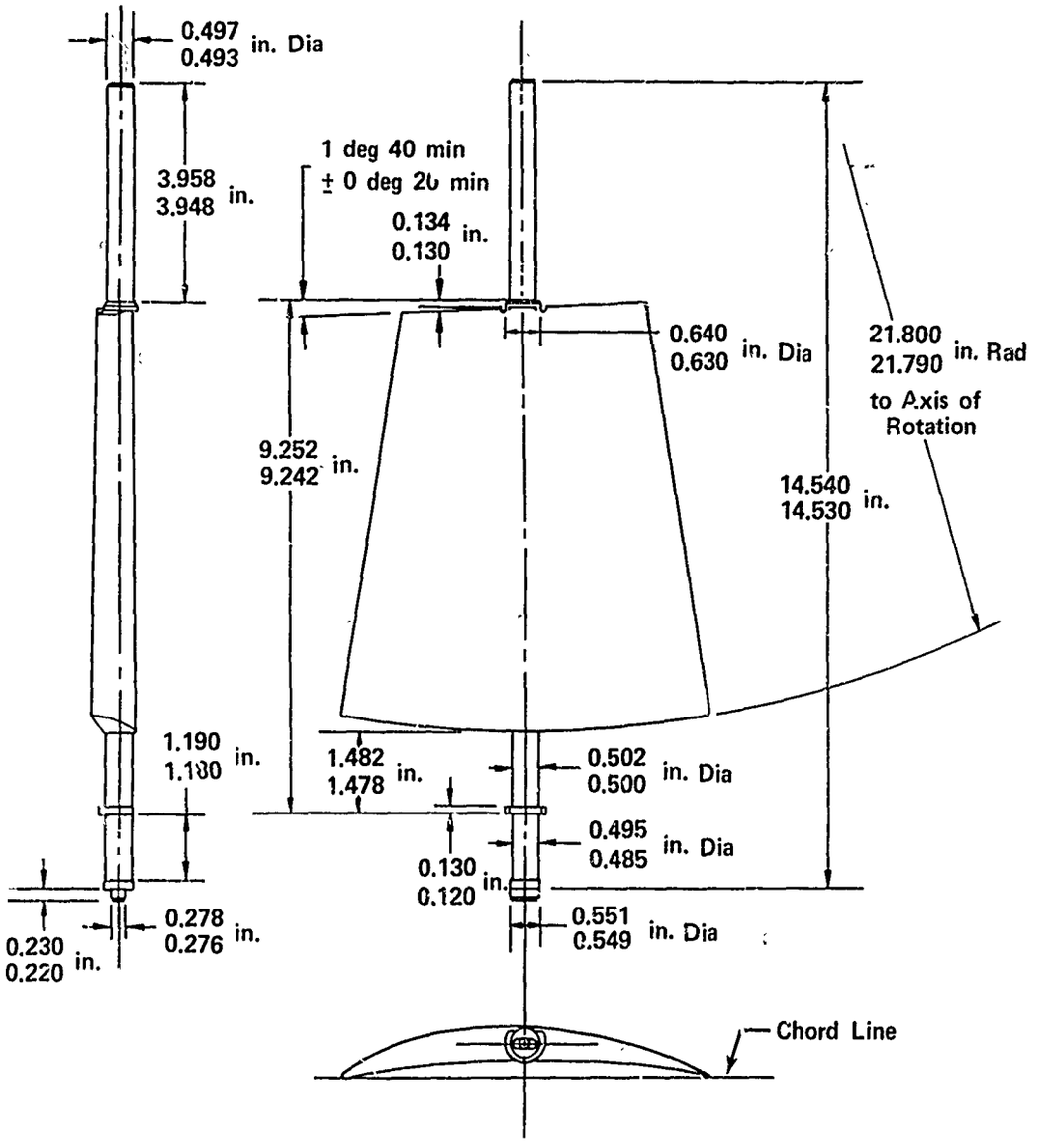

Figure 14. Duct Exit Guide Vane Design.

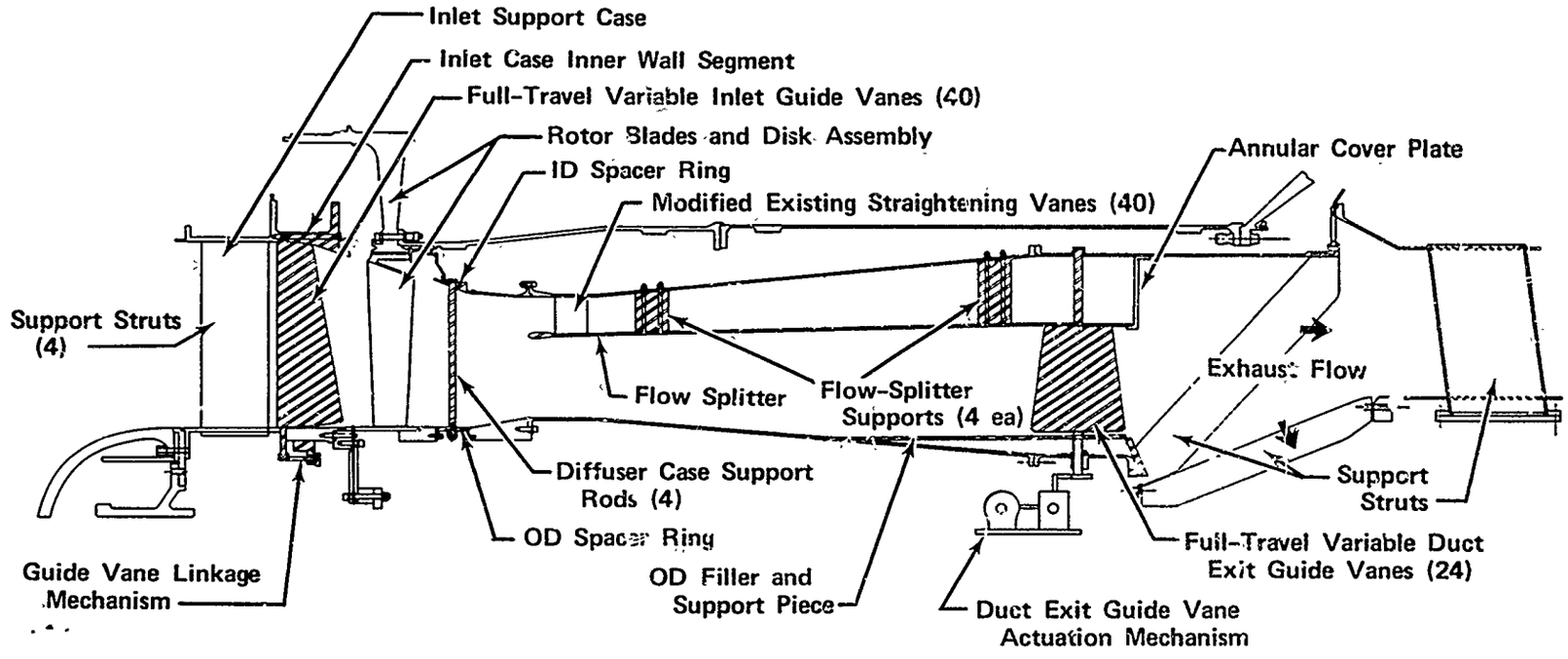

Figure 15. Sectional View of Low Hub-Tip Ratio Single-Stage Test Rig.

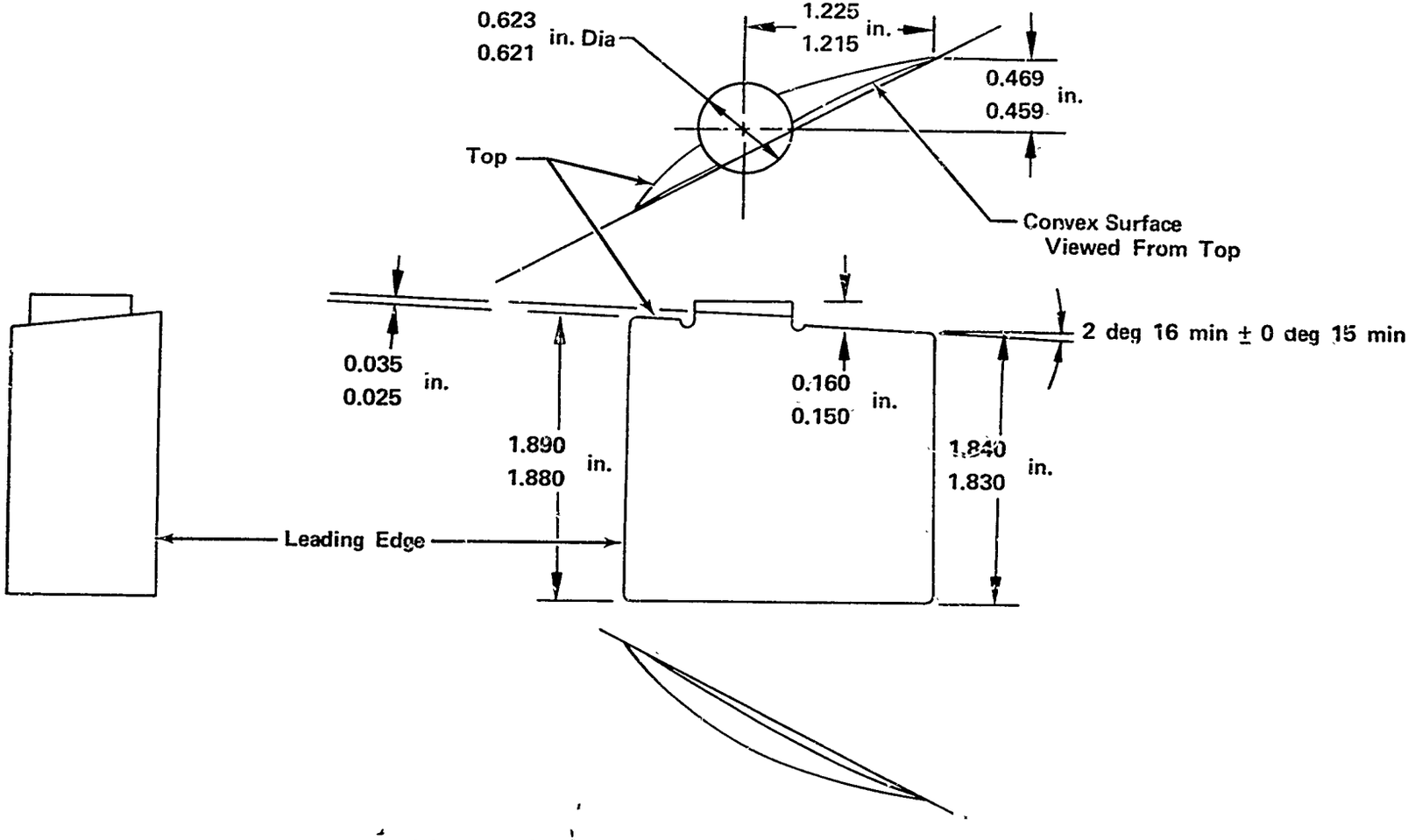

Figure 16. Gas Generator Flowpath Flow-Straightening Vane Design.

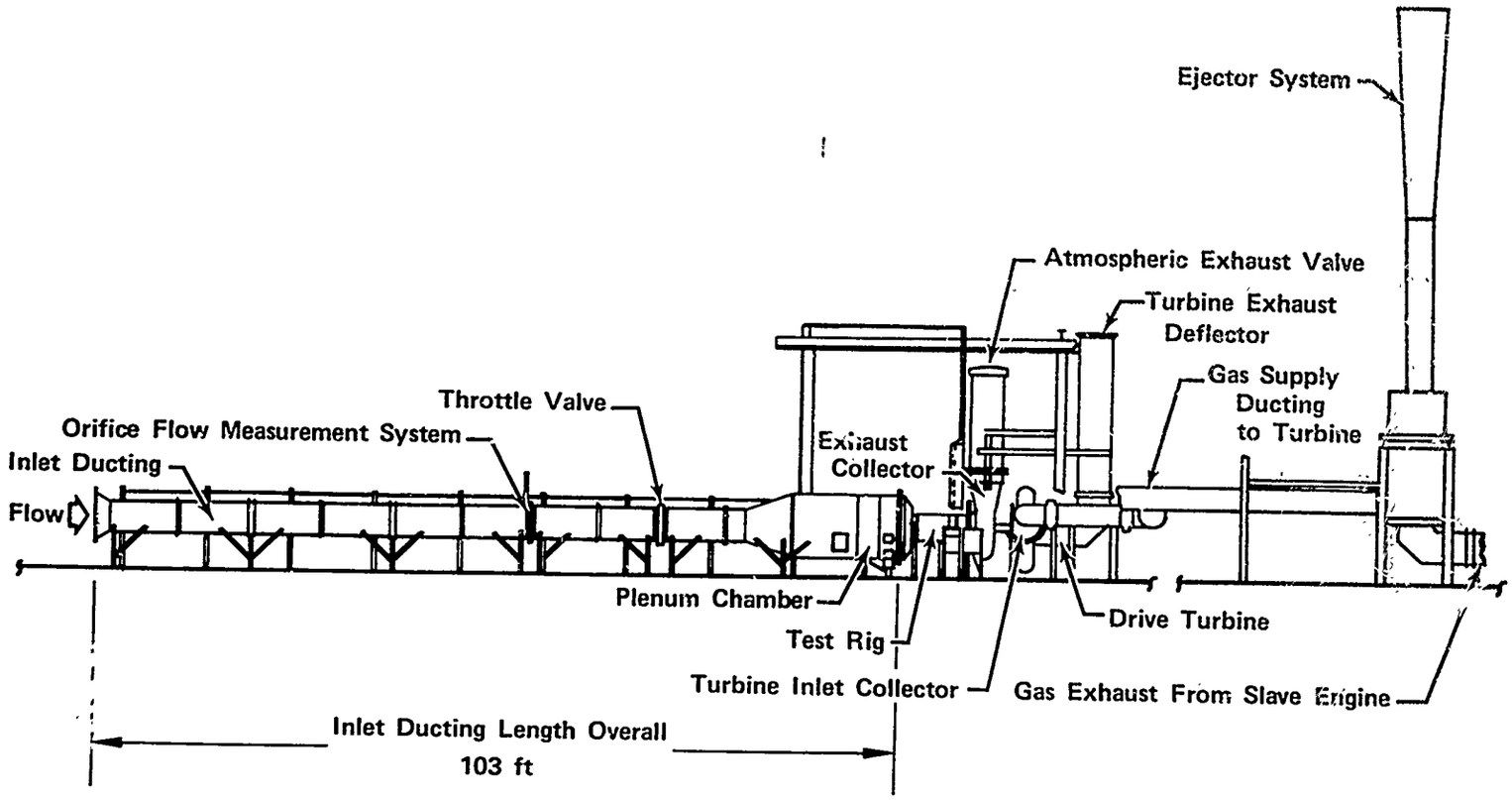

Figure 17. Compressor Research Facility.

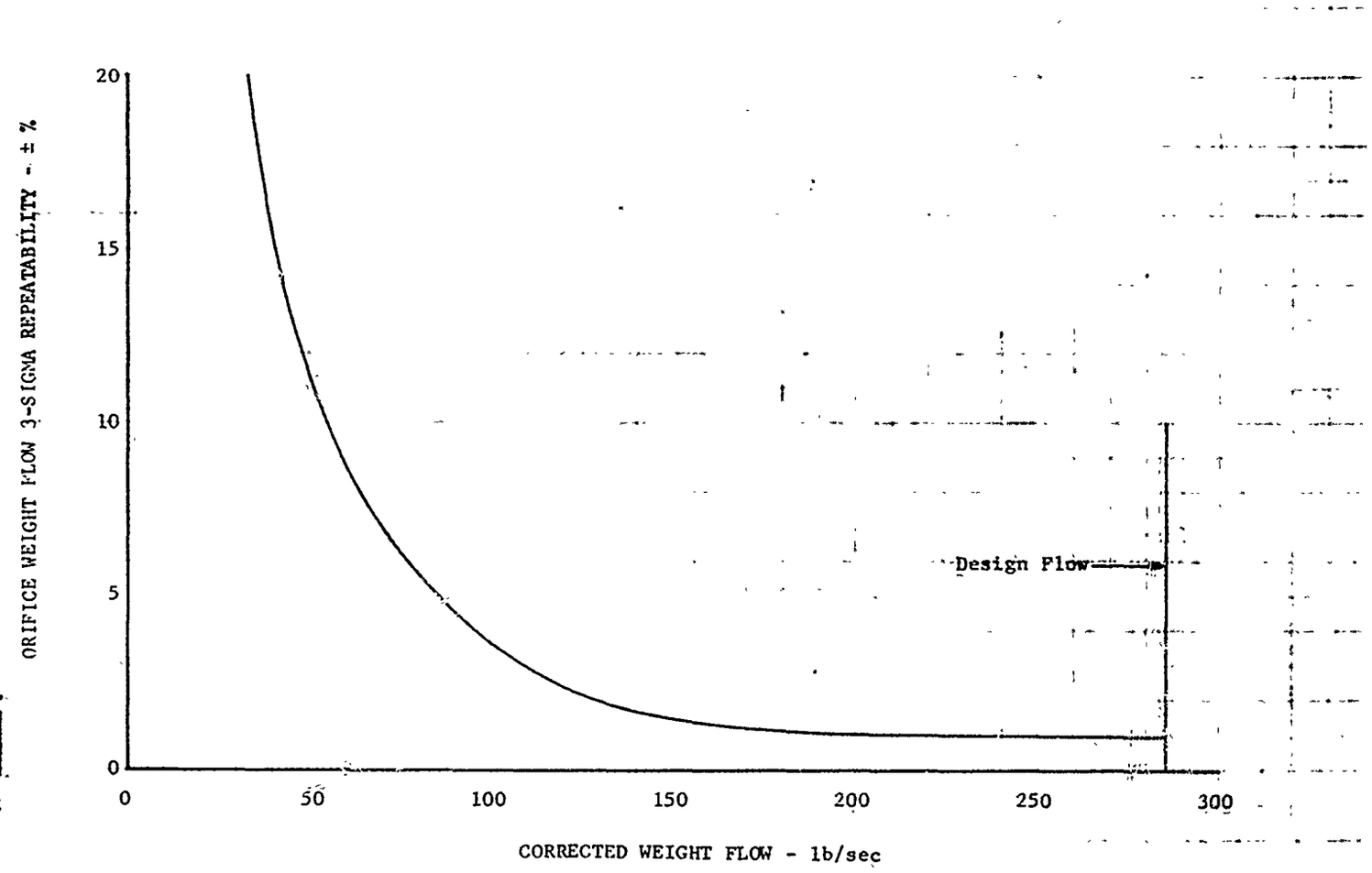

Figure 18. Orifice Weight Flow, 3-Sigma Repeatability.

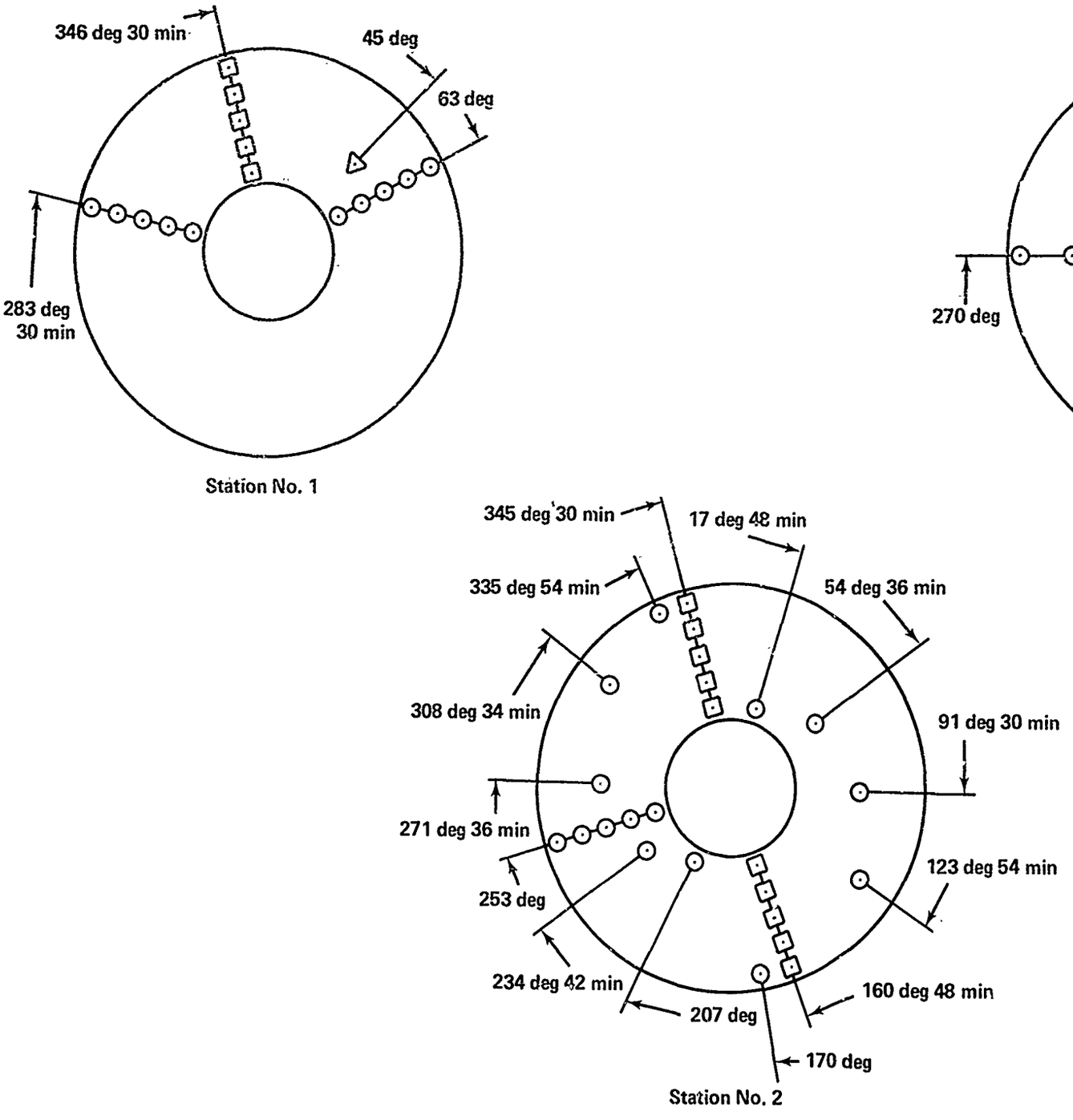

Figure 19. Circumferential Location of Fan Stage Performance Instrumentation.

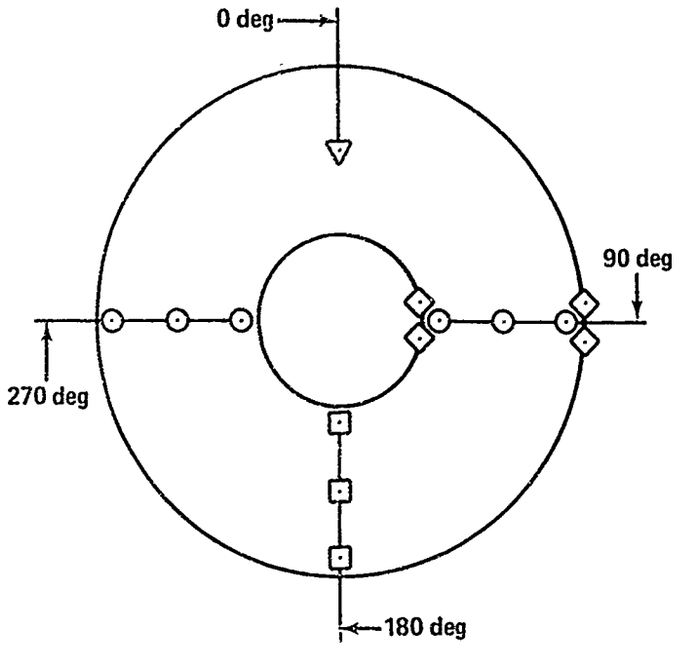

⊙ – Total Pressure
◇ – Static Pressure
⊡ – Total Temperature
△ – Air Angle

Stations No. 1, 2, and 4 Sensors are at 10, 30, 50, 70, and 90% Spans; Station No. 3 Sensors are at 10, 50, and 90% Spans

Station No. 3

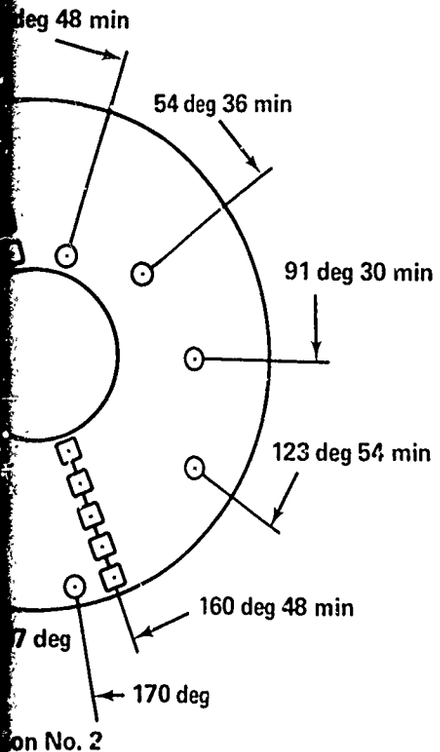

on No. 2

er-

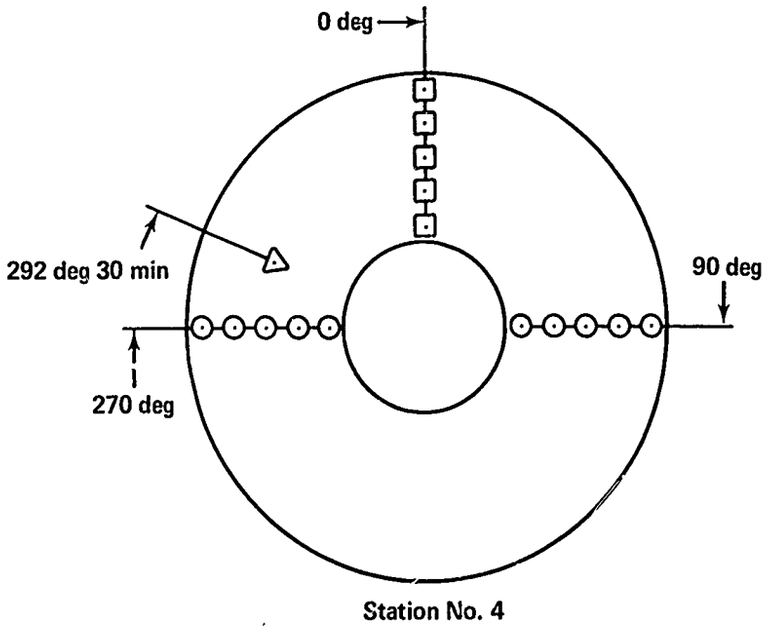

Station No. 4

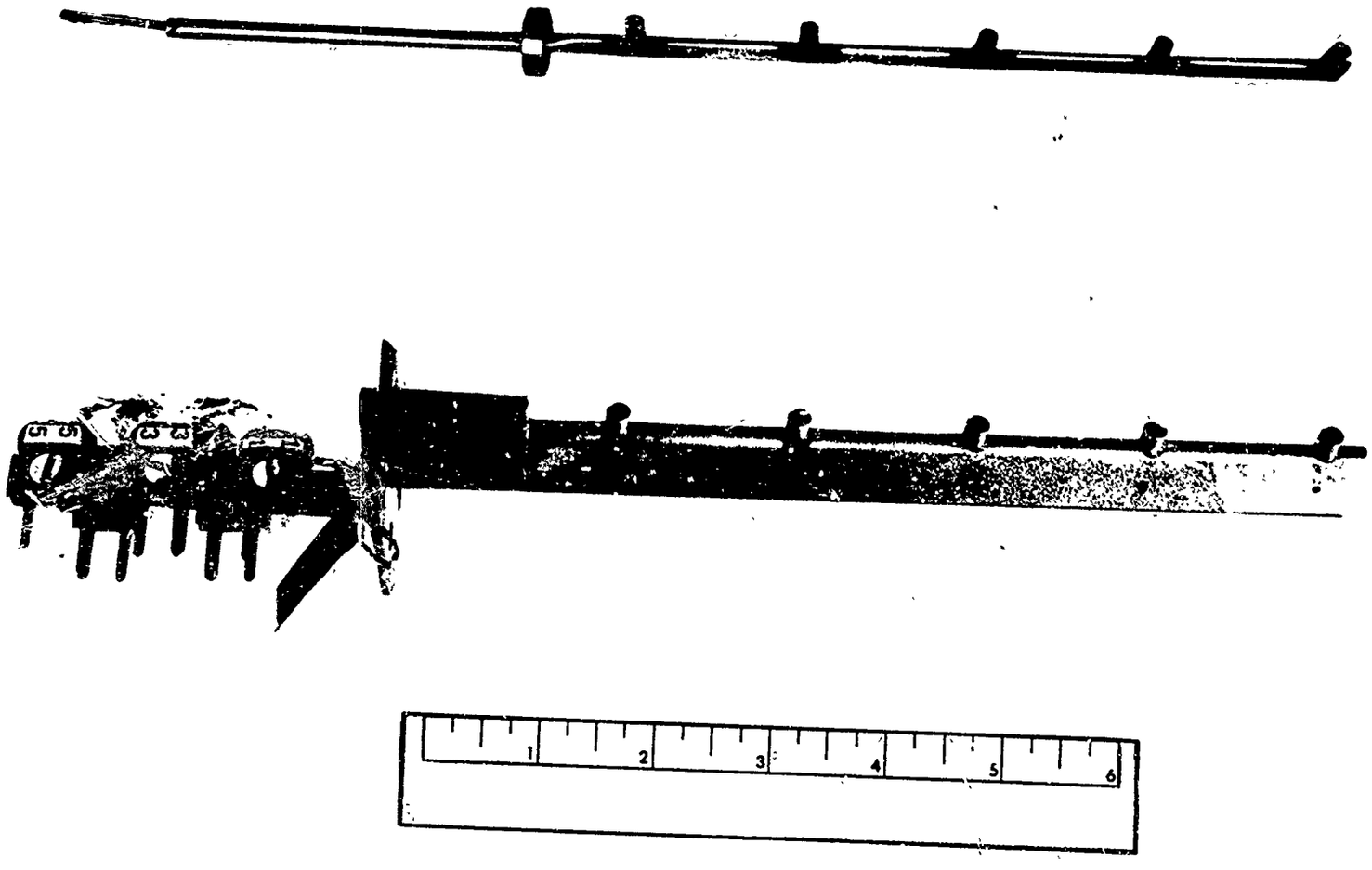

Figure 20. Total Temperature and Total Pressure Rakes.

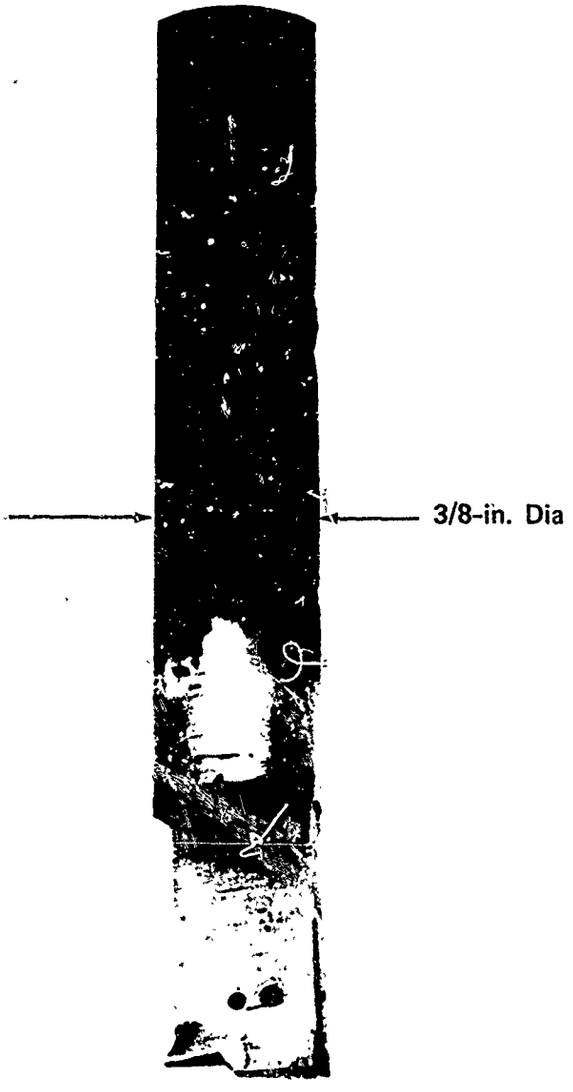

Figure 21. 20-Degree Wedge Probe.

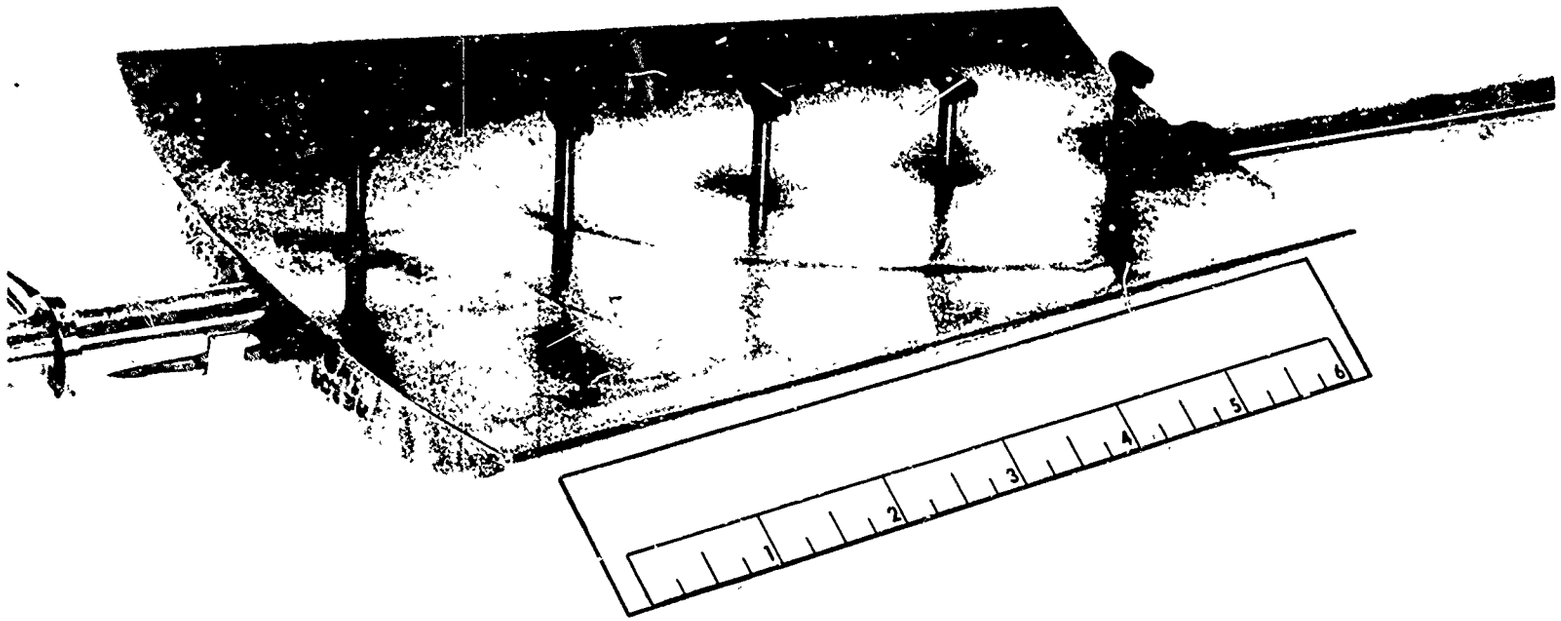

Figure 22. Duct Exit Guide Vane With Total Pressure Kiel Probes Installed.

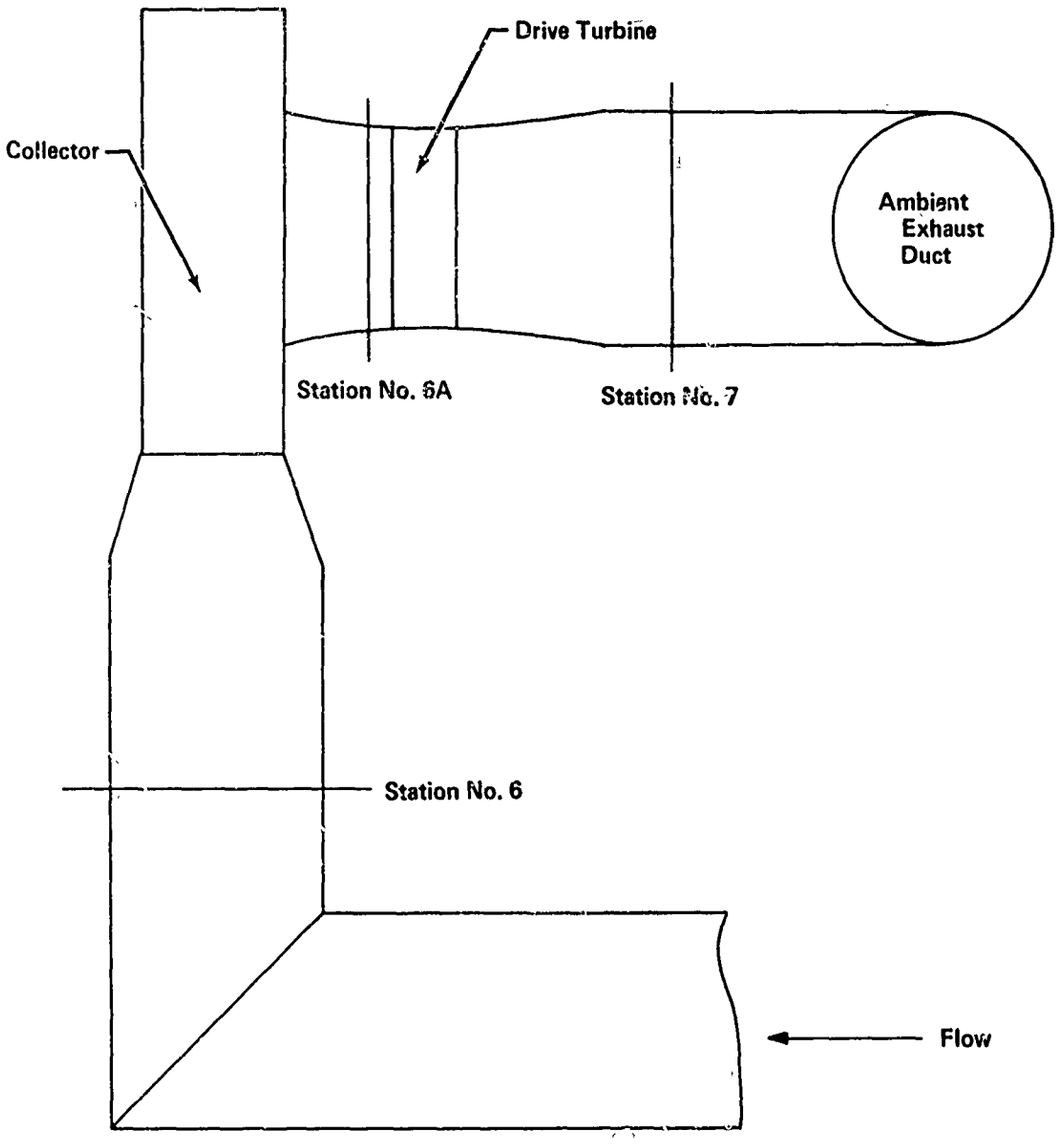

Figure 23. Drive Turbine Instrumentation Stations.

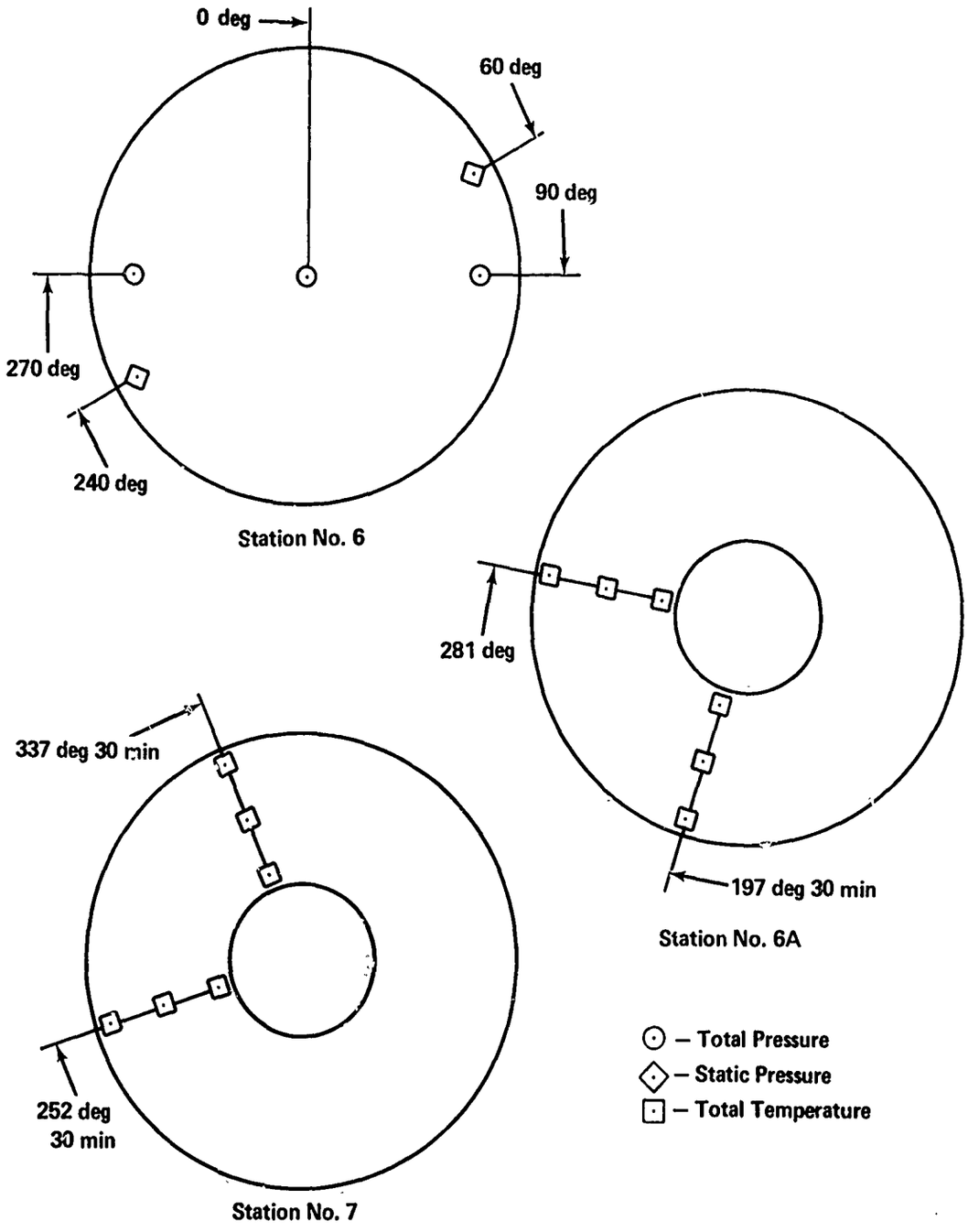

Figure 24. Circumferential Locations of Drive Turbine Instrumentation.

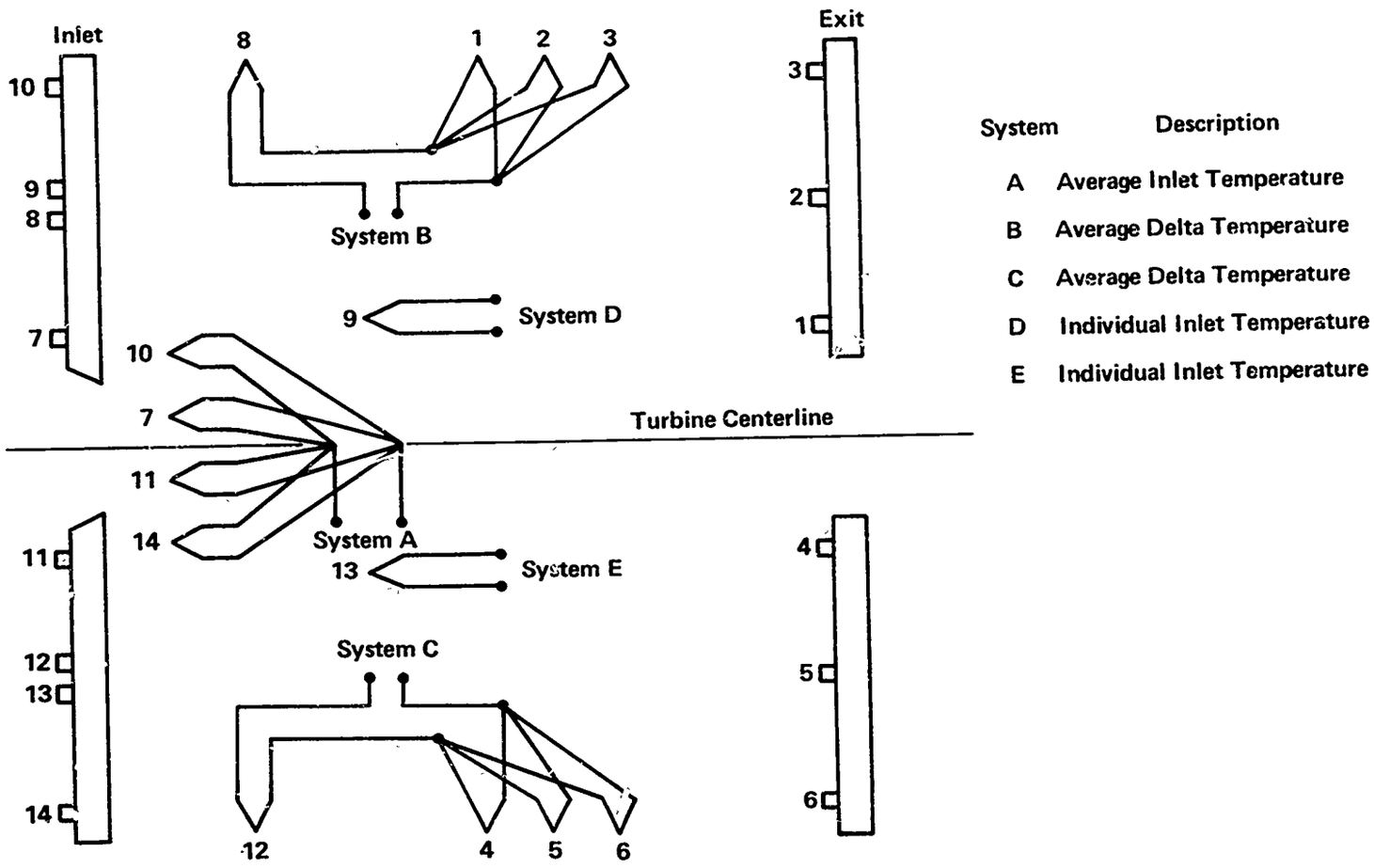

Figure 25. Drive Turbine Thermocouple Circuits.

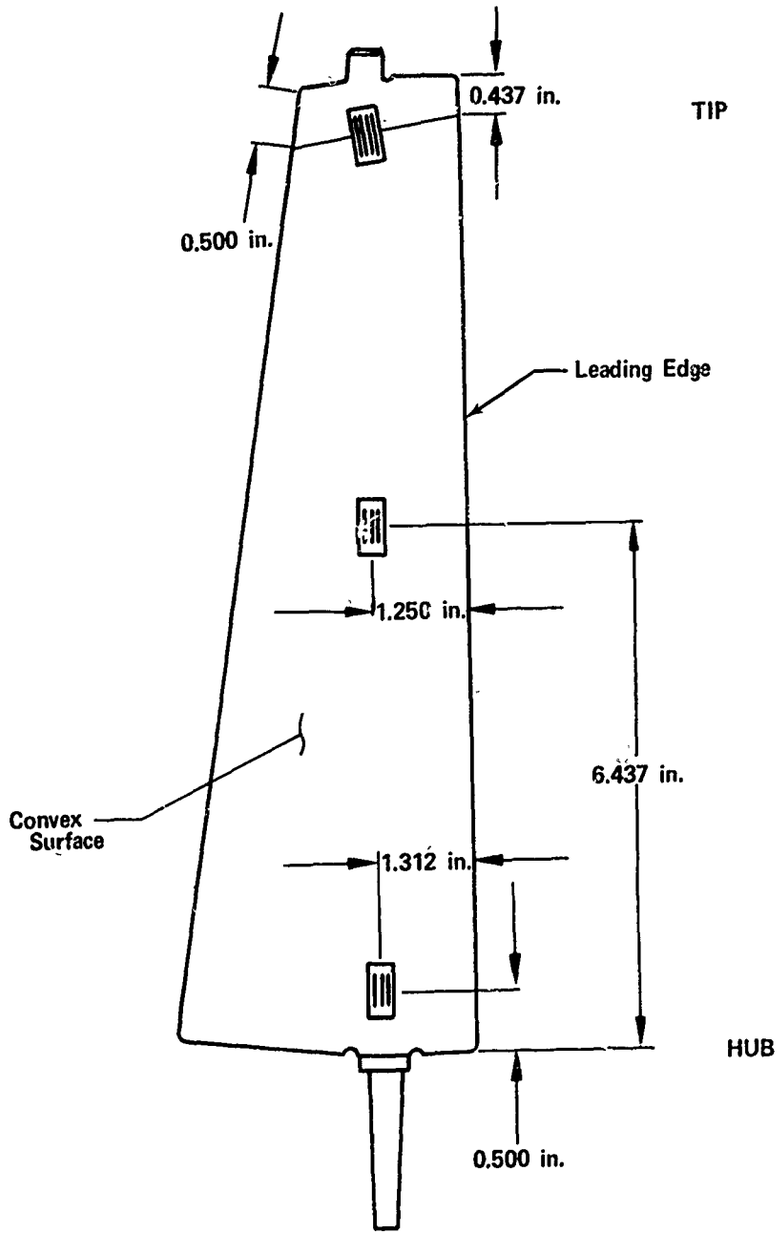

Figure 26. Inlet Guide Vane Strain Gage Locations.

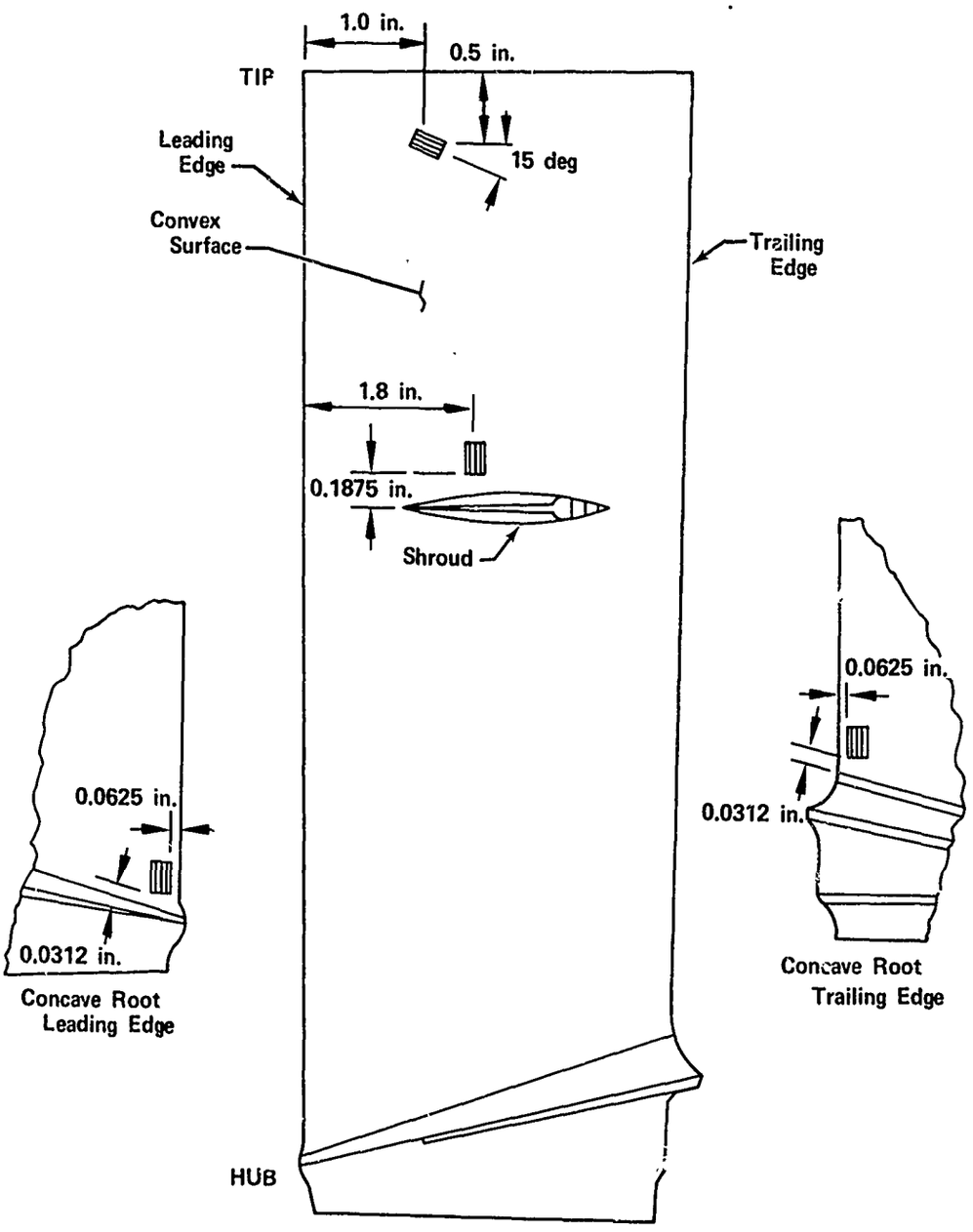

Figure 27. Rotor Blade Strain Gage Locations.

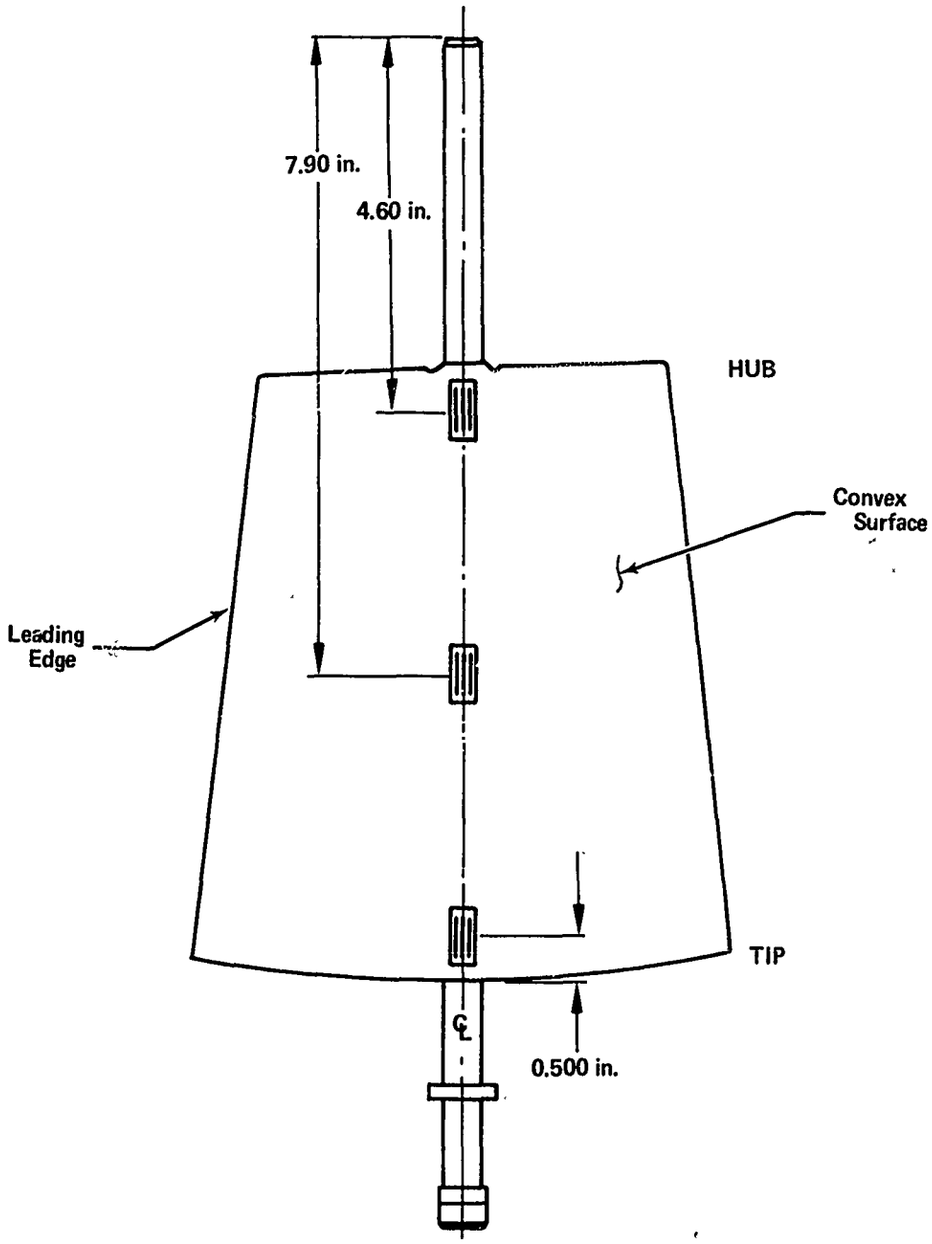

Figure 28. Duct Exit Guide Vane Strain Gage Locations.

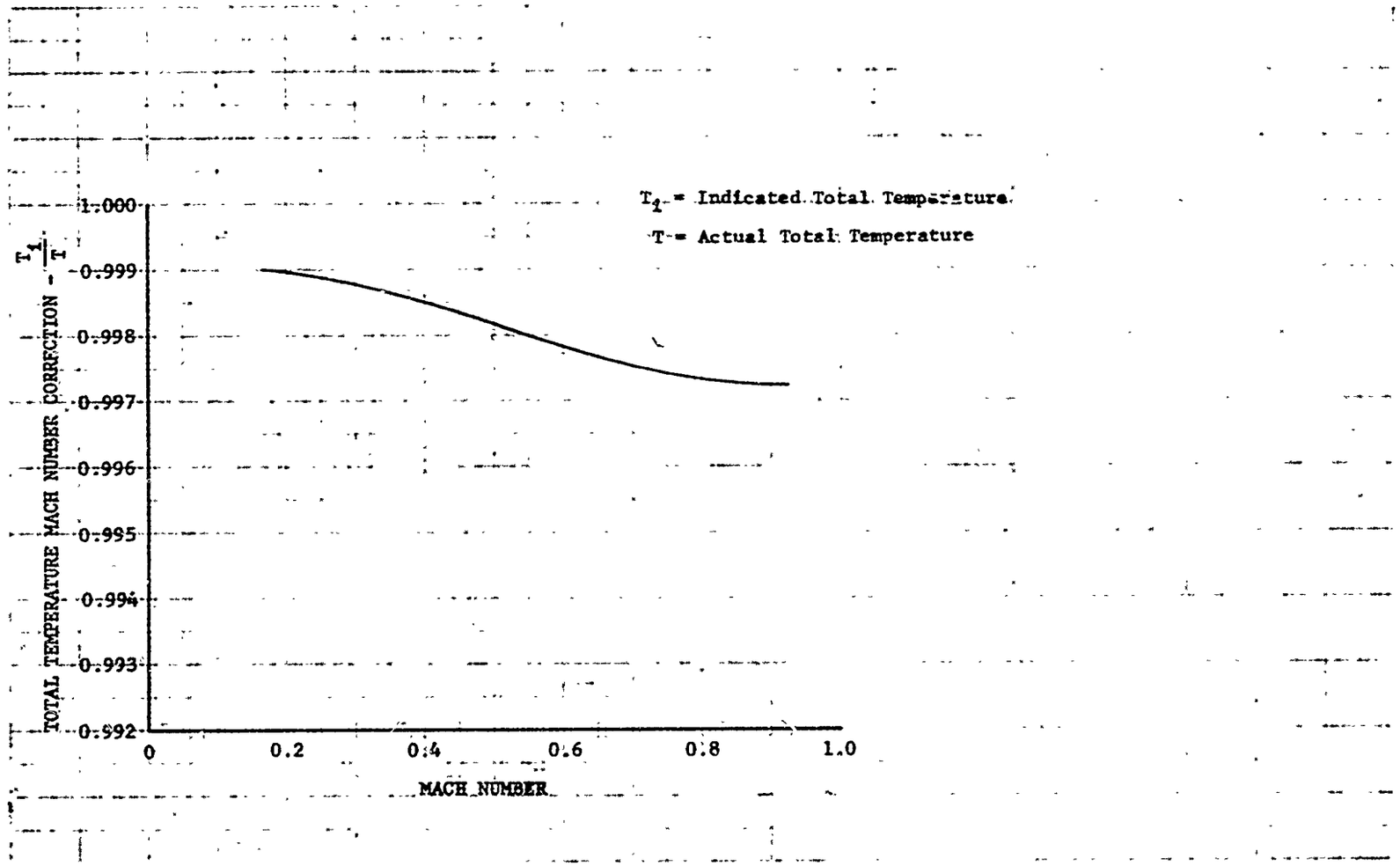

Figure 29. Total Temperature Probe Calibration Curve.

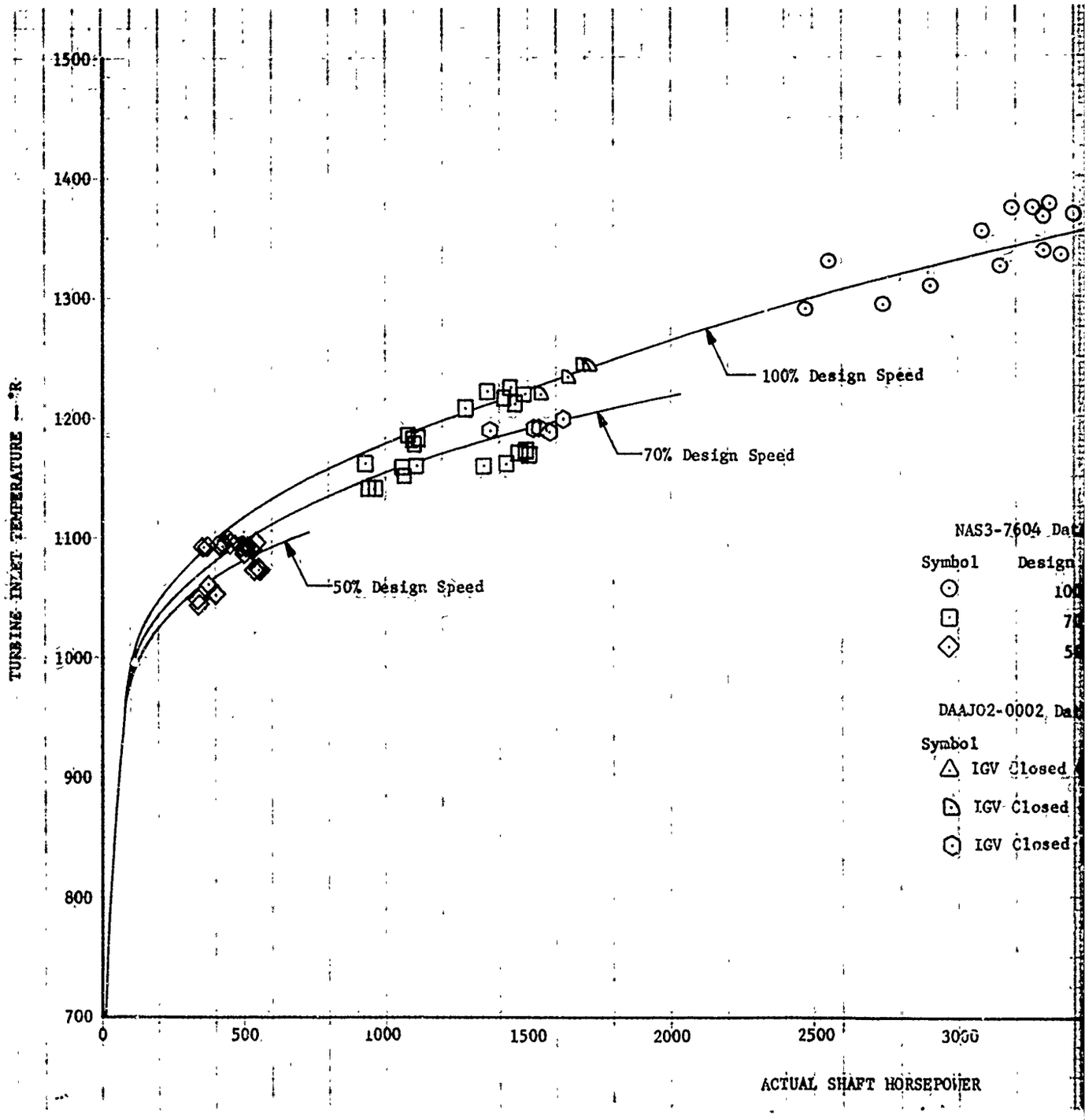

Figure 30. Shaft Horsepower - Drive Turbine Inlet Temperature Correlation.

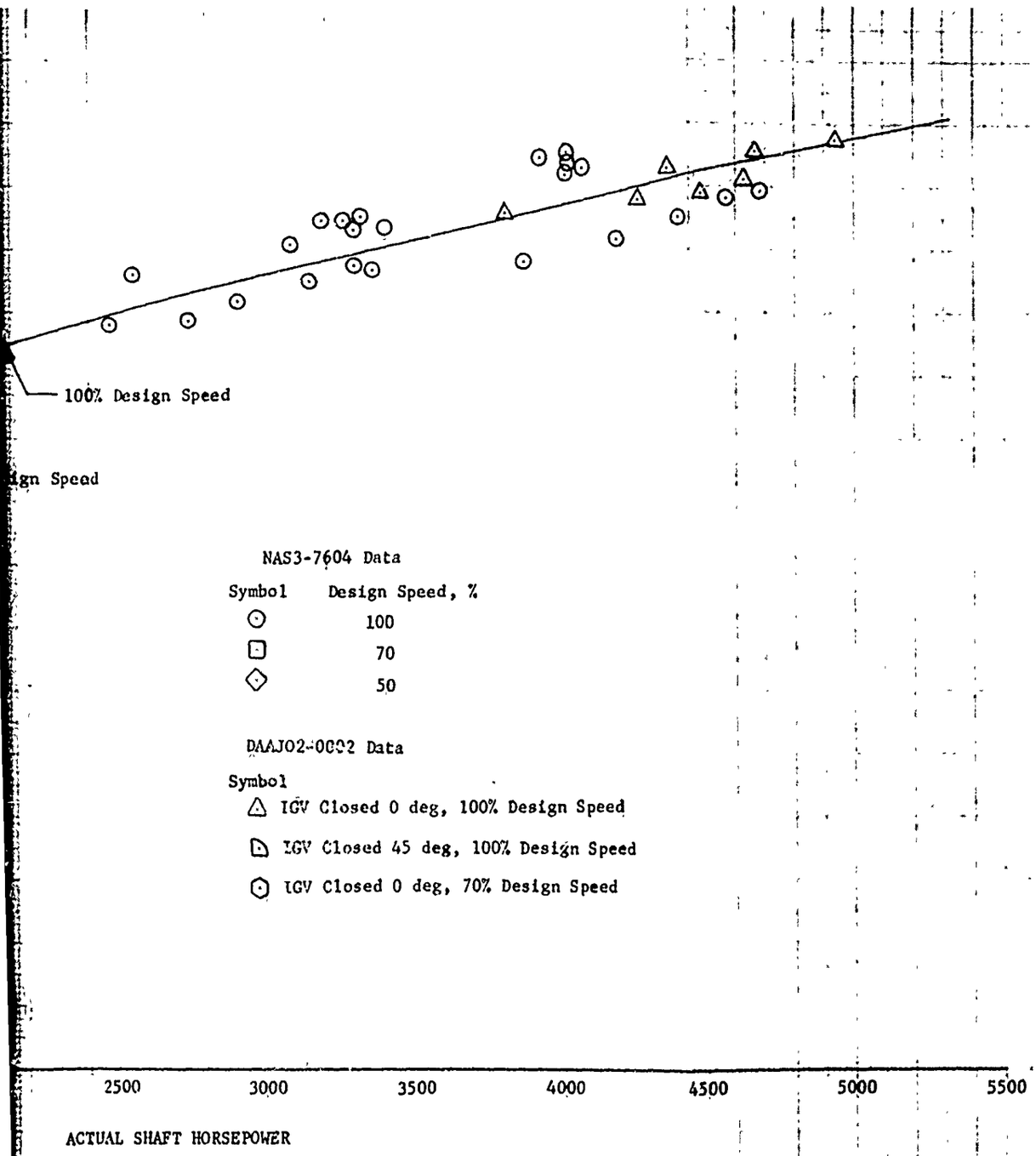
100% Design Speed
ign Speed
NAS3-7604 Data
Symbol
Design Speed, %
100
70
50
DAAJ02-0002 Data
Symbol
IGV Closed 0 deg, 100% Design Speed
IGV Closed 45 deg, 100% Design Speed
IGV Closed 0 deg, 70% Design Speed
2500
3000
3500
4000
4500
5000
5500
ACTUAL SHAFT HORSEPOWER

B

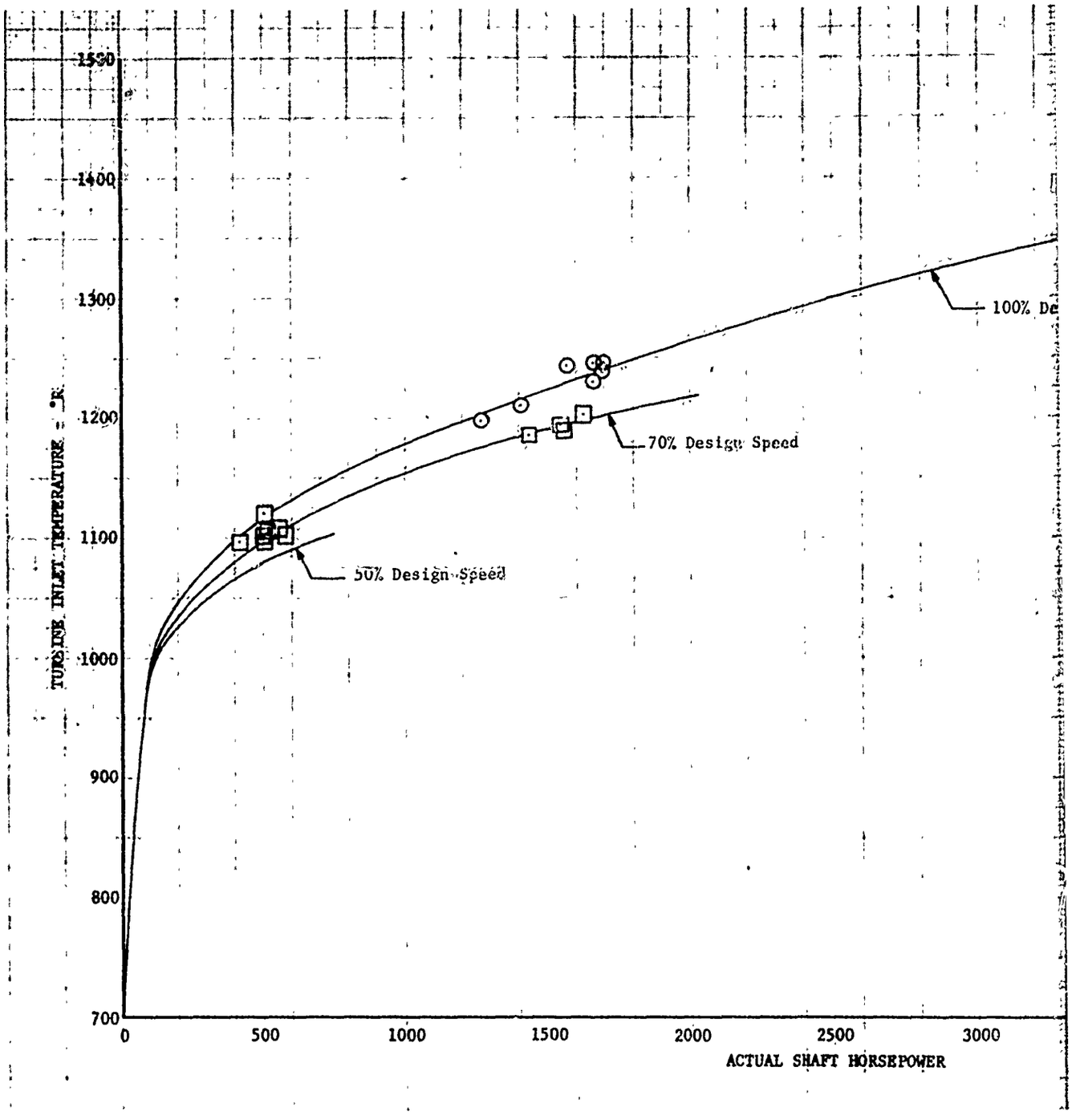

Figure 31. Comparison of Predicted Shaft Horsepower With Calculated Shaft Horsepower.

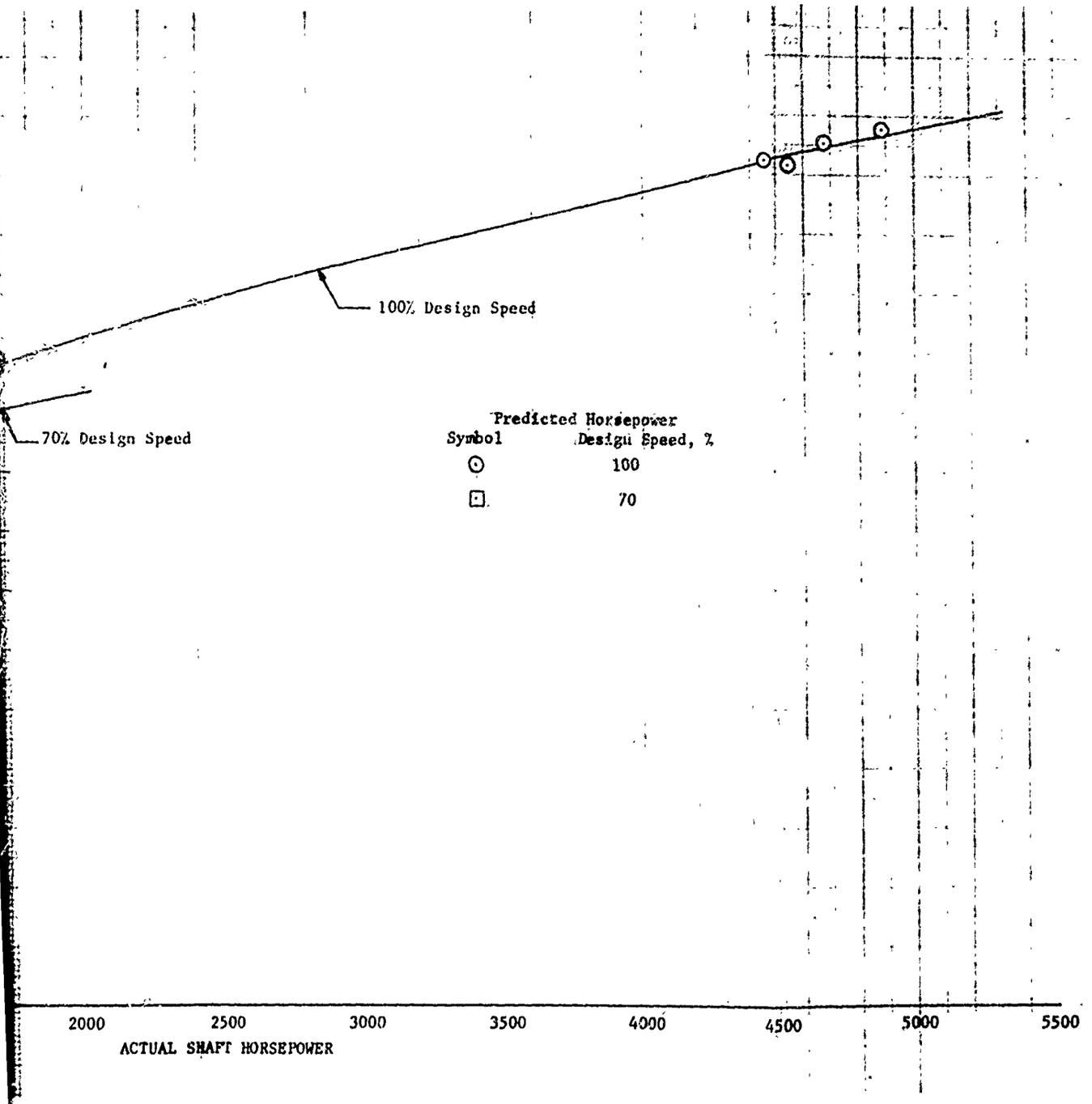

Horse-
rsepower.

B

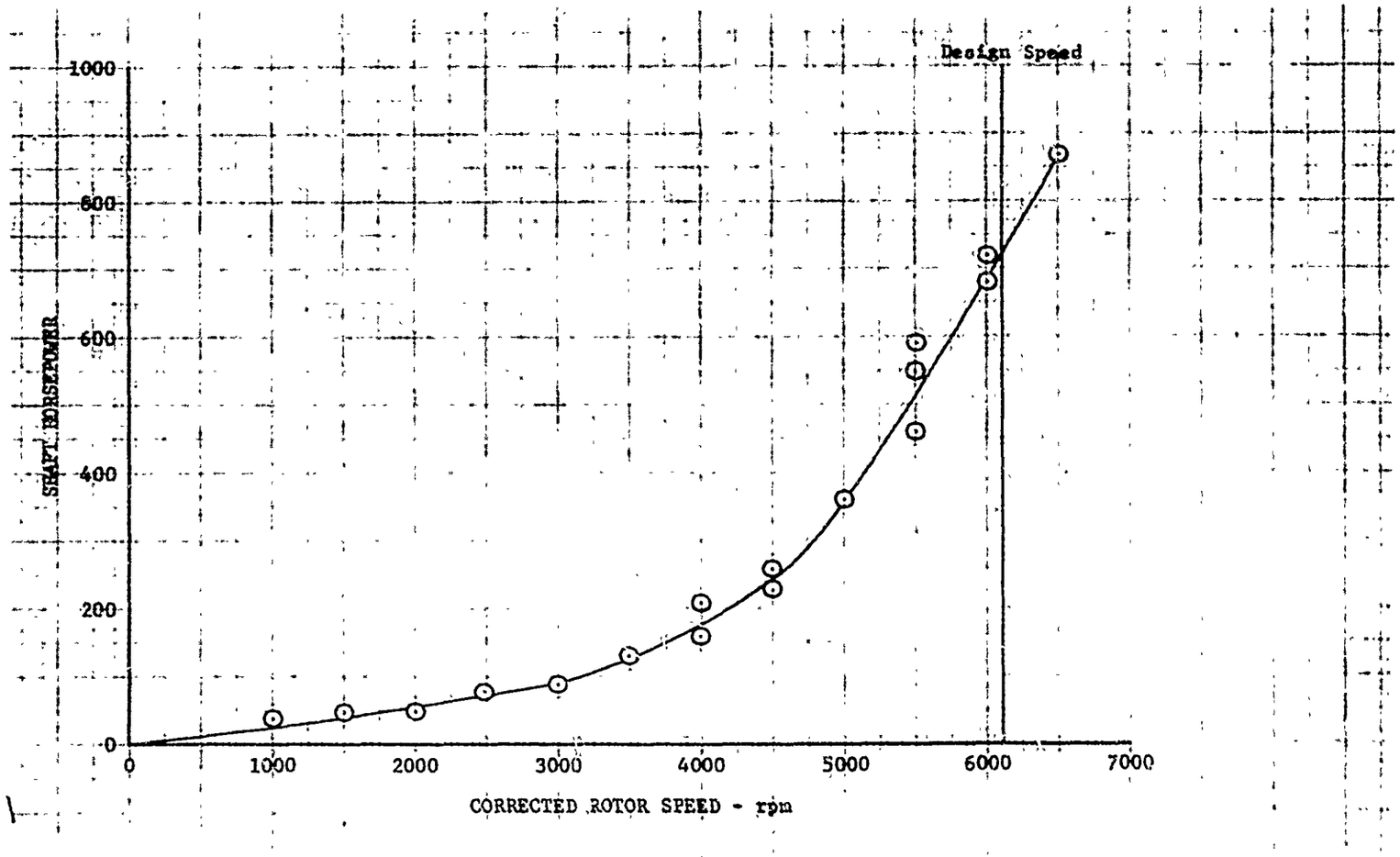

Figure 32. Shaft Horsepower vs Corrected Rotor Speed With Inlet and Exit Guide Vanes Fully Closed.

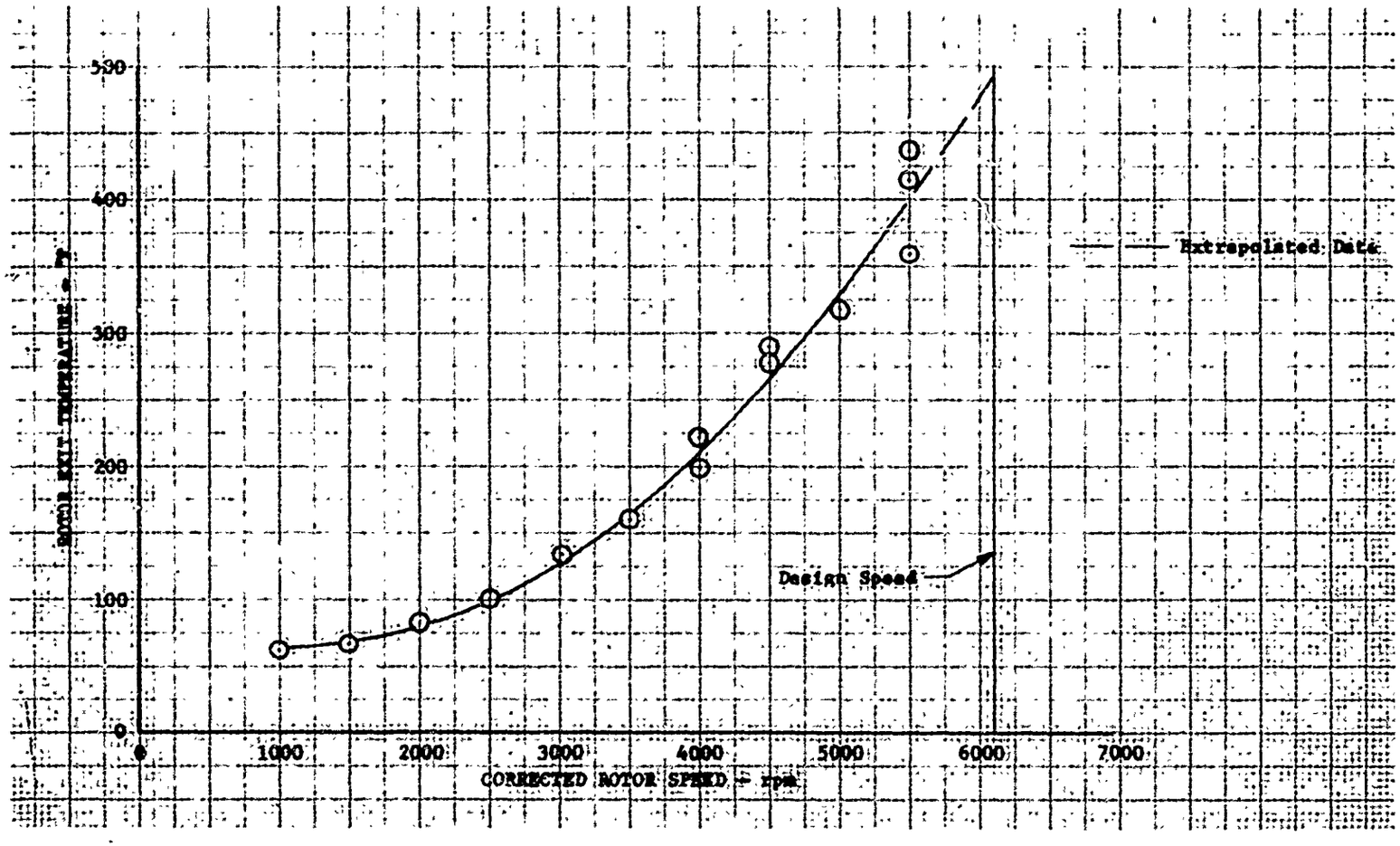

Figure 33. Rotor Exit Temperature vs Corrected Rotor Speed With Inlet and Exit Guide Vanes Fully Closed.

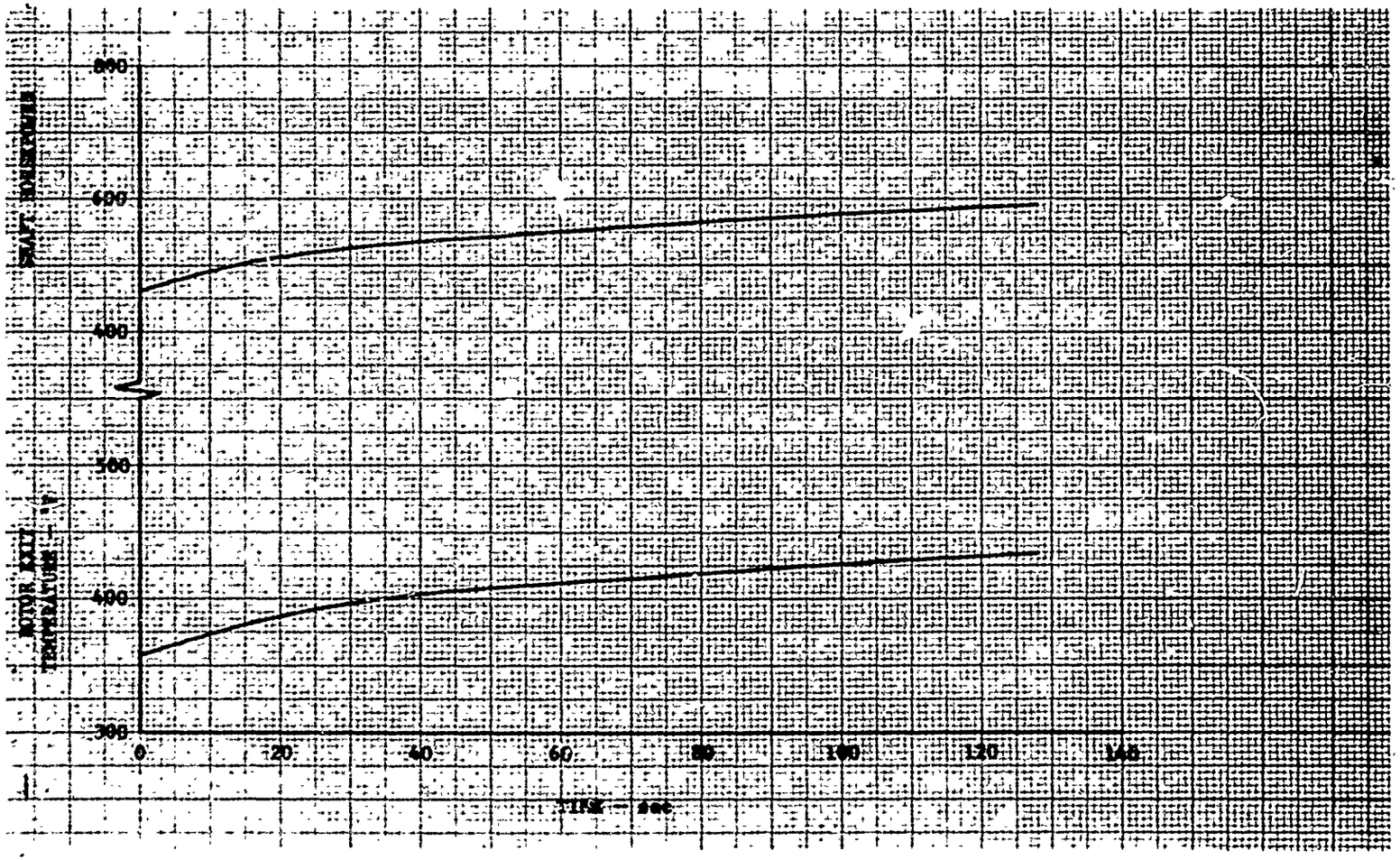

Figure 34. Increase of Shaft Horsepower and Rotor Exit Temperature With Time; Inlet and Exit Guide Vanes Fully Closed; 90-Percent Design Rotor Speed.

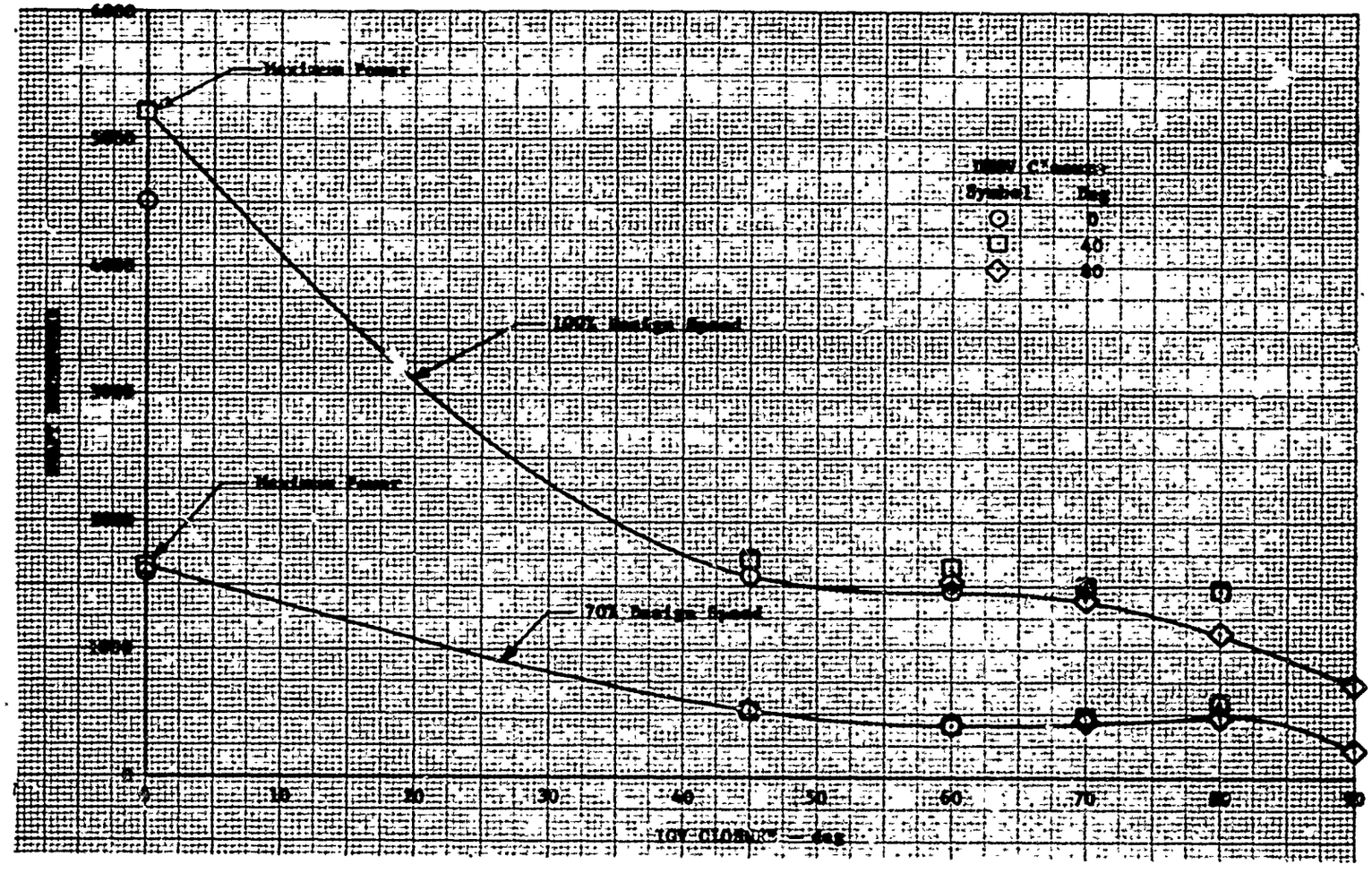

Figure 35. Effect of Guide Vane Position on Shaft Horsepower.

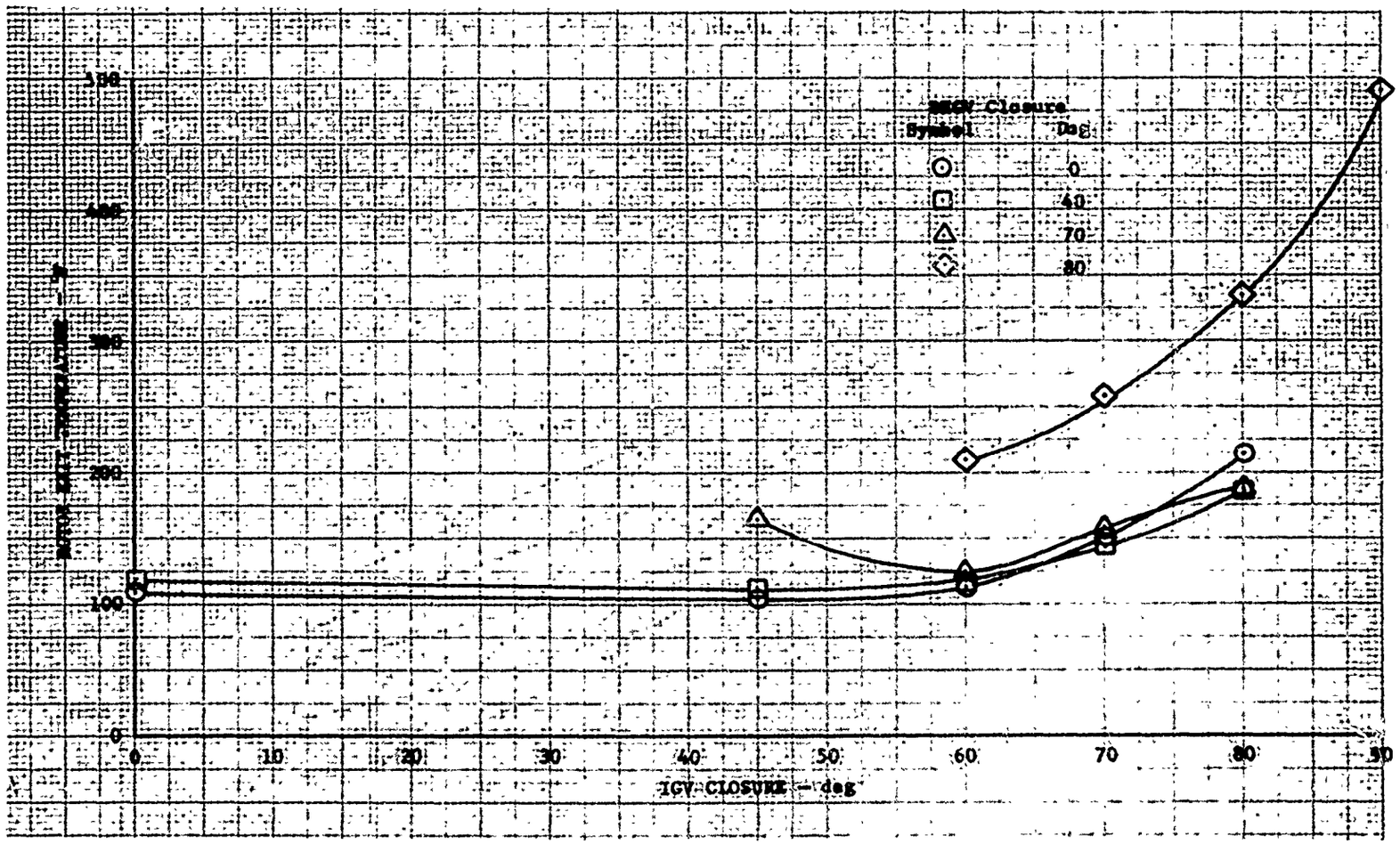

Figure 36. Effect of Guide Vane Position on Rotor Exit Temperature; Design Rotor Speed.

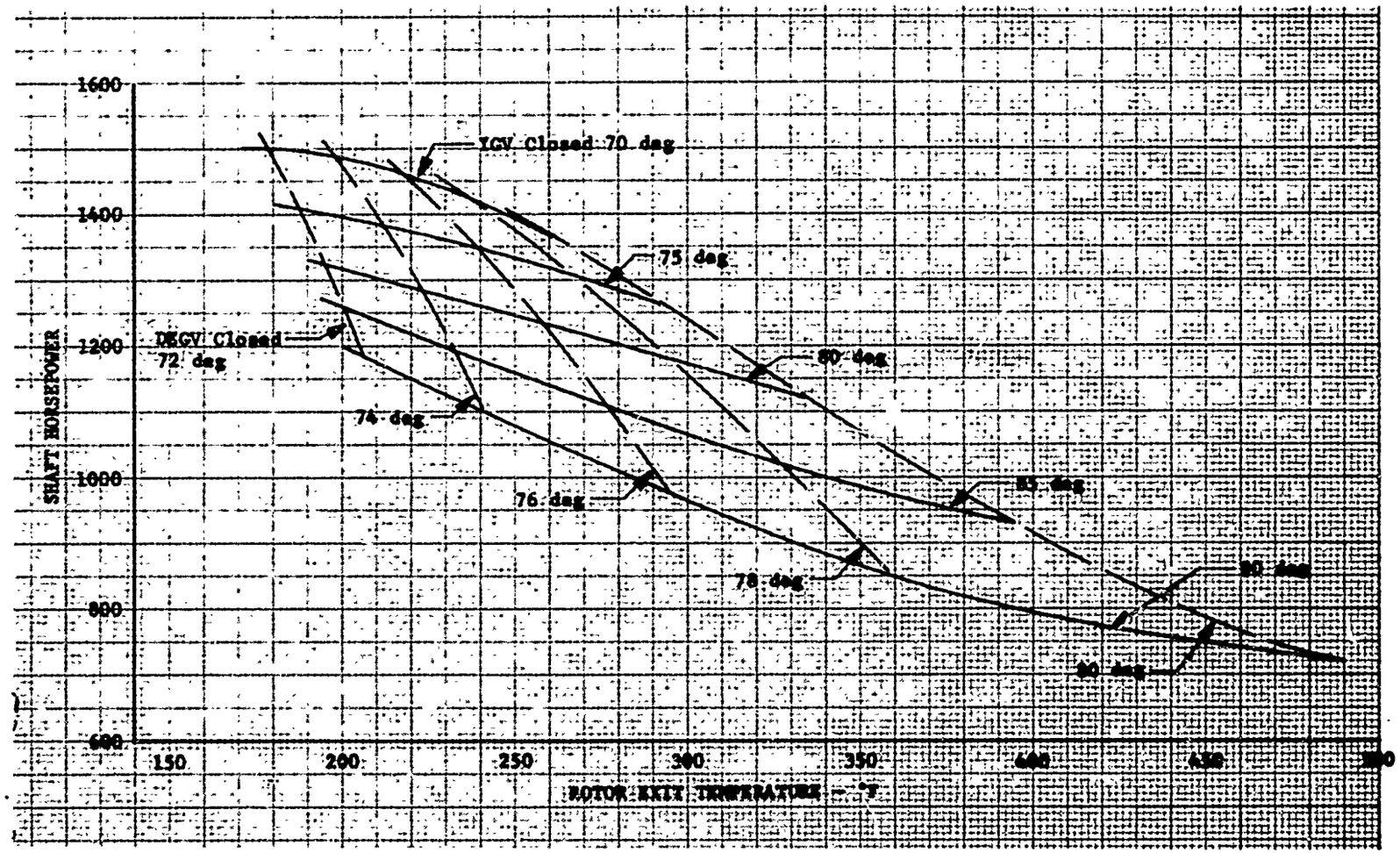

Figure 37. Shaft Horsepower vs Rotor Exit Temperature for High Guide Vane Closure Angles; Design Rotor Speed.

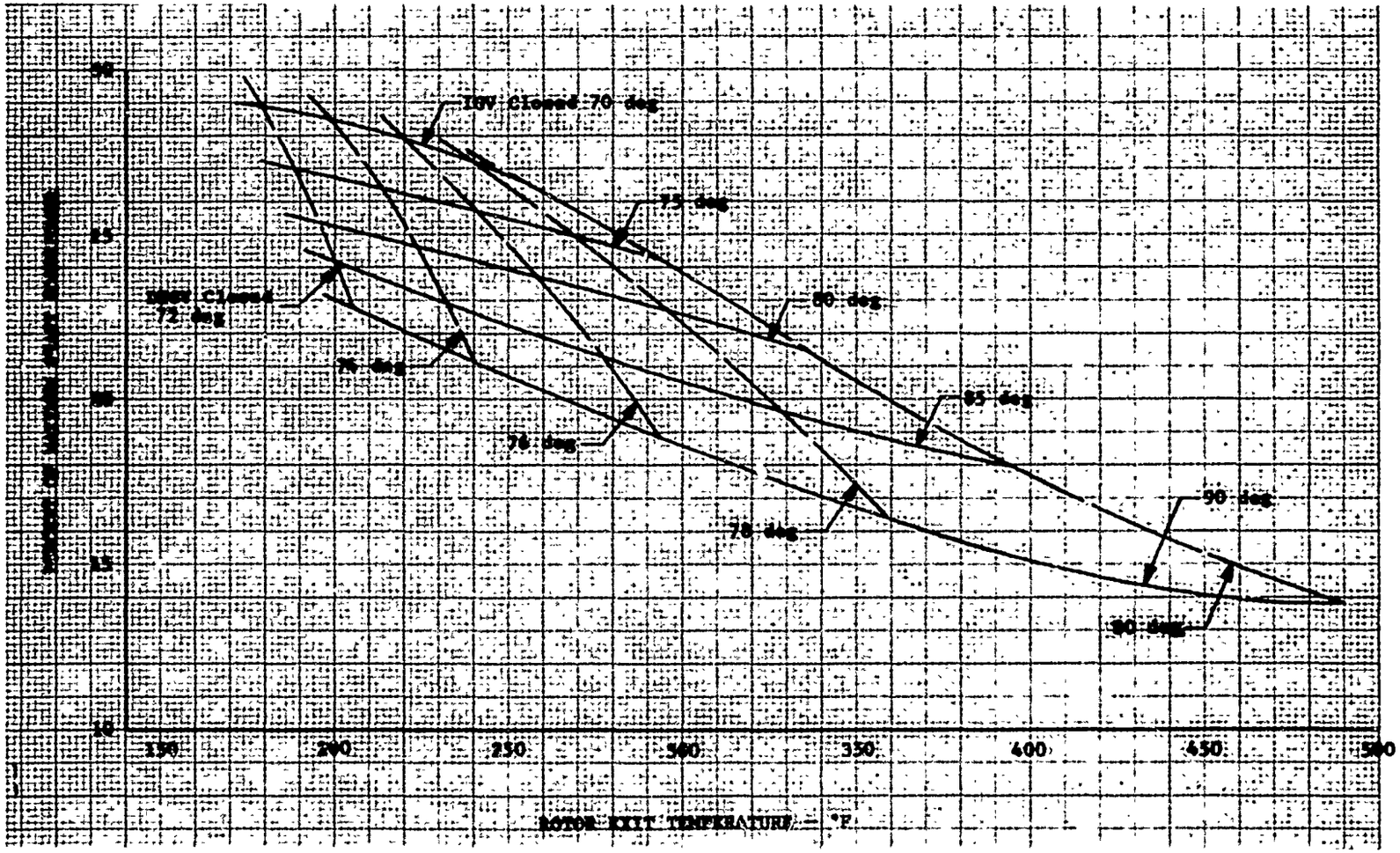

Figure 38. Percent of Maximum Shaft Horsepower vs Rotor Exit Temperature for High Guide Vane Closure Angles; Design Rotor Speed.

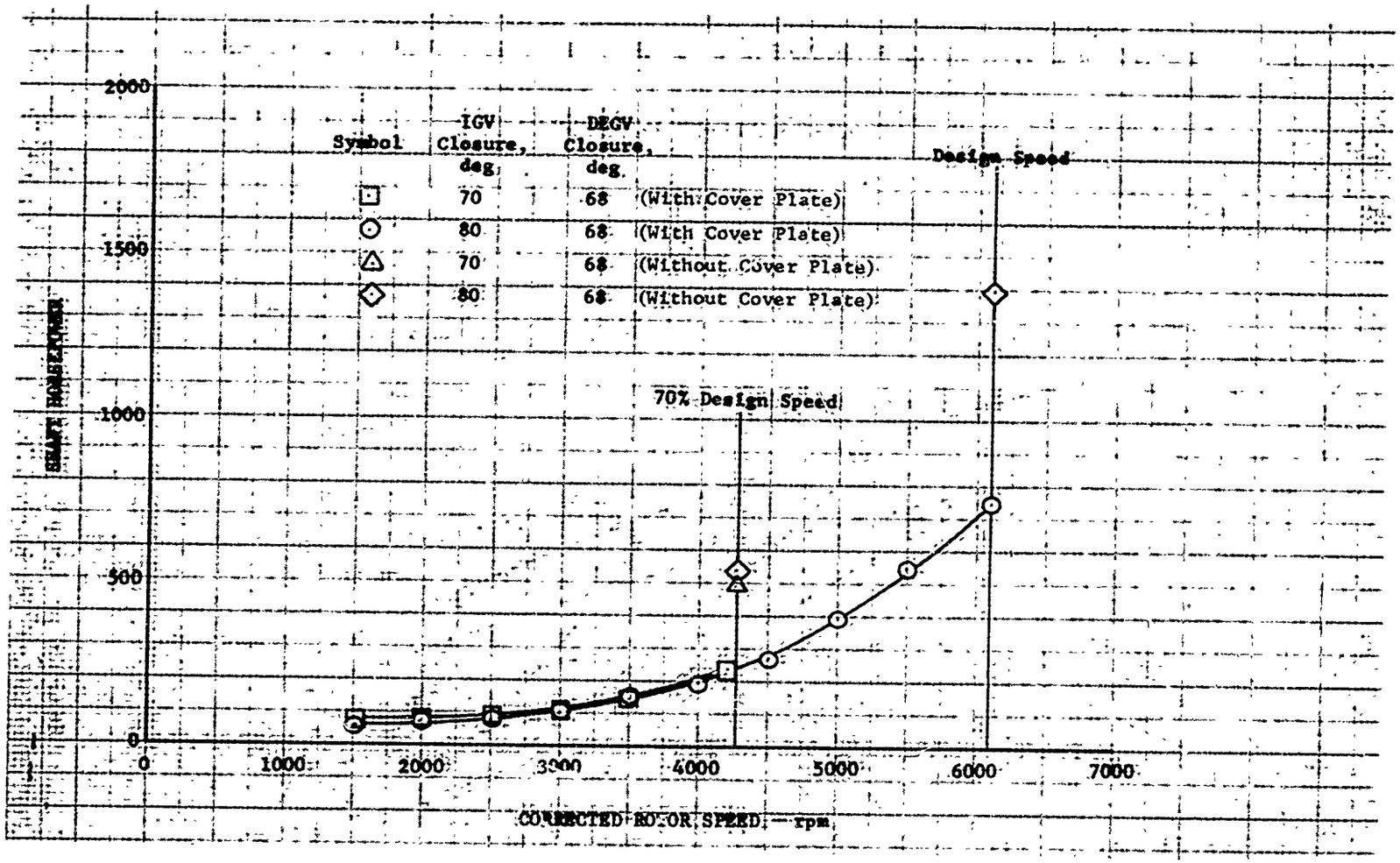

Figure 39. Shaft Horsepower vs Corrected Rotor Speed With Gas Generator Flowpath Cover Plate Installed.

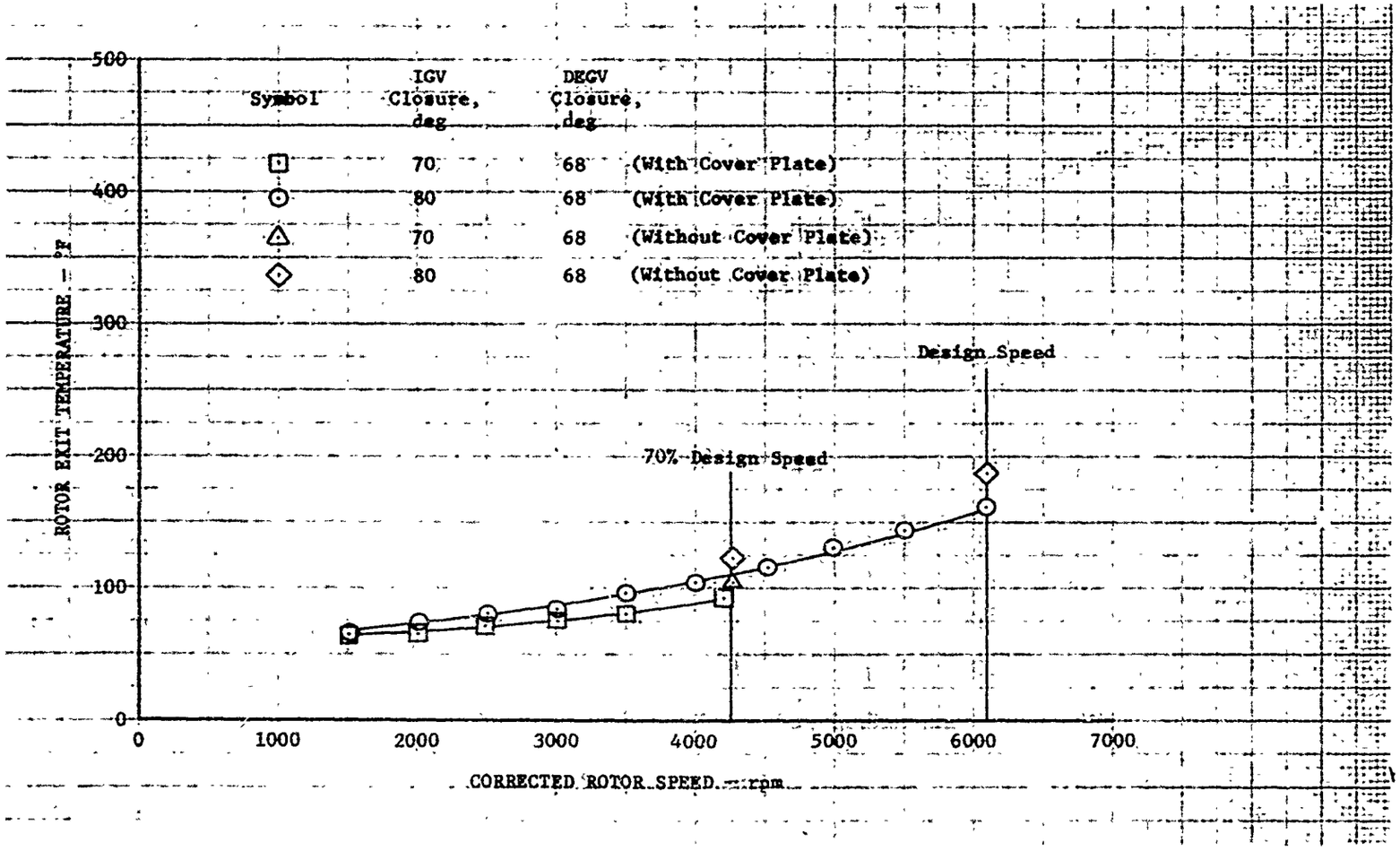

Figure 40. Rotor Exit Temperature vs Corrected Rotor Speed With Gas Generator Flowpath Cover Plate Installed.

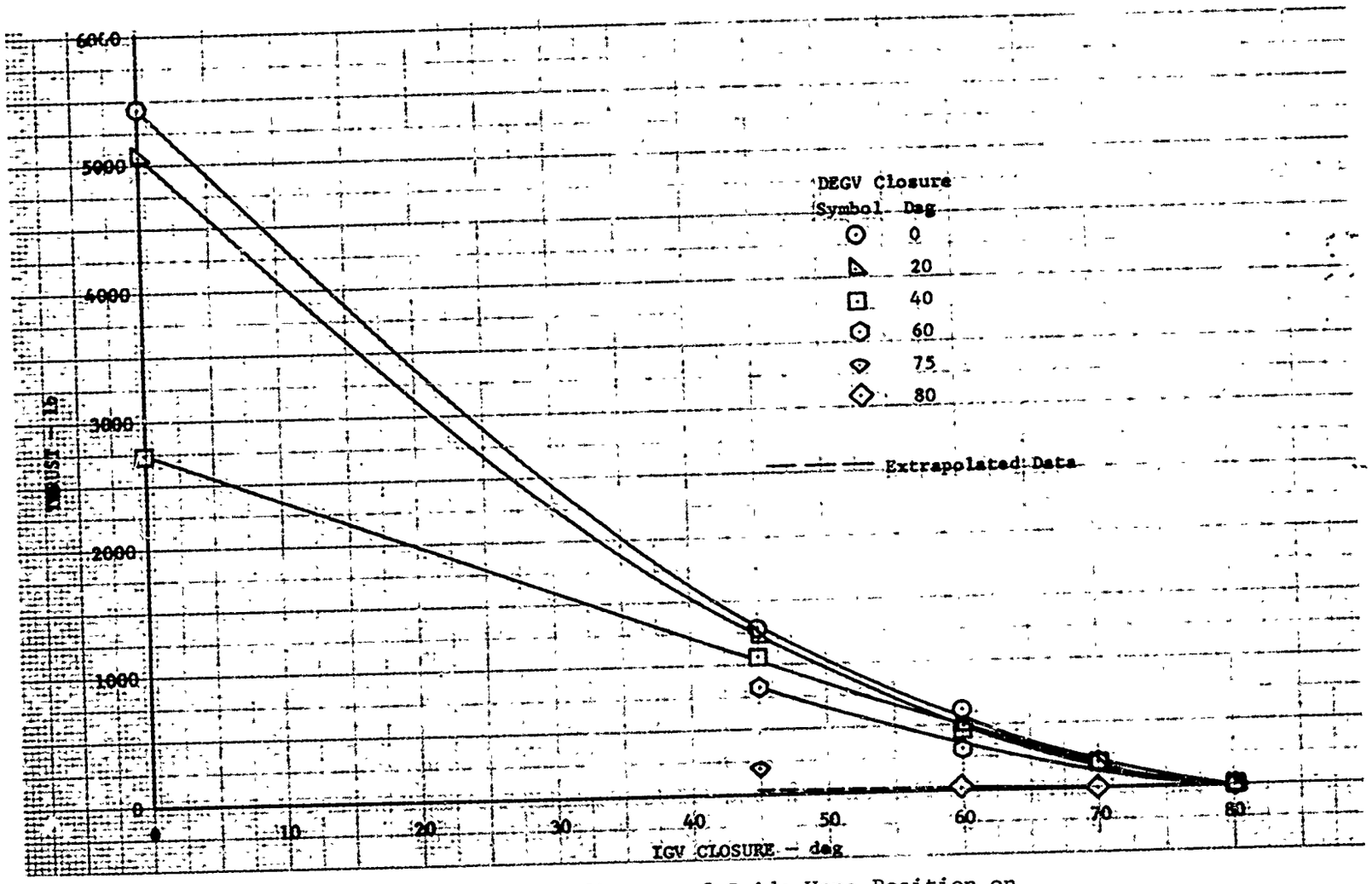

Figure 41. Influence of Guide Vane Position on Fan Thrust; Design Rotor Speed.

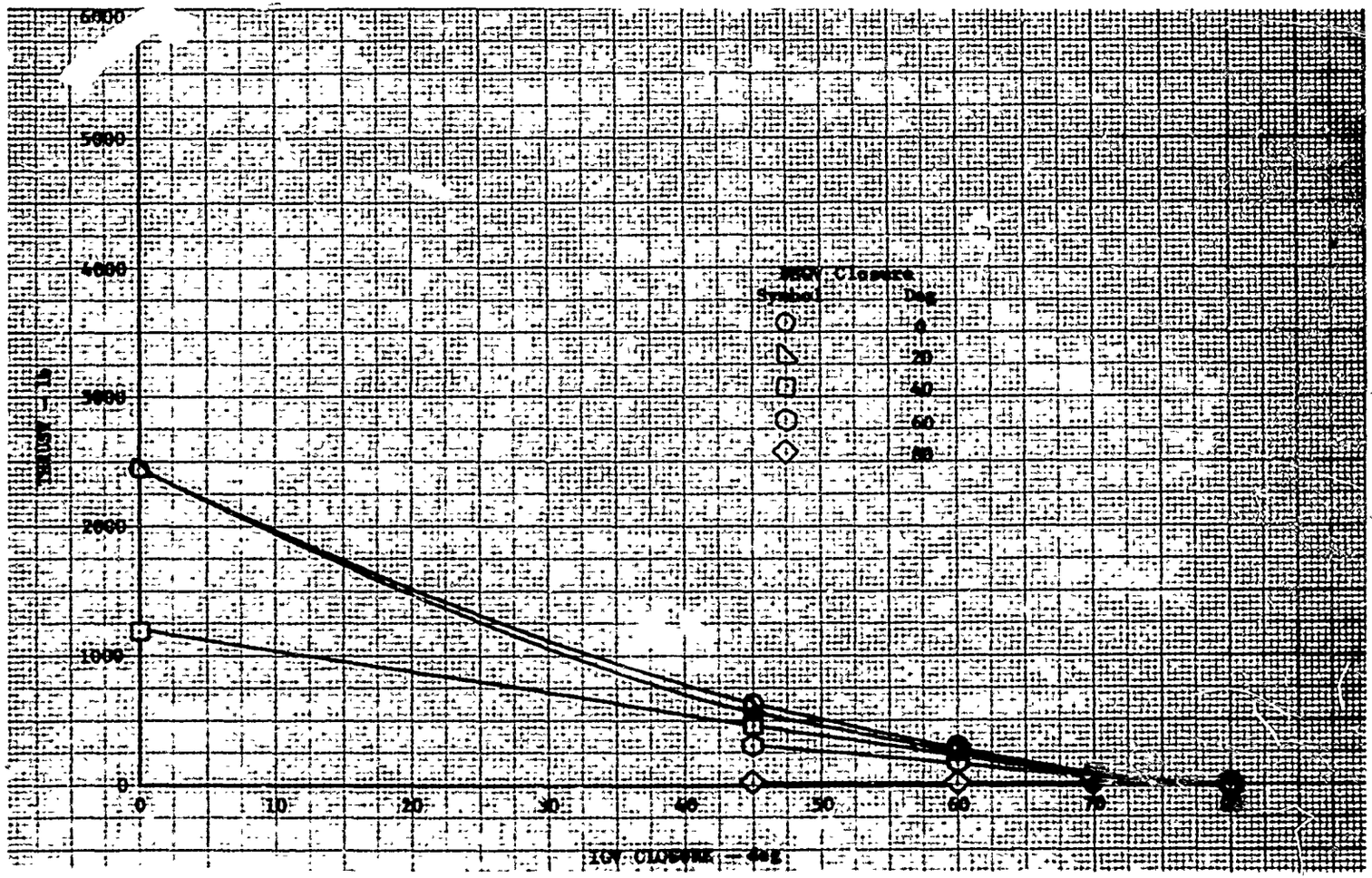

Figure 42. Influence of Guide Vane Position on Fan Thrust; 70-Percent Design Rotor Speed.

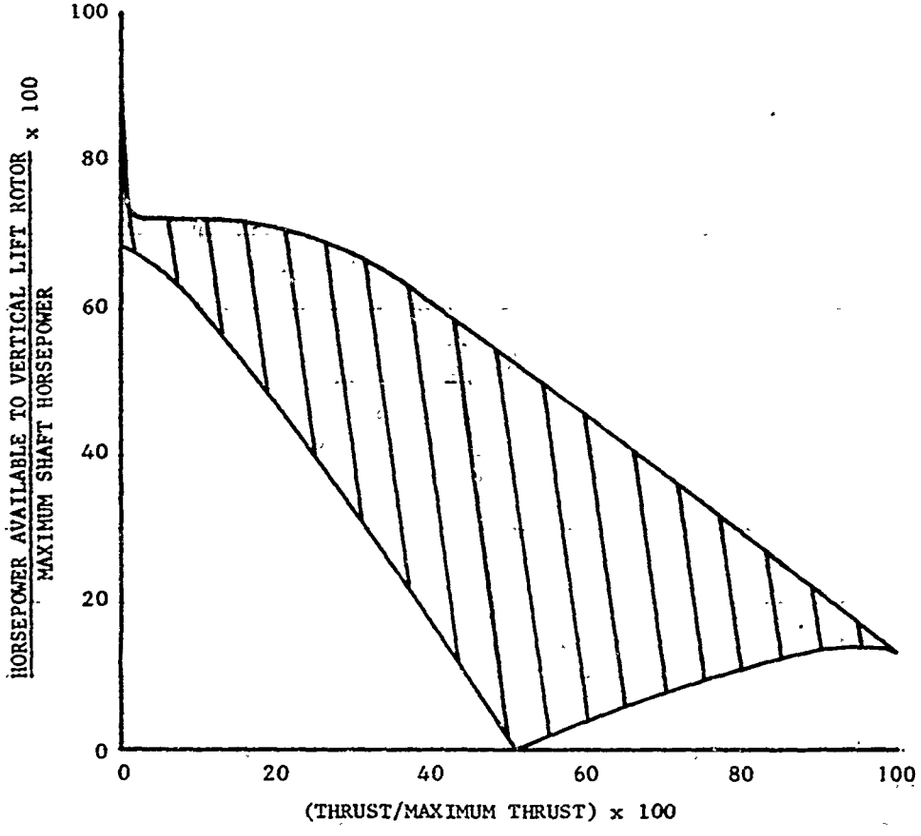

Figure 43. Operating Envelope of Available Shaft Horsepower and Thrust From Test Data.

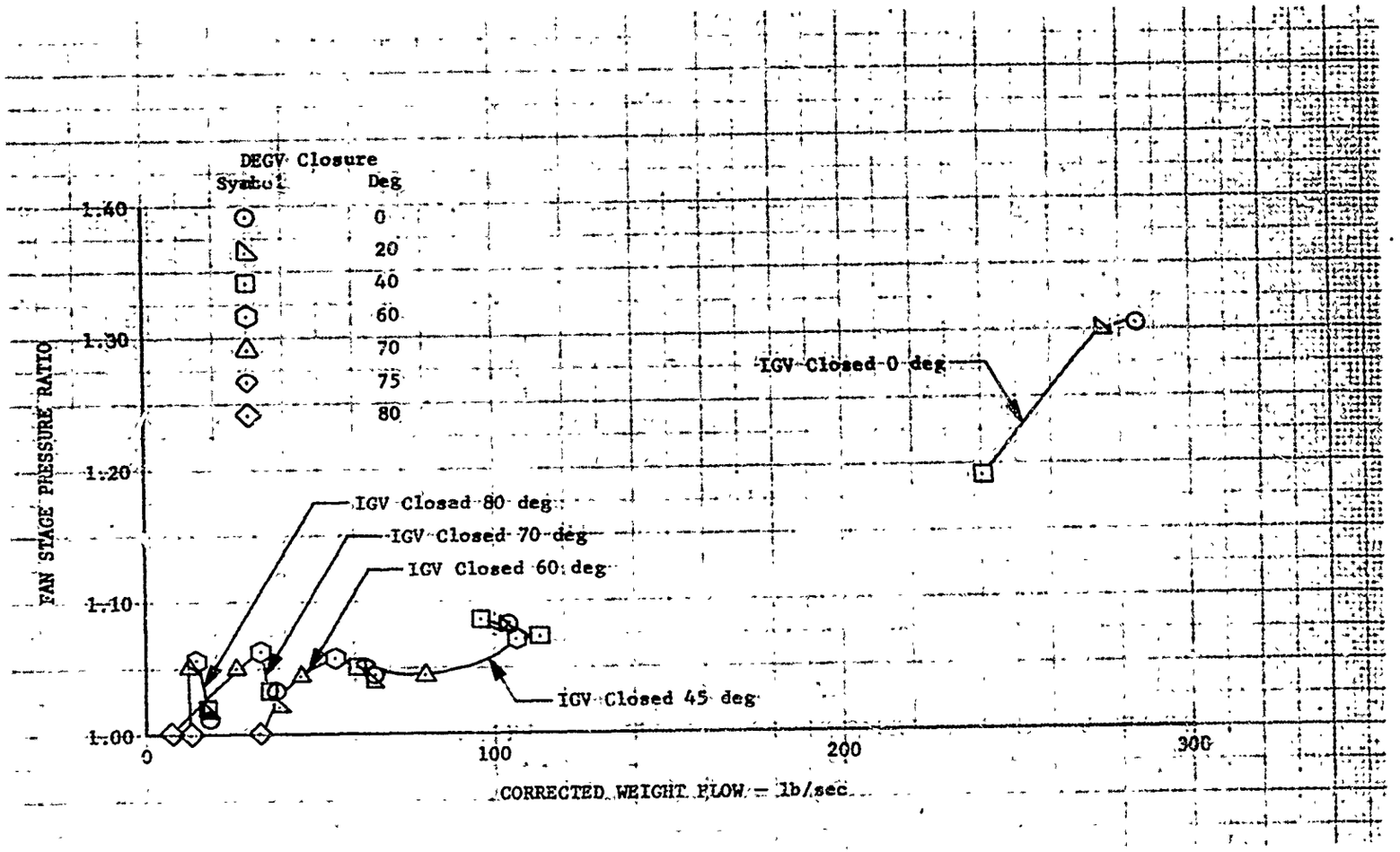

Figure 44. Fan Stage Pressure Ratio vs Corrected Weight Flow; Design Rotor Speed.

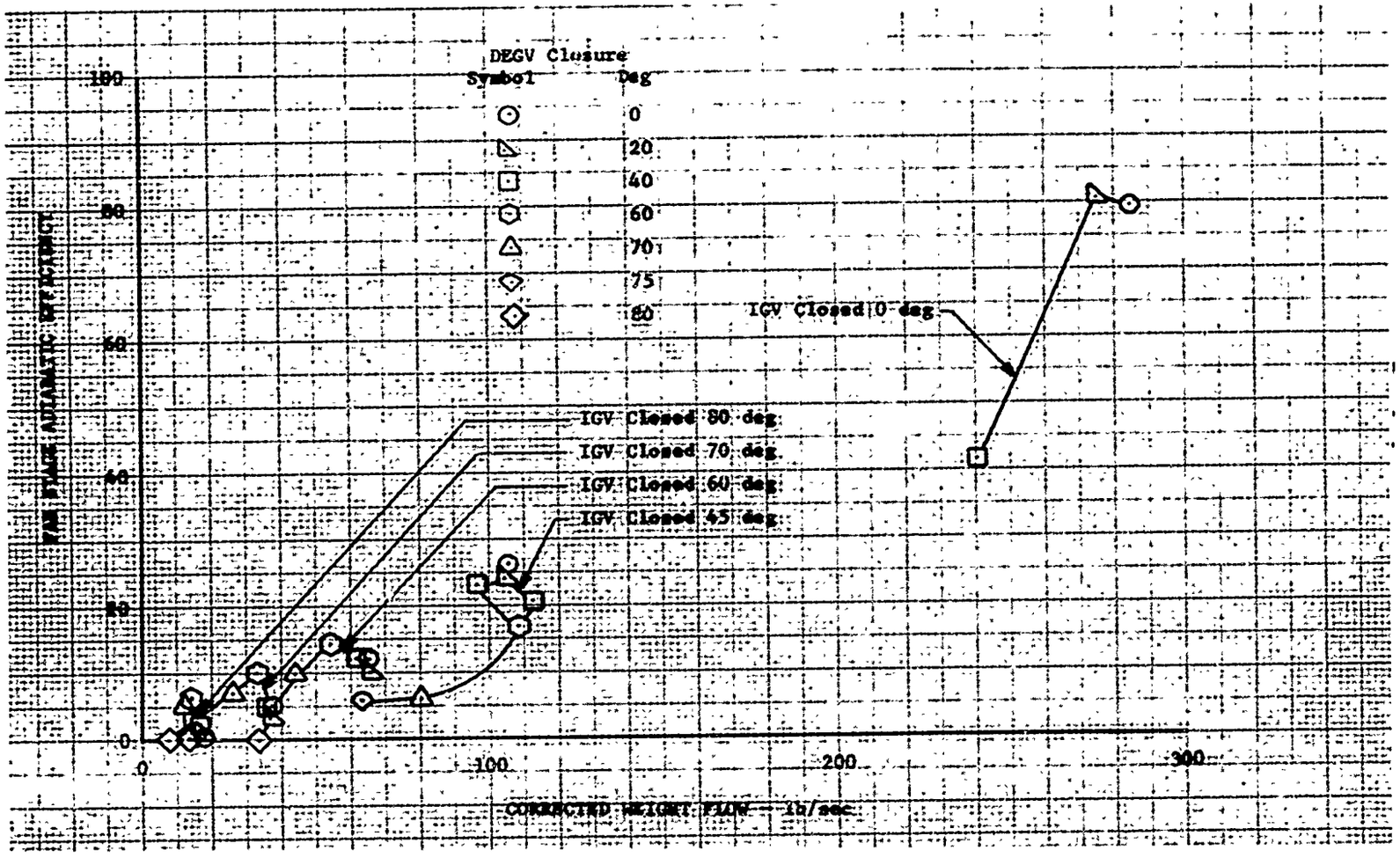

Figure 45. Fan Stage Adiabatic Efficiency vs Corrected Weight Flow; Design Rotor Speed.

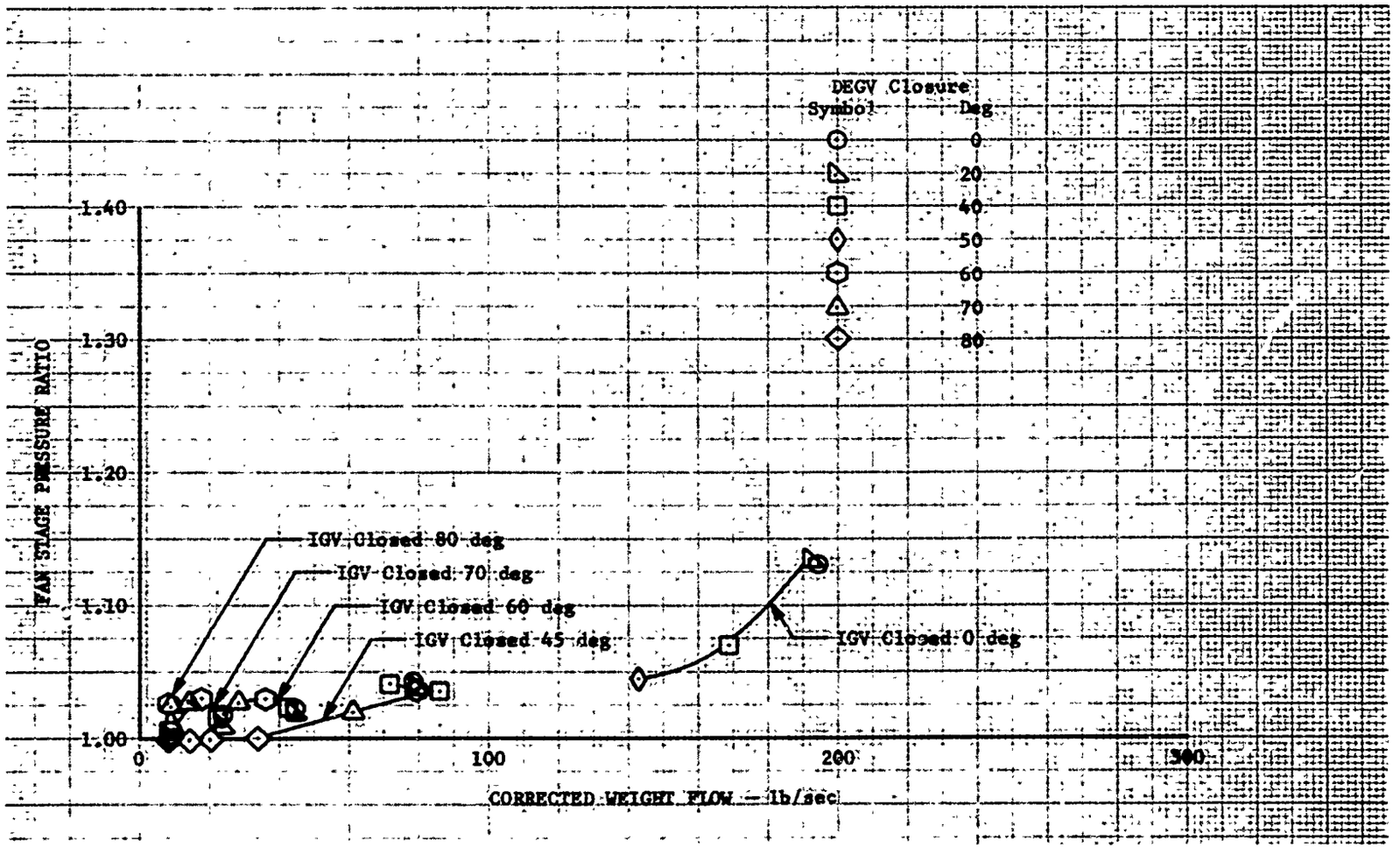

Figure 46. Fan Stage Pressure Ratio vs Corrected Weight Flow; 70-Percent Design Rotor Speed.

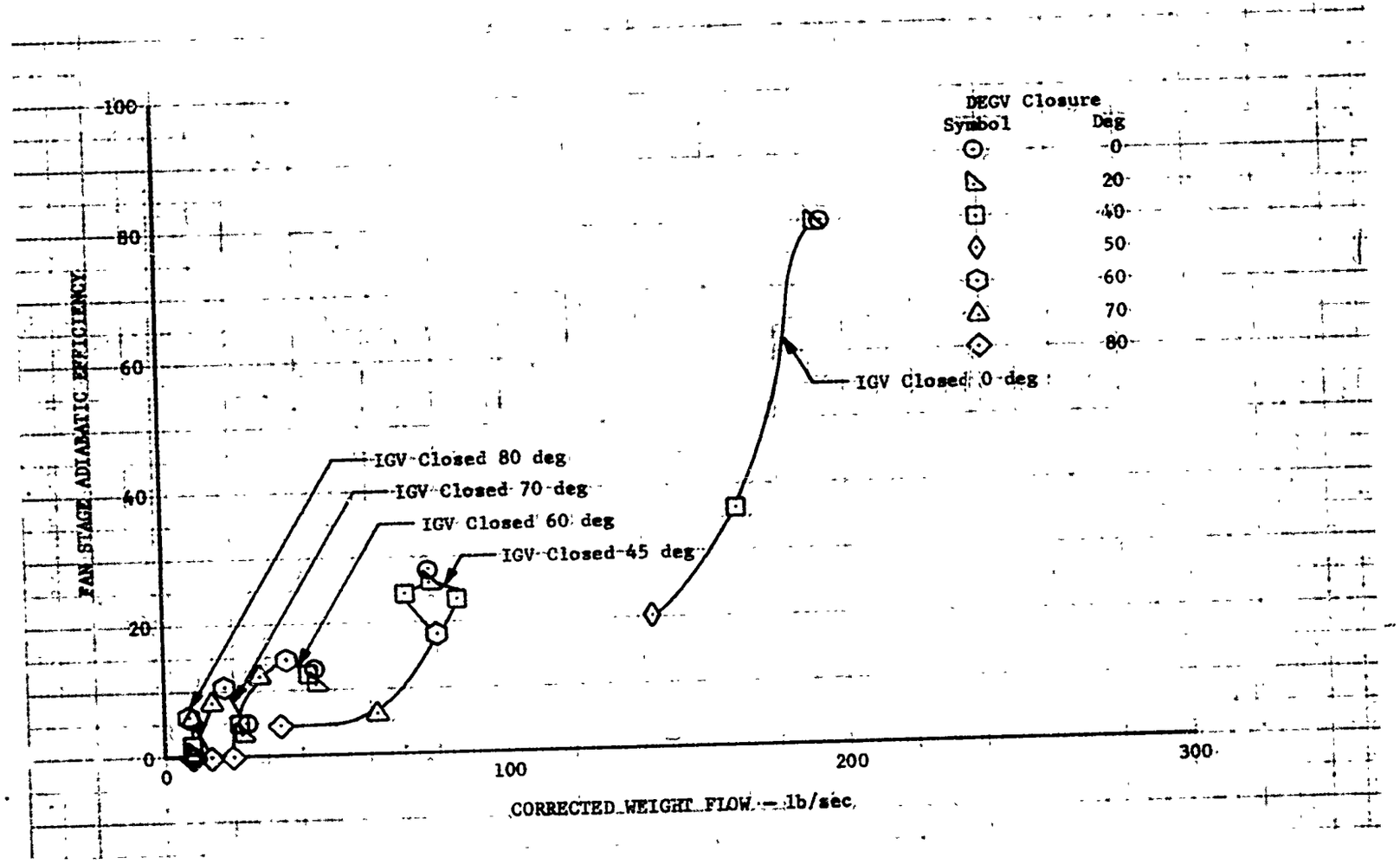

Figure 47. Fan Stage Adiabatic Efficiency vs Corrected Weight Flow; 70-Percent Design Rotor Speed.

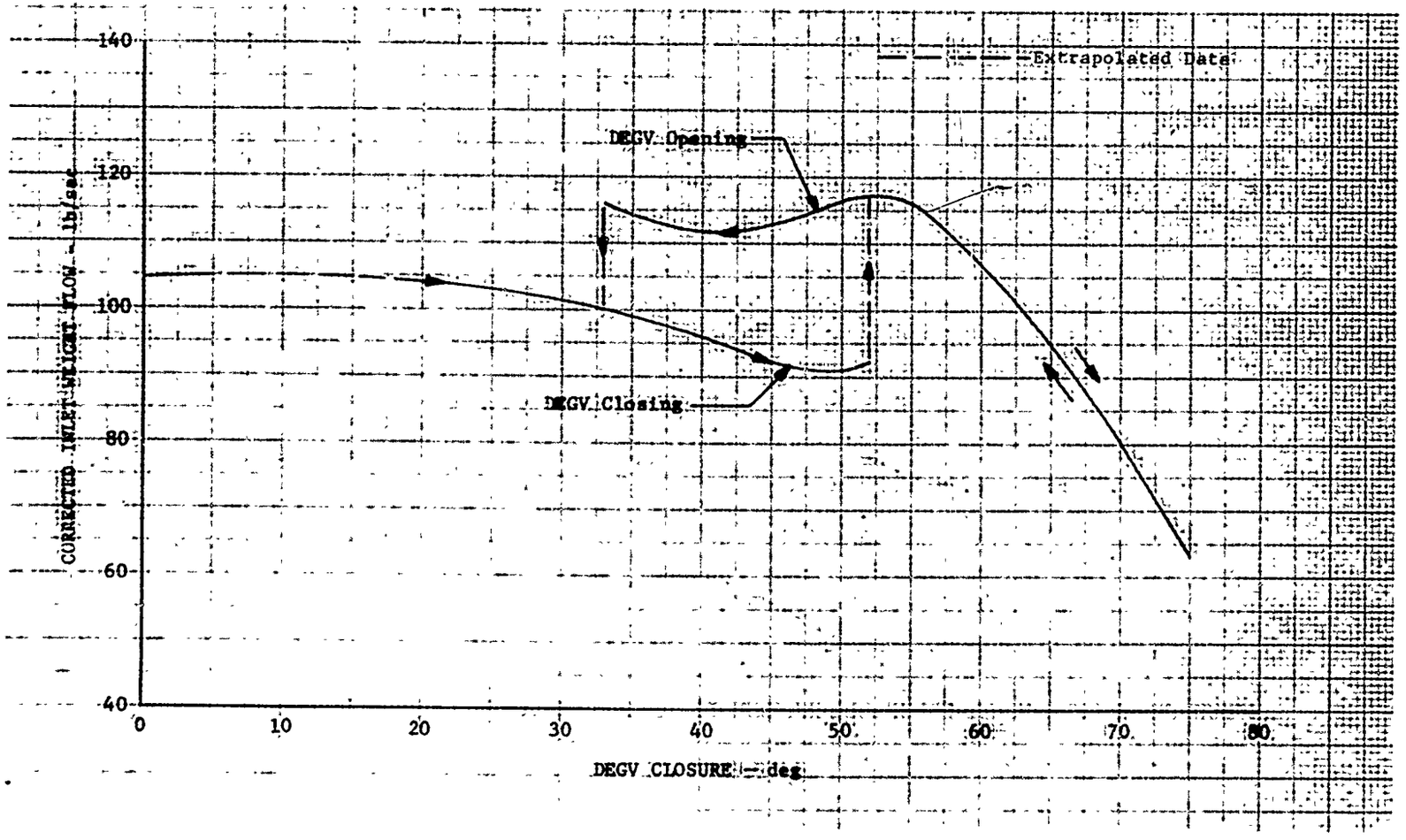

Figure 48. Weight Flow Discontinuity as a Function of Exit Guide Vane Closure Angle; Inlet Guide Vane Closed 45 Degrees; Design Rotor Speed.

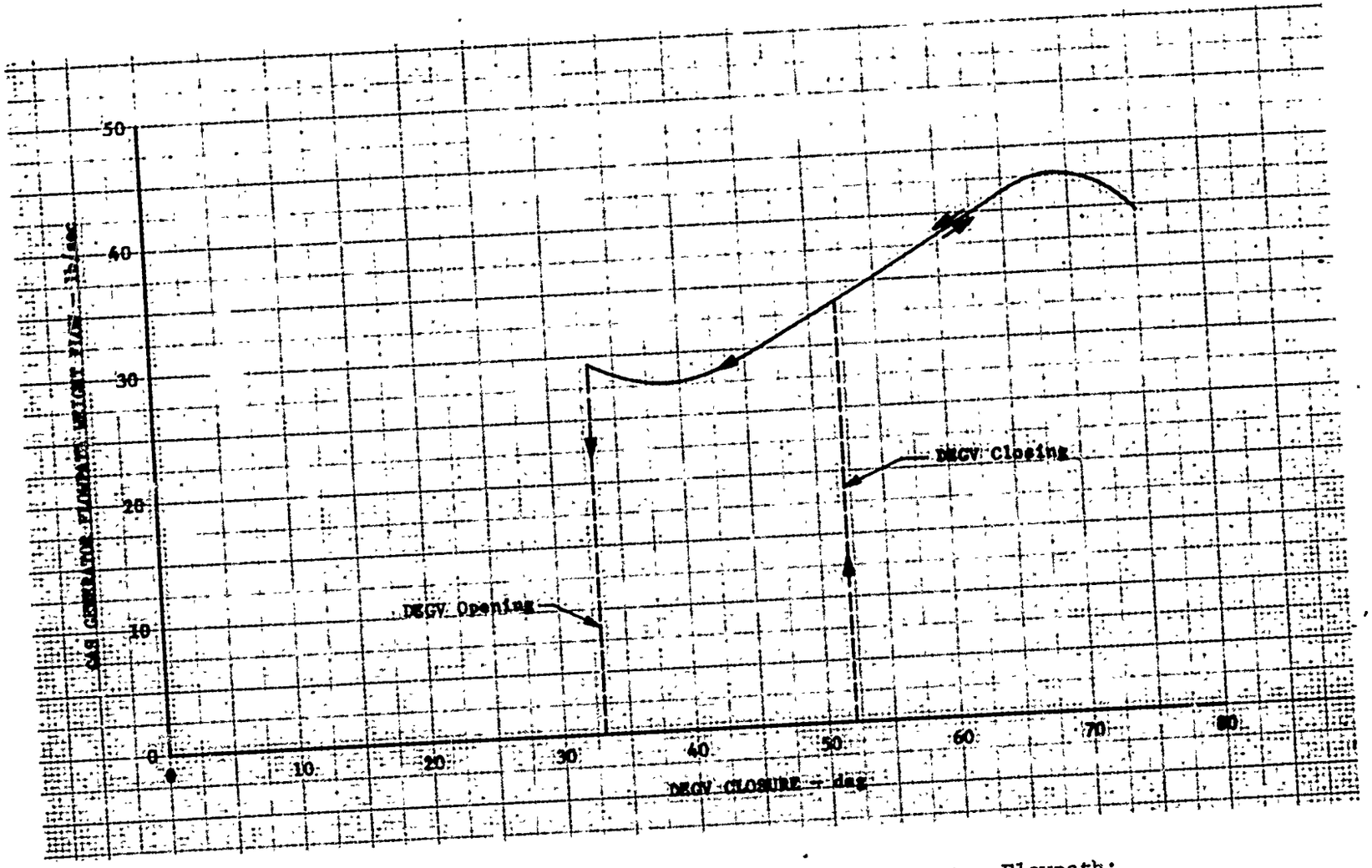

Figure 49. Weight Flow Discontinuities in Gas Generator Flowpath; Inlet Guide Vane Closed 45 Degrees; Design Rotor Speed.

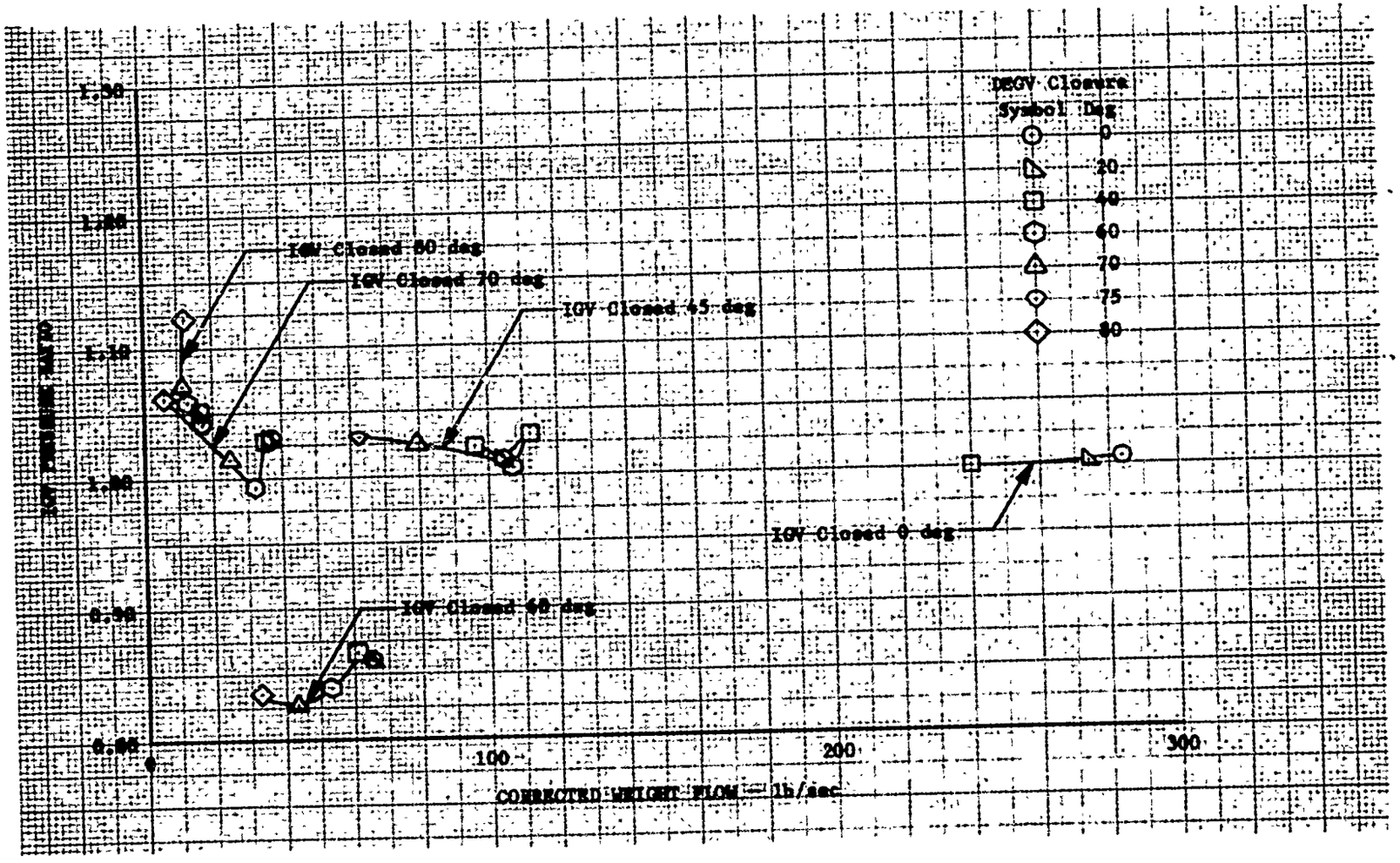

Figure 50. Inlet Guide Vane Pressure Ratio vs Corrected Weight Flow; Design Rotor Speed.

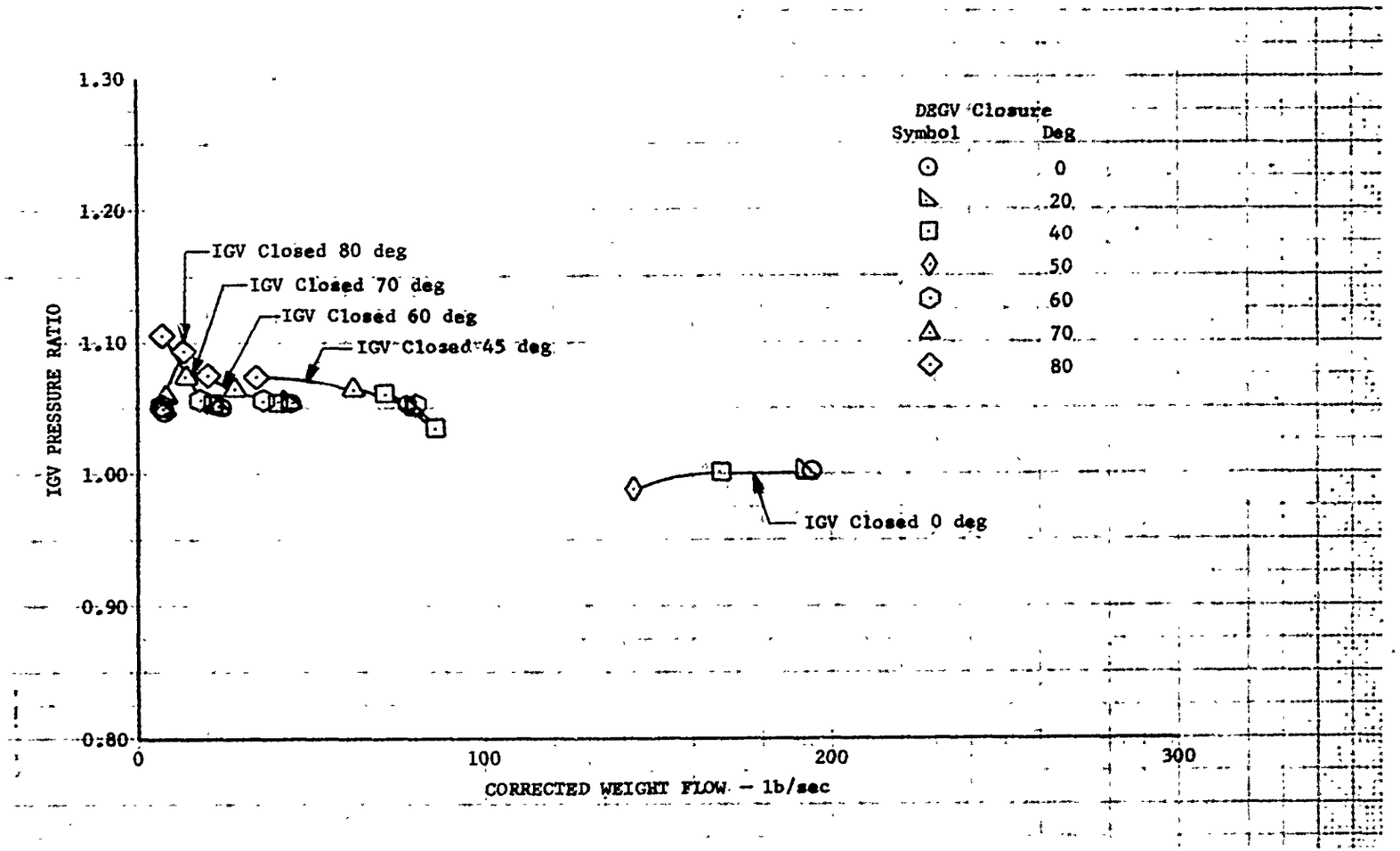

Figure 51. Inlet Guide Vane Pressure Ratio vs Corrected Weight Flow; 70-Percent Design Rotor Speed.

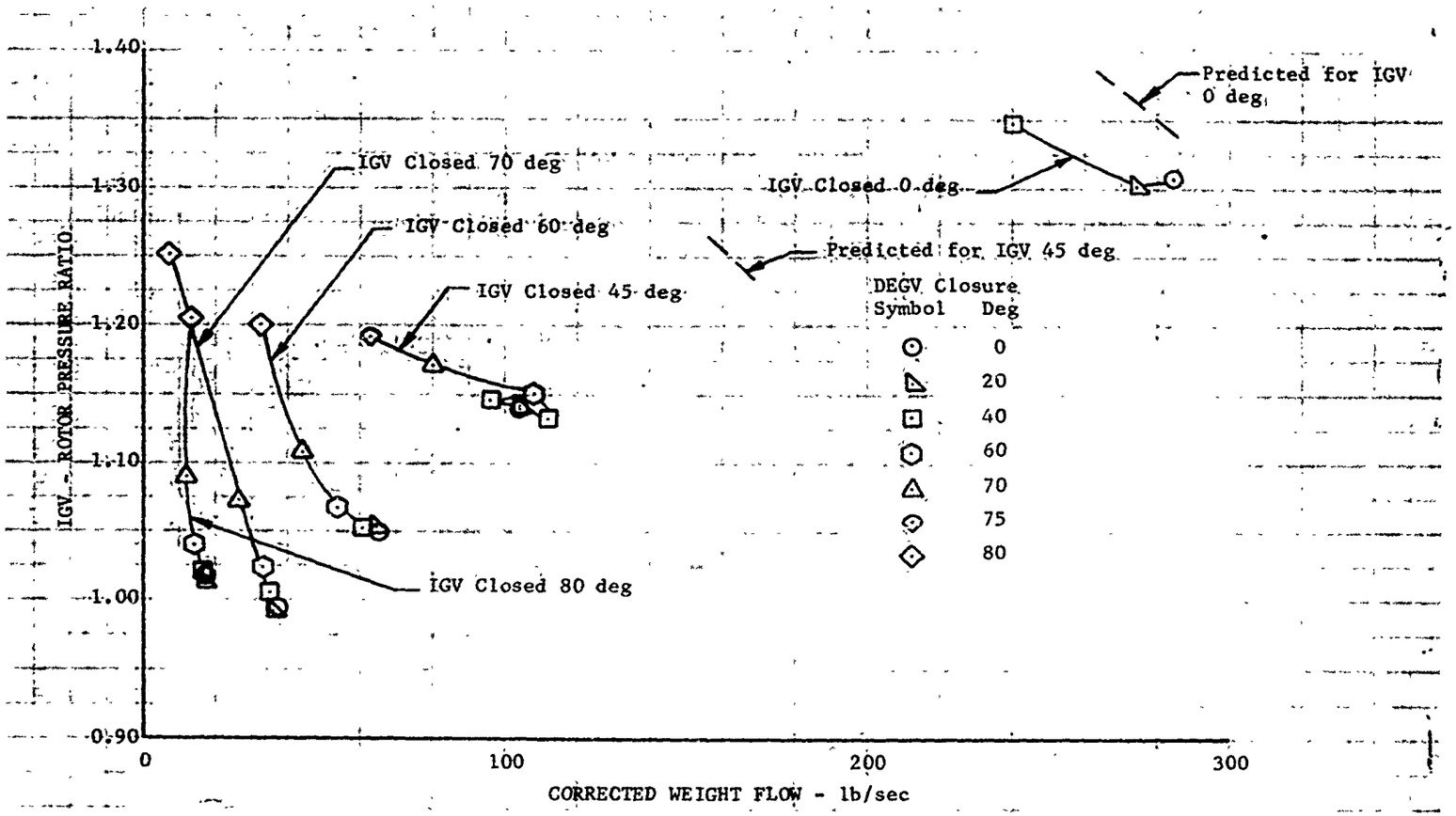

Figure 52. Inlet Guide Vane - Rotor Pressure Ratio vs Corrected Weight Flow; Design Rotor Speed.

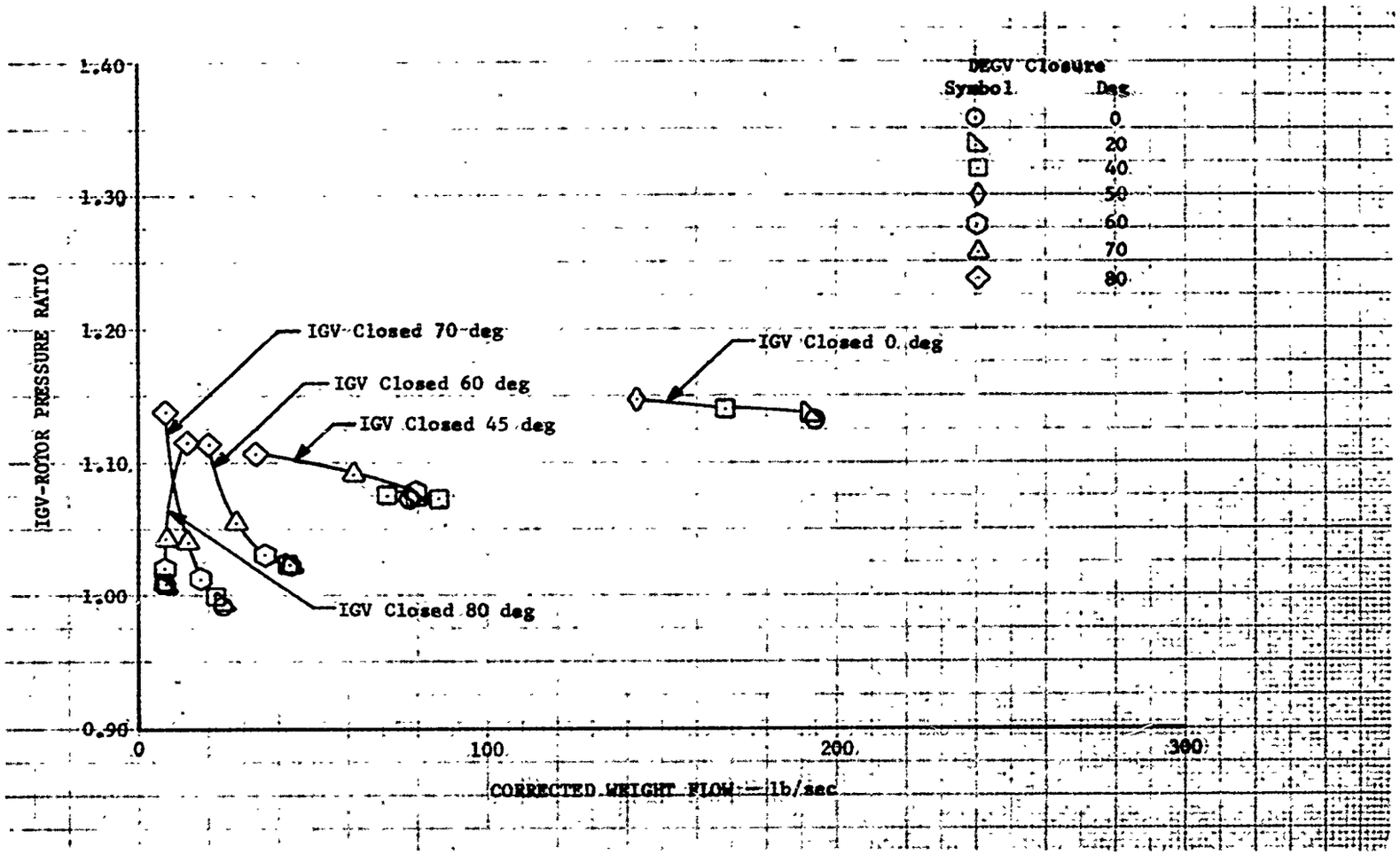

Figure 53. Inlet Guide Vane - Rotor Pressure Rotor vs Corrected Weight Flow; 70-Percent Design Rotor Speed.

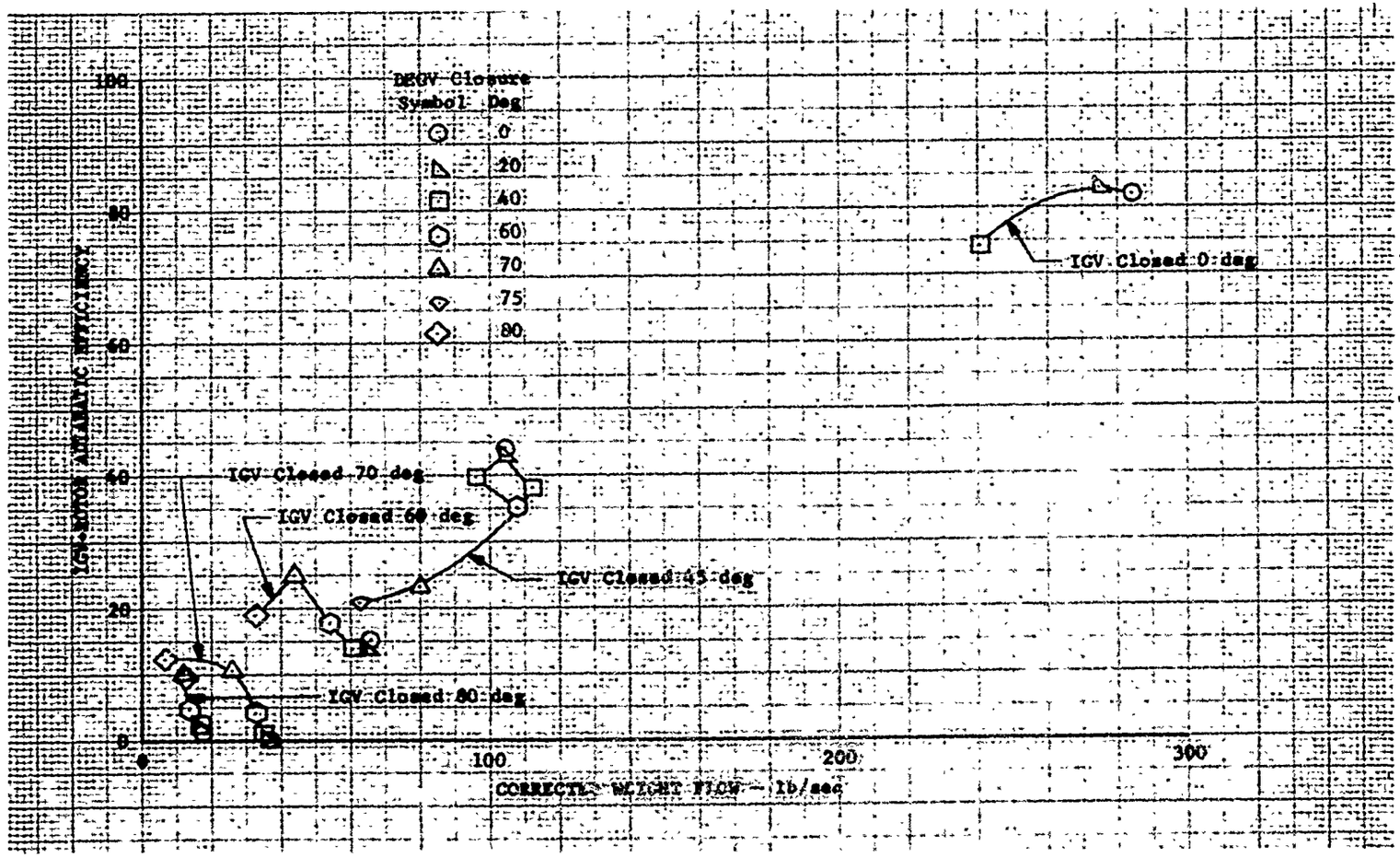

Figure 54. Inlet Guide Vane - Rotor Adiabatic Efficiency vs Corrected Weight Flow; Design Rotor Speed.

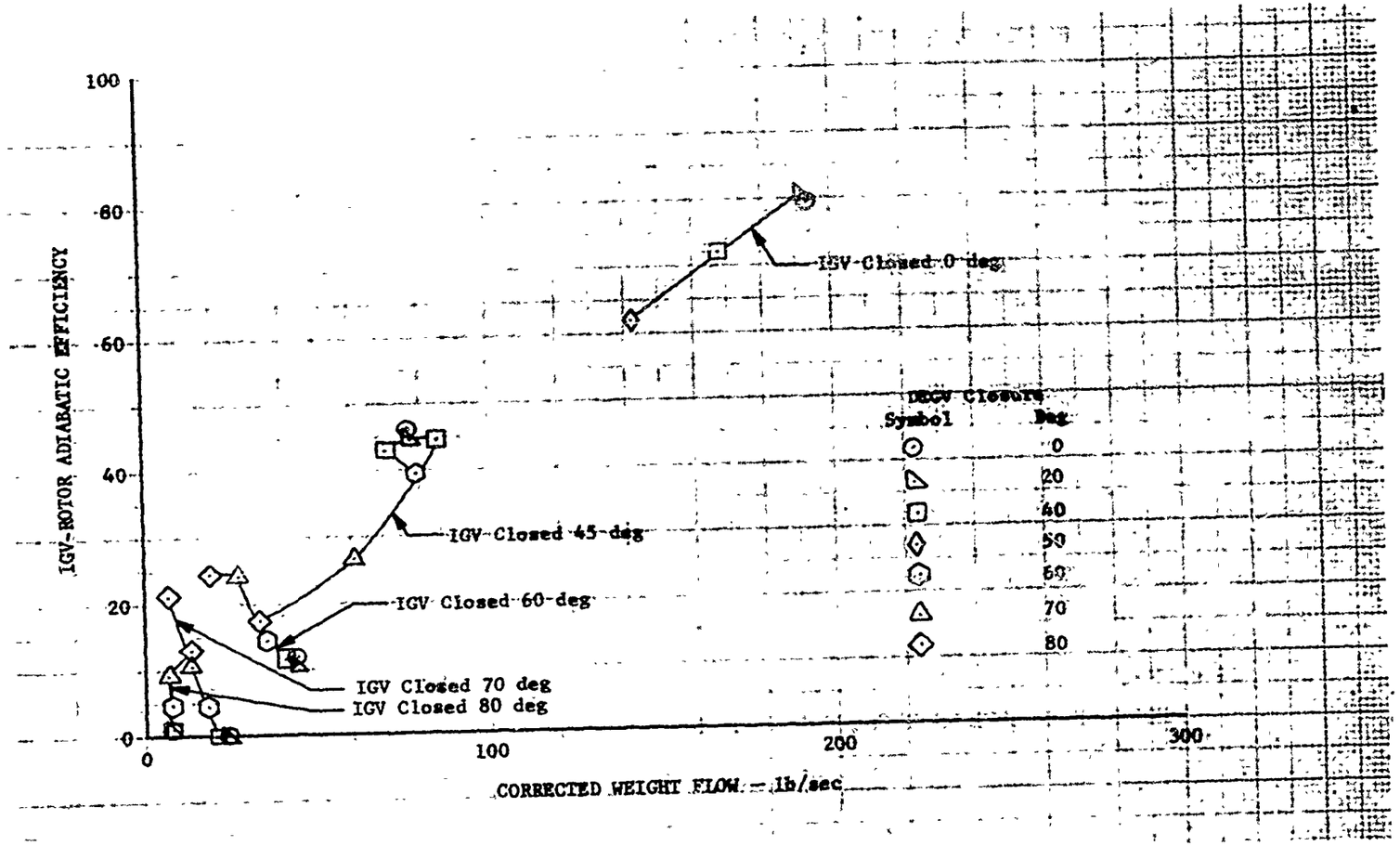

Figure 55. Inlet Guide Vane - Rotor Adiabatic Efficiency vs Corrected Weight Flow; 70-Percent Design Rotor Speed.

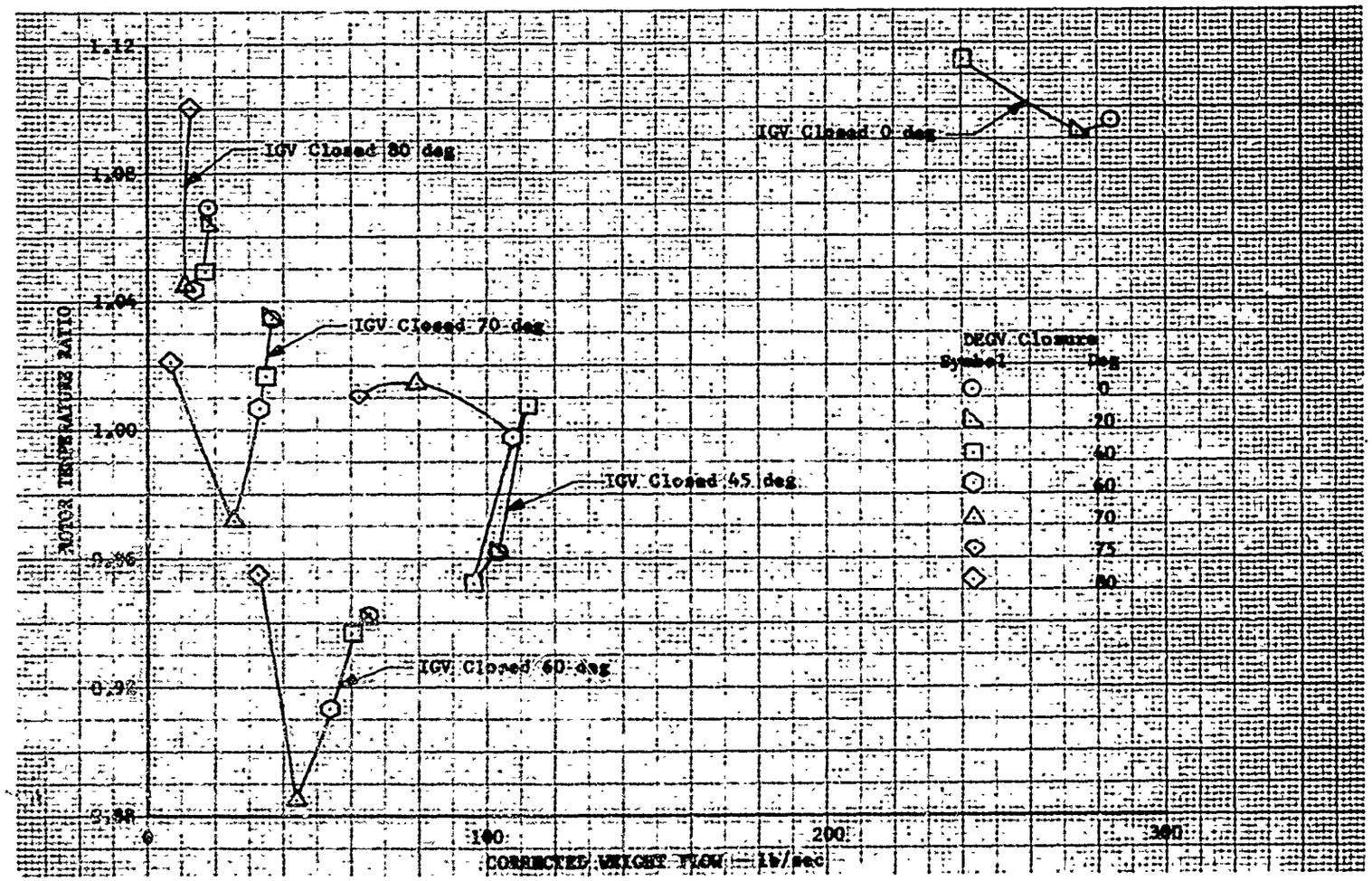

Figure 56. Rotor Temperature Ratio vs Corrected Weight Flow; Design Rotor Speed.

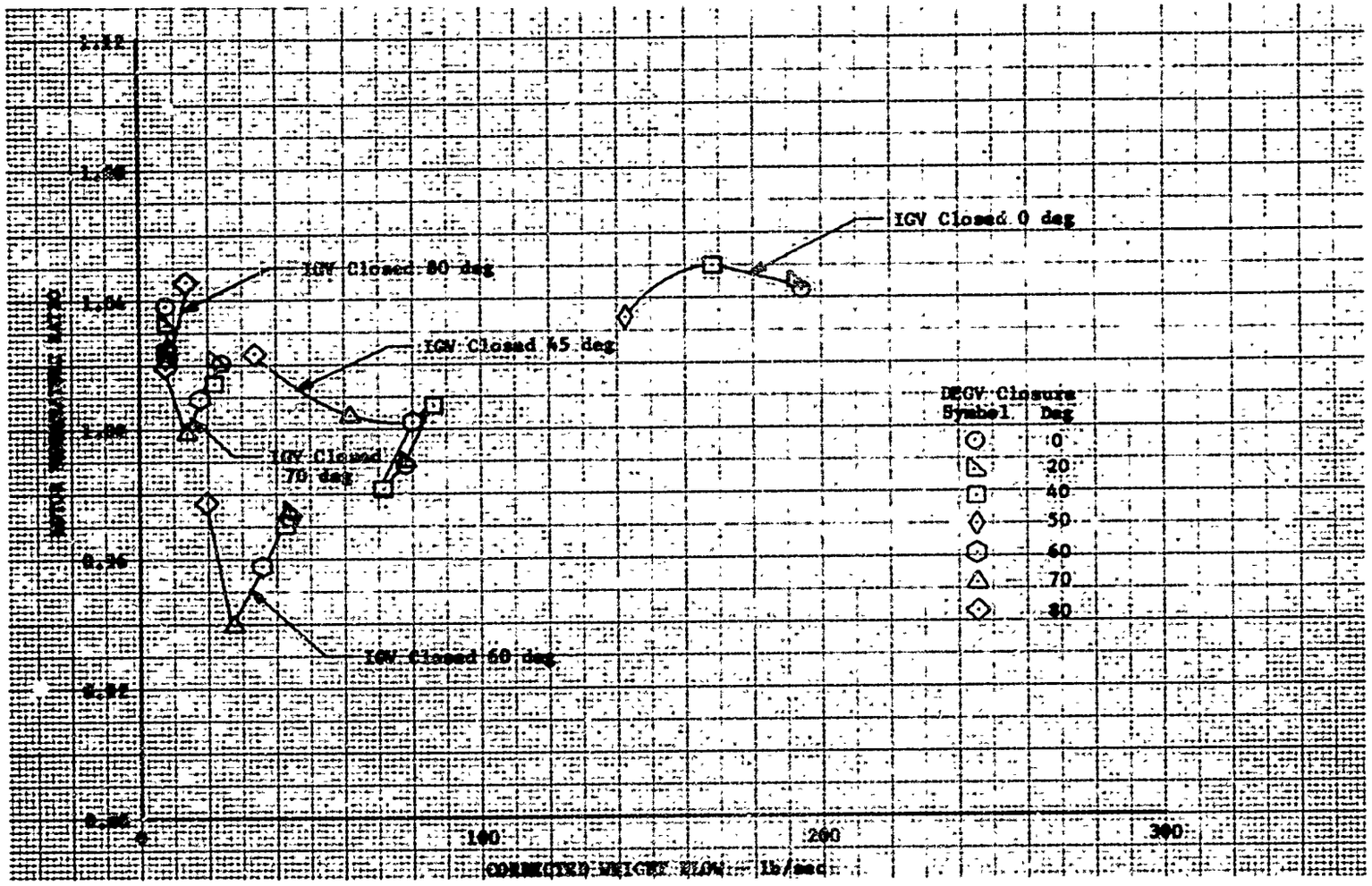

Figure 57. Rotor Temperature Ratio vs Corrected Weight Flow; 70-Percent Design Rotor Speed.

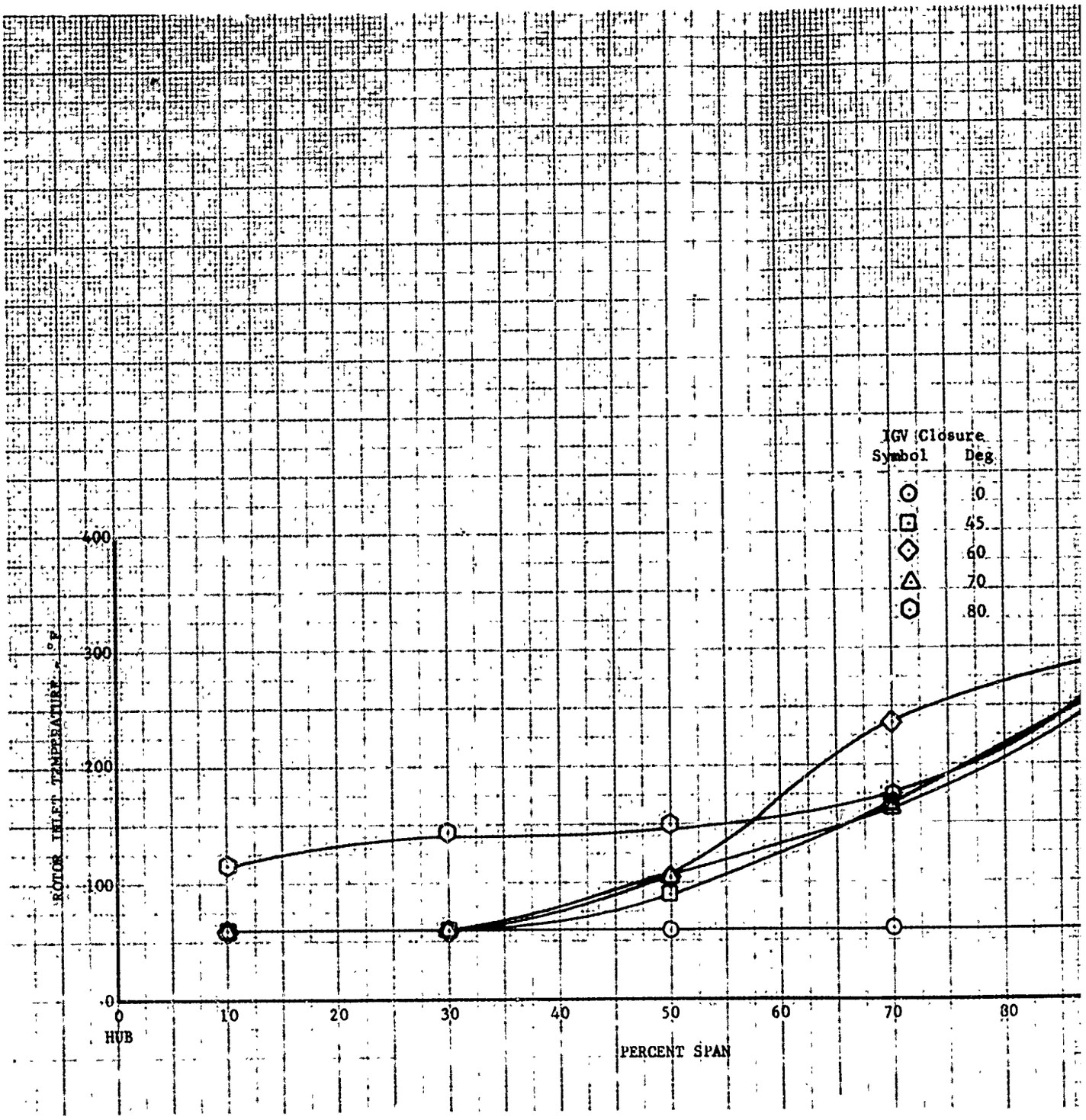

Figure 58. Rotor Inlet Temperature Distributions; Exit Guide Vane Fully Open; Design Rotor Speed.

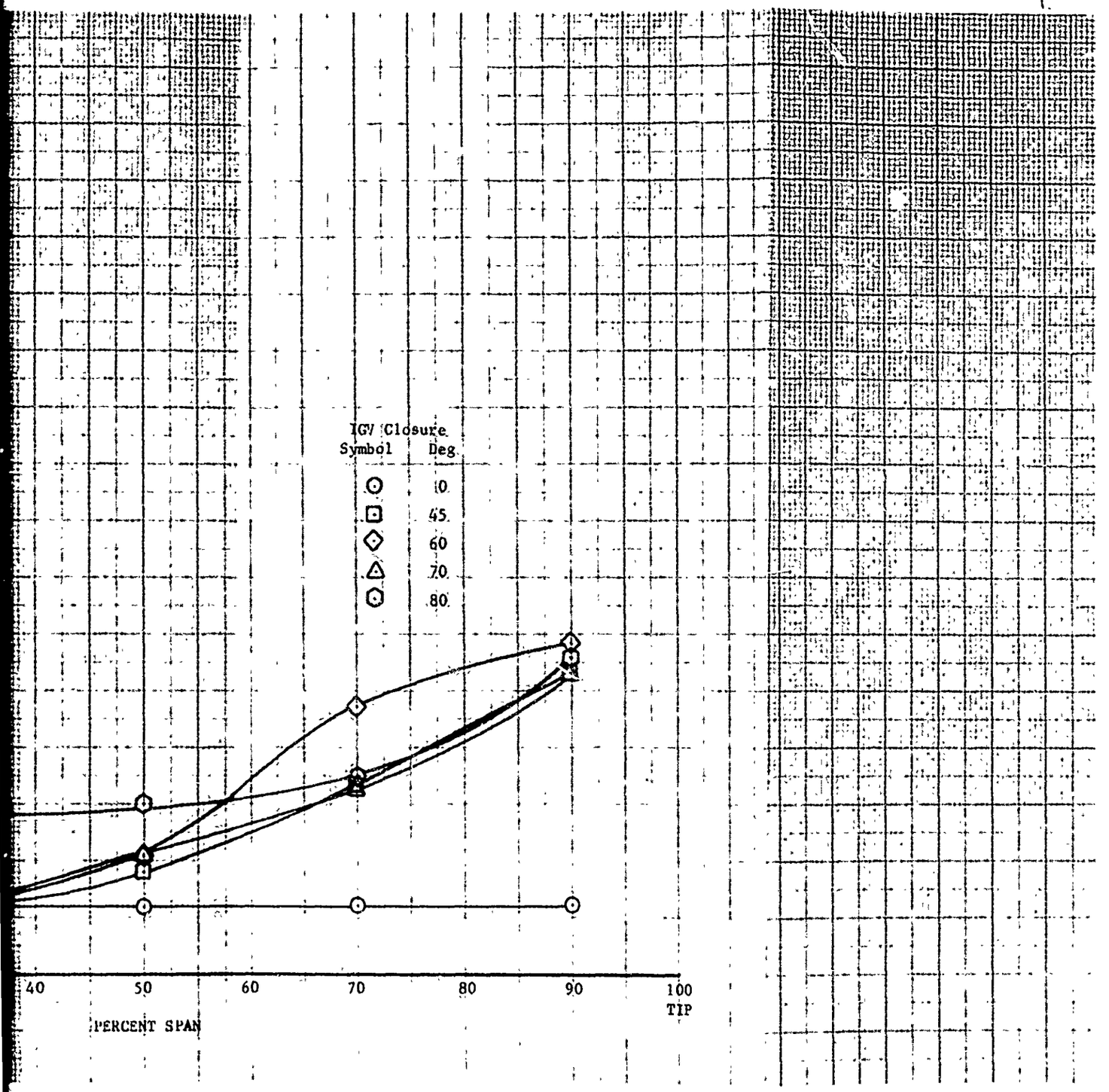

ributions; Exit
n Rotor Speed.

B

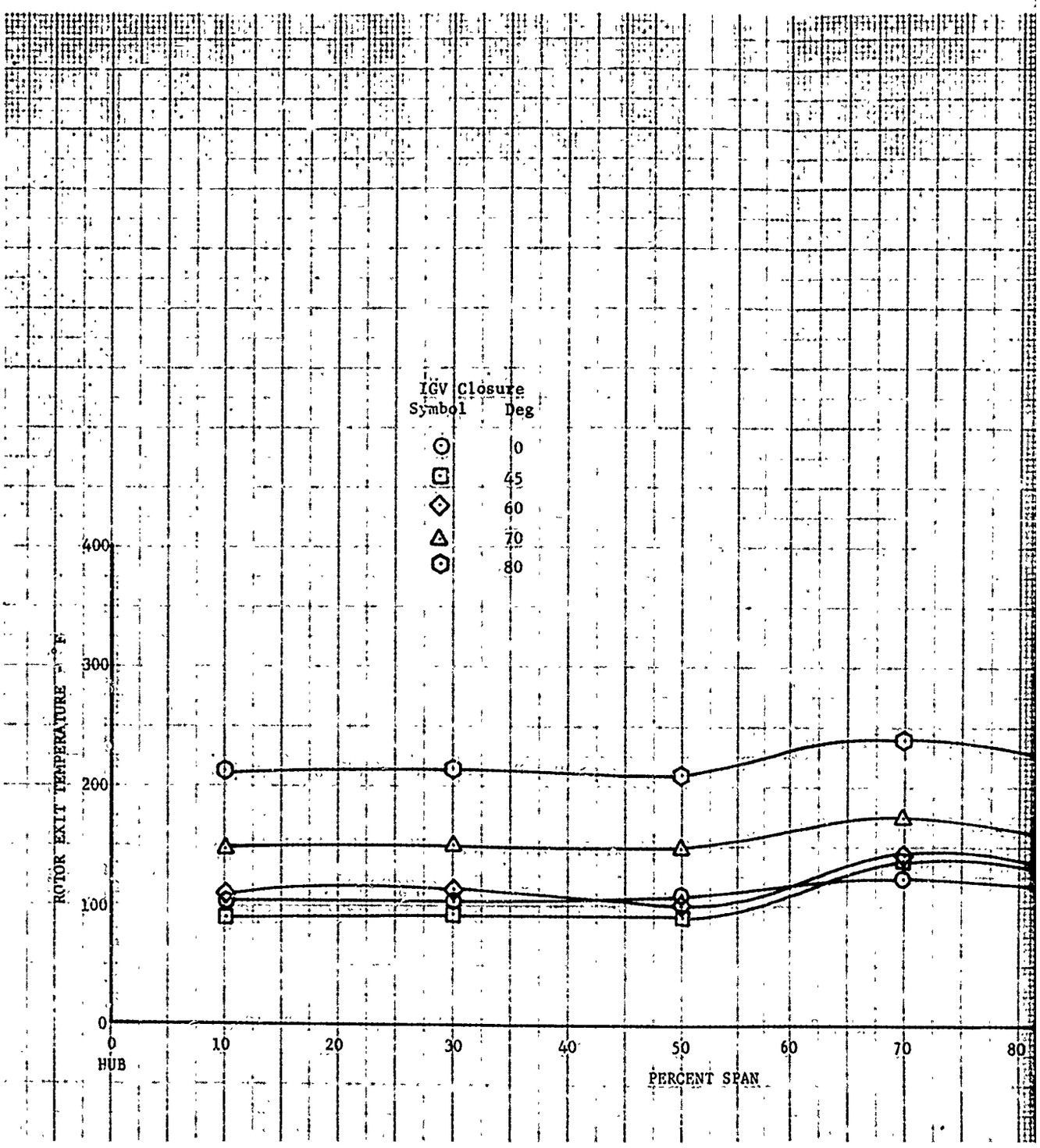

Figure 59. Rotor Exit Temperature Distributions; Exit Guide Vane Fully Open; Design Rotor Speed.

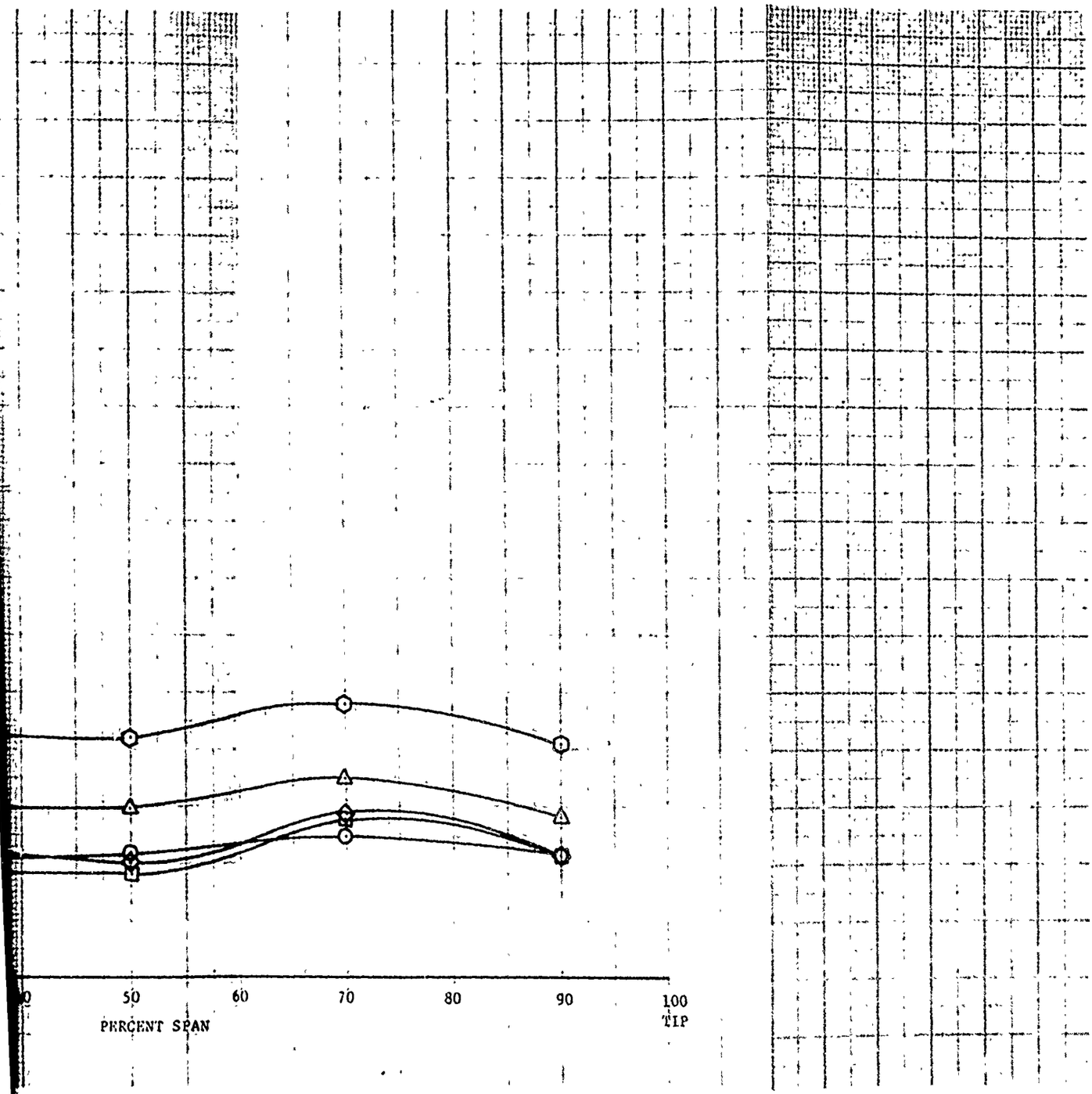

ibutions; Exit
n Rotor Speed.

B

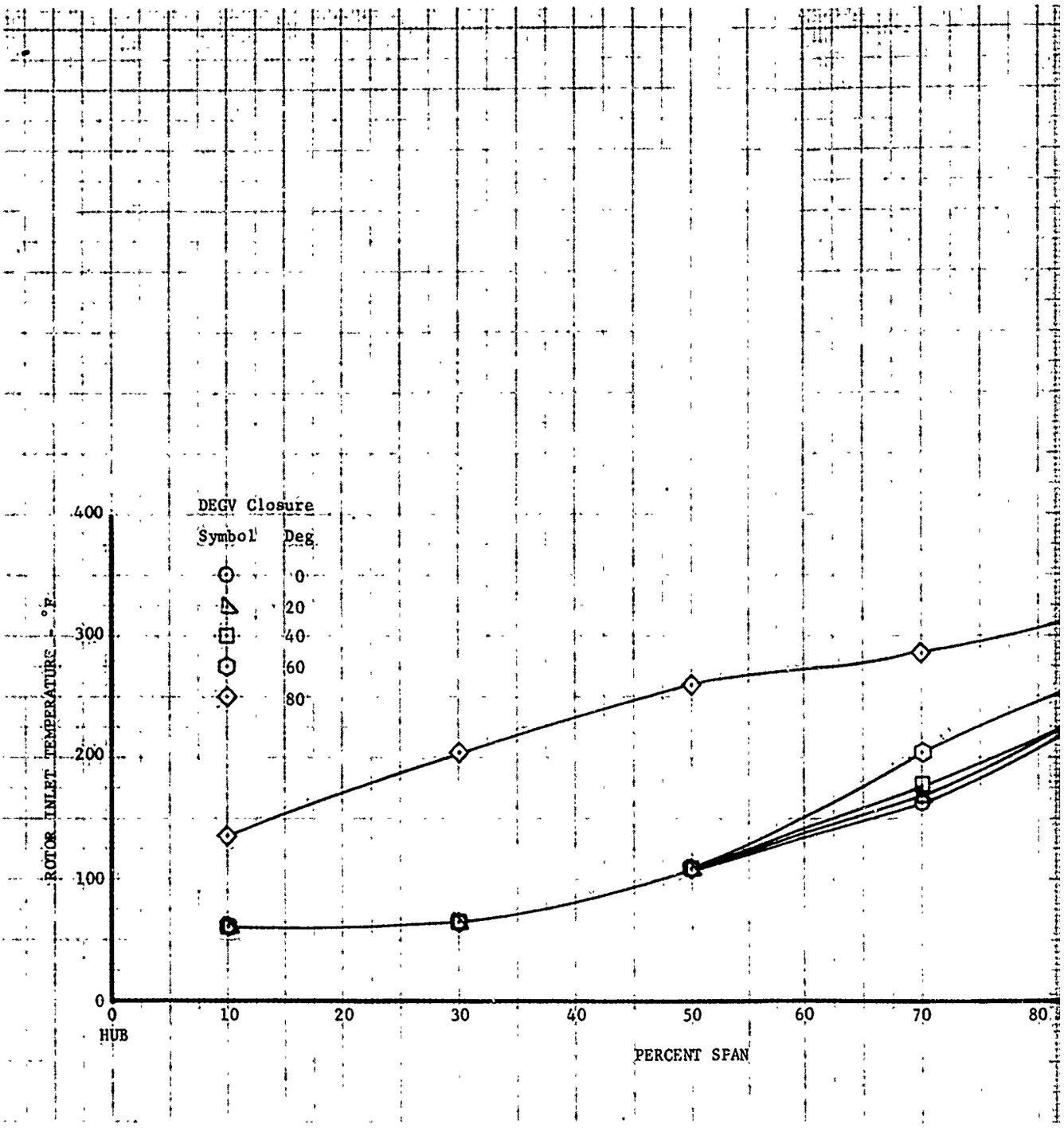

Figure 60. Rotor Inlet Temperature Distributions; Inlet Guide Vane Closed 70 Degrees; Design Rotor Speed.

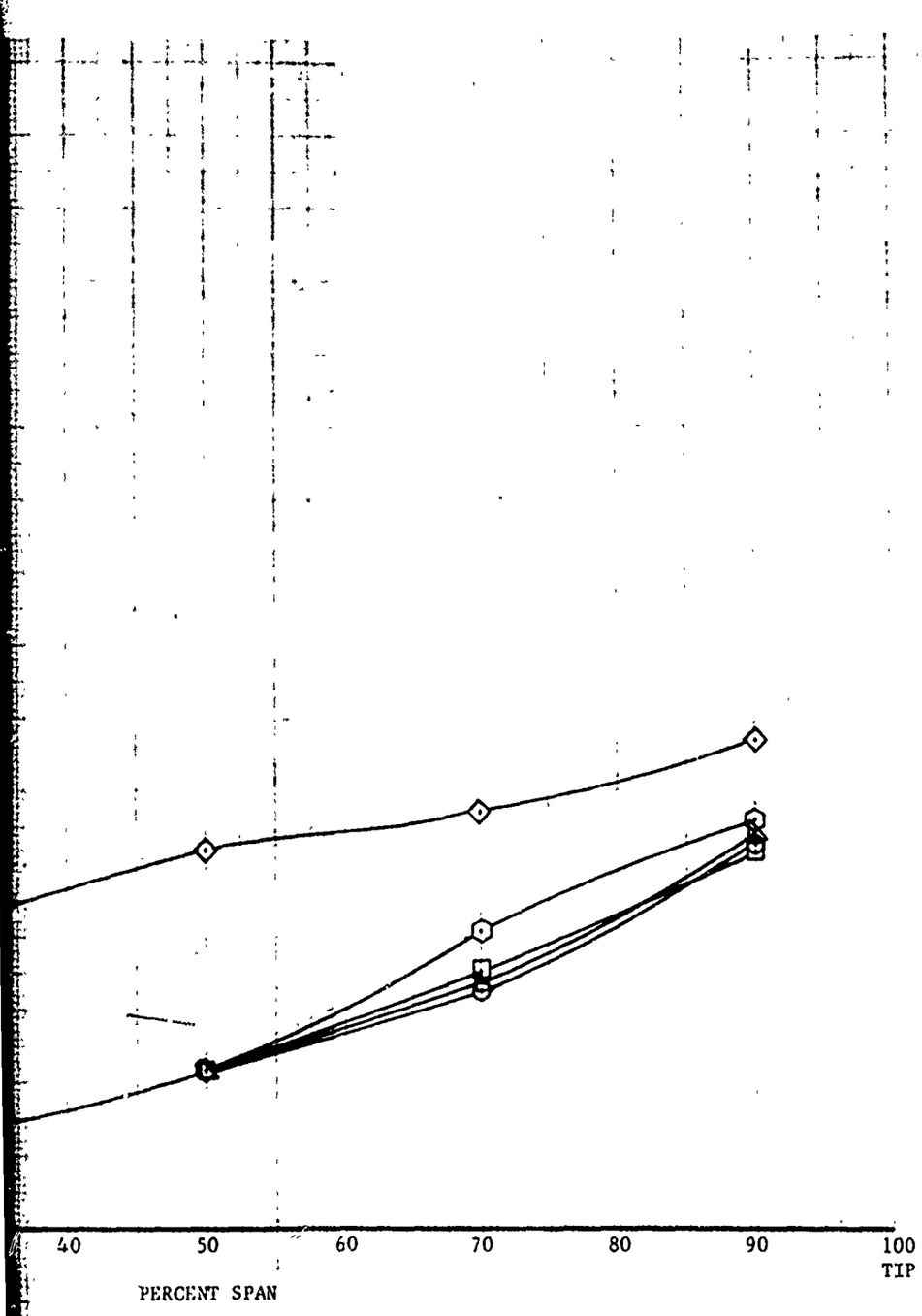

e Distributions;
d 70 Degrees;

B

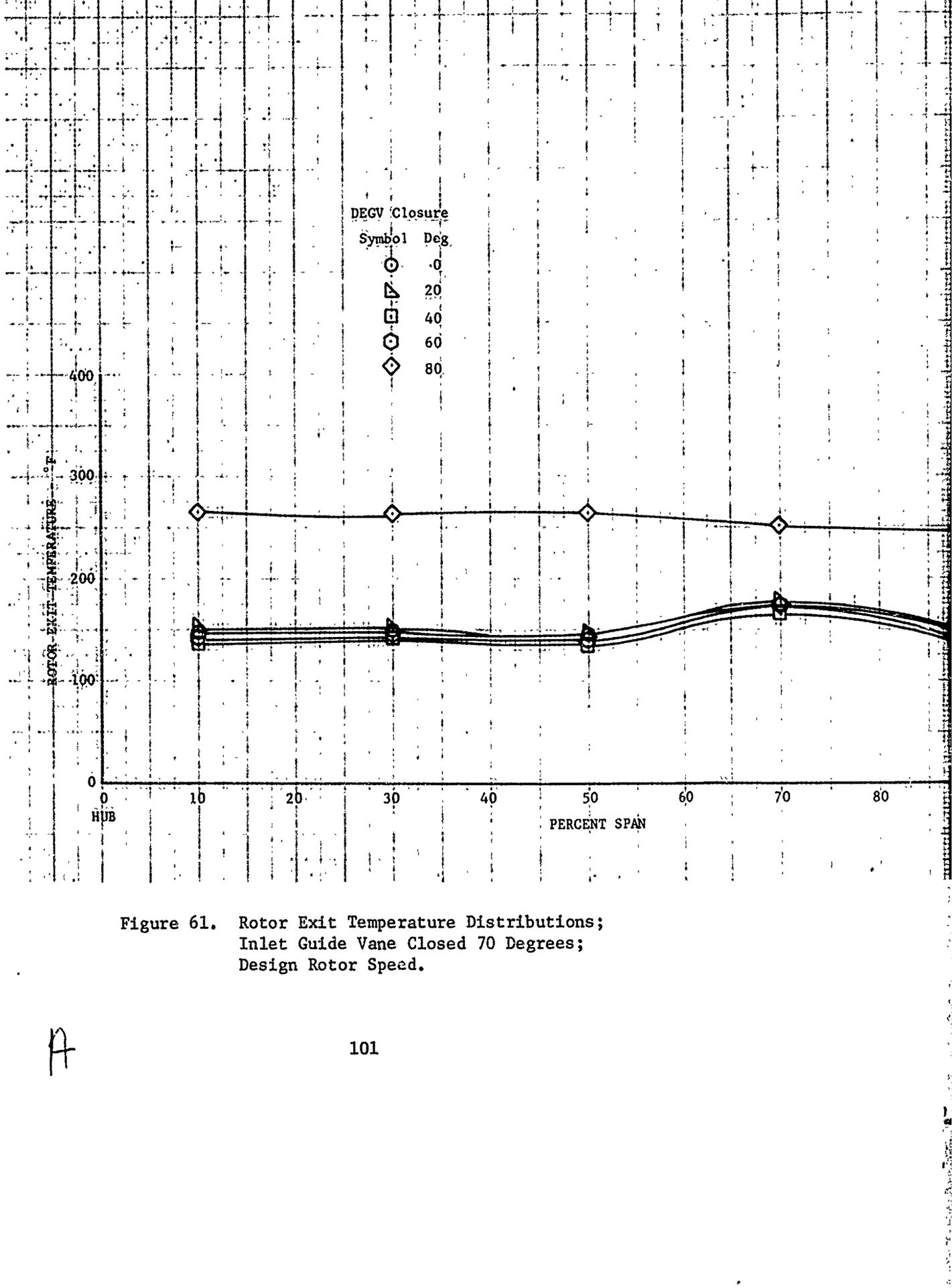

Figure 61. Rotor Exit Temperature Distributions; Inlet Guide Vane Closed 70 Degrees; Design Rotor Speed.

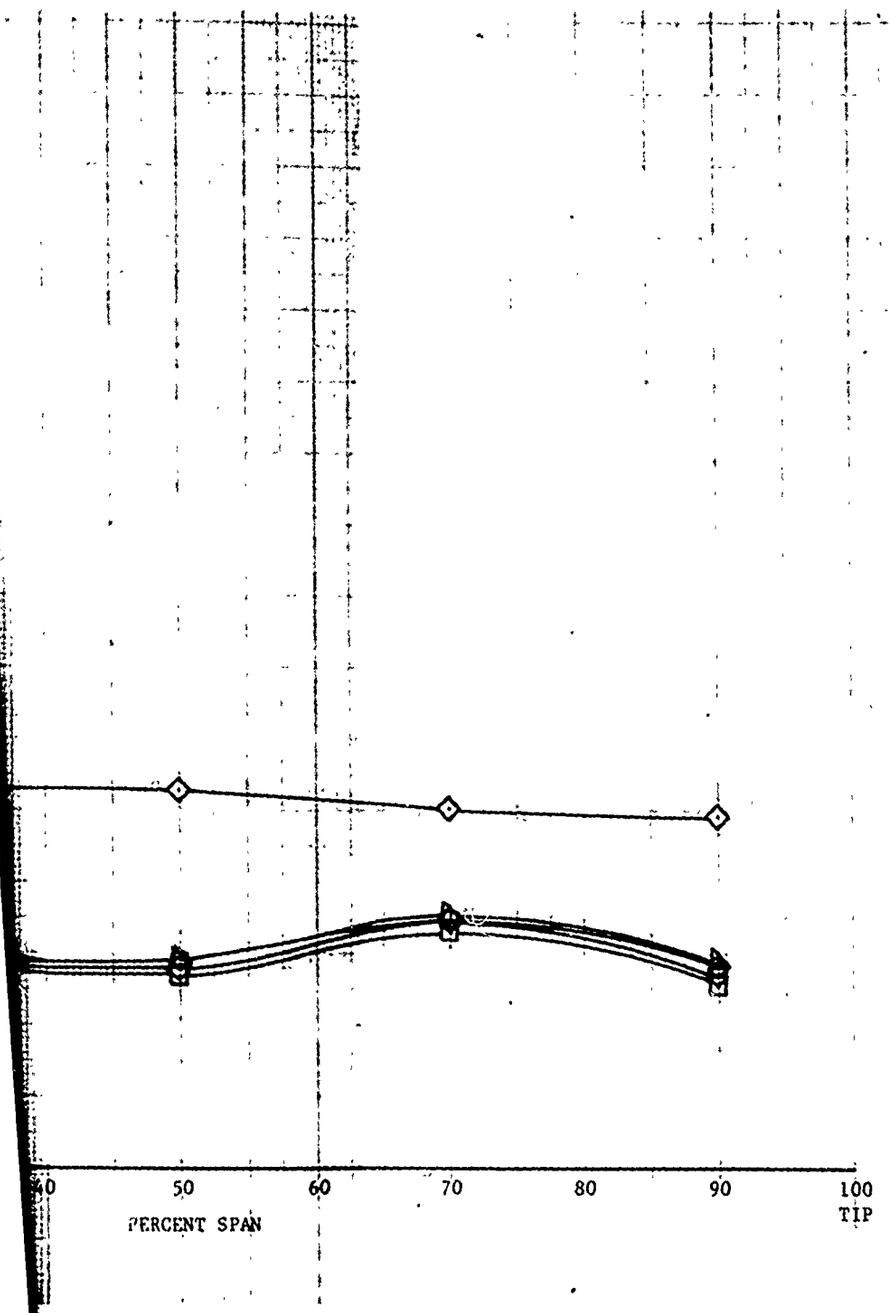

tributions;
0 Degrees;

B

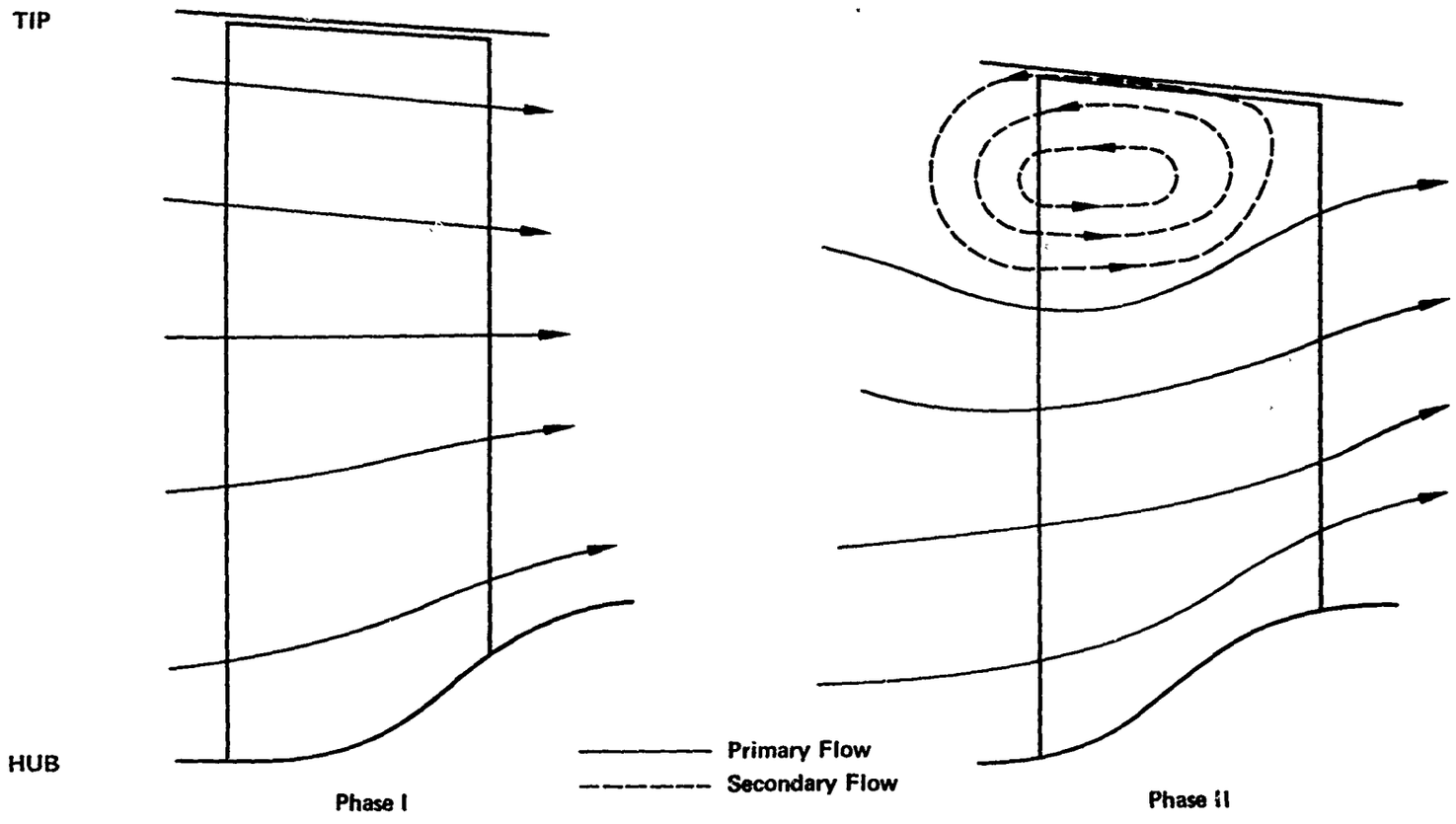

Figure 62. Recirculation Flow Model.

LITERATURE CITED

1. Atkinson, R. P., and Raymond C. C., PRELIMINARY DESIGN STUDY OF CONVERTIBLE FAN/SHAFT ENGINES FINAL REPORT; General Motors, Allison Division; USAAVLABS Technical Report 68-26, U.S. Army Aviation Materiel Laboratories, Fort Eustis, Virginia, April 1968, AD 673148.

2. Crigler, John, and Copeland, W. Latham, NOISE STUDIES OF INLET GUIDE VANE-ROTOR INTERACTION OF A SINGLE STAGE AXIAL FLOW COMPRESSOR; NASA TN D-2962, Langley Research Center, Langley Station, Hampton, Virginia, September 1965.

3. Fincher, H. M., FAN NOISE - THE EFFECT OF A SINGLE UPSTREAM STATOR, Journal of Sound and Vibration, Vol. 3, 1963, pp. 100-110.

4. Smith, L. F., Emerson, T. E., Dietrich, C. W., and Morfrey, C. L., NOISE REDUCTION FOR FORCED-DRAFT BLOWERS VOLUME I - BLOWER DESIGN GUIDE; Technical Report No. BBN 1454, Bolt, Beranek and Newman Inc., Cambridge, Massachusetts, October 24, 1966.

5. AERODYNAMIC DESIGN OF AXIAL FLOW COMPRESSORS (REVISED); NASA SP-36, NASA Lewis Research Center, Cleveland, Ohio, 1965.

6. Steinke, Ronald J., and Crouse, James E., PRELIMINARY ANALYSIS OF THE EFFECTIVENESS OF VARIABLE-GEOMETRY GUIDE VANES TO CONTROL ROTOR-INLET FLOW CONDITIONS; NASA TN D-3823, Lewis Research Center, Cleveland, Ohio, January 1967.

7. Jones, B. A., and Wright, D. L., SINGLE STAGE EXPERIMENTAL EVALUATION OF VARIABLE GEOMETRY GUIDE VANES AND STATORS: PART I - ANALYSIS AND DESIGN, Pratt & Whitney Aircraft; NASA CR-54554, Lewis Research Center, Cleveland, Ohio, August 1968.

8. Osborn, Walter M., and Lewis, George W., EFFECTS OF THREE OUTLET-ANNULUS AREA BLOCKAGE CONFIGURATIONS ON THE PERFORMANCE OF A 20-INCH (50.8 CM) AXIAL-FLOW COMPRESSOR ROTOR; NASA TN-D-5506, Lewis Research Center, Cleveland, Ohio, October 1969.

APPENDIX I
COMPUTER PROGRAMS USED FOR AERODYNAMIC DESIGN

Two computer programs are used to model axial flow compressor aerodynamics: (1) Axial Flow Compressor Calculation and (2) Streamline Calculation Deck. The functions of these two programs are summarized as follows.

AXIAL FLOW COMPRESSOR CALCULATION (AFCC)

This computer program calculates the entrance and discharge conditions for each blade row of an axial flow compressor. The calculation is required to satisfy the equation of motion for an axisymmetric flow field at each of these transverse planes with the assumption that the streamline curvature in the meridional plane may be neglected. Thus, the radial distribution of static pressure reflects swirl velocities but does not account for wall curvature. Radial velocity components, although not calculated, may be introduced to the program as an input item. The program is provided with optional subroutines to calculate the loss coefficient, minimum loss incidence angle, and unstalled operating range, for all of the compressor blade types currently in use at Pratt & Whitney Aircraft, at relative Mach numbers up to 1.5. At higher Mach numbers, these data must be specially input. Various methods of calculating deviation angle are also provided as subroutines.

The program has the capacity to iterate to a solution along several optional paths. The two major paths permit (1) selection of blade metal geometry that satisfies input vector diagrams and (2) solution of the flow field for arbitrary blading, thus permitting solution of both the "design" and "off-design" problems.

STREAMLINE CALCULATION DECK

Many variations of this computer procedure are used for the solution of specific flow problems. The basic procedure, however, permits the calculation of an axisymmetric flow field for a specified flow annulus containing rotor and stator blade rows. The major difference between this and the AFCC program is that the equations of motion are herein solved, including those terms reflecting the influence of streamline curvature in the meridional plane on the radial static pressure gradient.

TABLE VI. PERFORMANCE DATA SUMMARY - DESIGN ROTOR SPEED

IGV Closure (deg)	DEGV Closure (deg)	Inlet Flow (lb/sec)	Shaft Horse-Power (hp)	Thrust (lb)	Fan Stage Pressure Ratio	Fan Stage Efficiency (%)	Rotor Temperature Ratio	IGV Pressure Ratio	IGV-Rotor Pressure Ratio	IGV-Rotor Efficiency (%)
0	0	284	4500	5420	1.302	79.2	1.095	1.003	1.308	81.6
0	10	279	4430	5160	1.292	80.0	1.090	1.002	1.298	82.1
0	20	274	4380	5040	1.297	80.7	1.092	1.001	1.302	82.7
0	30	268	4730	4260	1.273	69.5	1.097	1.001	1.325	82.6
0	40	240	5200	2740	1.188	41.4	1.114	1.000	1.348	74.0
45	0	104.5	1570	1300	1.082	25.7	0.962	1.010	1.141	43.7
45	20	104	1720	1230	1.079	23.7	0.962	1.010	1.143	42.7
45	30	101	1720	1170	1.083	24.3	0.959	1.017	1.144	41.6
45	40*	95.5	1690	1030	1.084	23.0	0.953	1.021	1.147	39.5
45	40**	112	1690	1100	1.071	20.2	1.007	1.030	1.133	37.8
45	50*	91	1710	780	1.072	16.5	0.946	0.992	1.148	35.9
45	50**	116	1710	1160	1.090	25.2	1.007	0.991	1.138	37.3
45	60	107	1730	830	1.071	16.5	0.997	1.006	1.152	34.8
45	70	80	1760	380	1.042	5.8	1.014	1.025	1.172	23.1
45	75	63	1750	200	1.049	5.4	1.011	1.029	1.193	20.4
60	0	65	1460	620	1.045	12.4	0.942	0.862	1.049	15.1
60	10	65	1510	540	1.041	10.9	0.941	0.859	1.053	14.0
60	20	65	1520	500	1.040	10.2	0.941	0.861	1.054	13.8
60	30	62	1540	470	1.041	10.8	0.938	0.863	1.052	13.8
60	40	61	1640	460	1.049	12.2	0.936	0.867	1.052	13.6
60	50	58	***	410	1.051	13.7	0.935	0.844	1.053	14.4
60	60	54	1670	340	1.055	14.2	0.913	0.840	1.069	17.8
60	70	44	1700	220	1.045	10.0	0.885	0.828	1.109	24.4
60	80	32	1520	20	1.000	0.0	0.955	0.835	1.200	19.0

*Exit Vane Closing
**Exit Vane Opening
*** Rotor Speed Beyond 2.0 Percent Acceptance Band

TABLE VI - CONTINUED

IGV Closure (deg)	DEGV Closure (deg)	Inlet Flow (lb/sec)	Shaft Horse-Power (hp)	Thrust (lb)	Fan Stage Pressure Ratio	Fan Stage Efficiency (%)	Rotor Temperature Ratio	IGV Pressure Ratio	IGV-Rotor Pressure Ratio	IGV-Rotor Efficiency (%)
70	0	37	1460	200	1.032	5.2	1.034	1.029	0.995	0.0
70	10	37.5	1560	200	1.023	3.4	1.036	1.030	0.994	0.0
70	20	36.5	1540	160	1.022	3.2	1.034	1.030	0.994	0.0
70	30	37	1530	200	1.024	3.8	1.025	1.032	1.001	0.1
70	40	35	1490	190	1.030	5.2	1.016	1.028	1.007	1.2
70	50	34	1500	190	1.042	7.2	1.010	1.030	1.011	1.8
70	60	33	1490	170	1.062	10.2	1.006	0.993	1.024	4.1
70	70	26	1490	110	1.049	7.2	0.972	1.014	1.072	10.7
70	80	7	1380	0	1.000	0.0	1.021	1.061	1.252	12.1
80	0	17.5	1450	0	1.011	1.0	1.068	1.044	1.018	1.7
80	10	18	1490	20	1.012	1.1	1.064	1.046	1.016	1.5
80	20	17.5	1550	40	1.014	1.3	1.063	1.047	1.013	1.2
80	30	17	1600	20	1.015	1.6	1.052	1.047	1.014	1.4
80	40	17	1450	20	1.019	2.1	1.048	1.050	1.019	2.2
80	50	17.5	1520	30	1.032	3.6	1.042	1.053	1.026	3.0
80	60	14	1470	20	1.056	6.2	1.042	1.057	1.040	4.6
80	70	12	1350	10	1.049	5.5	1.044	1.072	1.090	10.0
80	80	13	1120	0	1.000	0.0	1.100	1.122	1.206	9.1

TABLE VII. PERFORMANCE DATA SUMMARY - 70-PERCENT DESIGN ROTOR SPEED

IGV Closure (deg)	DEGV Closure (deg)	Inlet Flow (lb/sec)	Shaft Horse-Power (hp)	Thrust (lb)	Fan Stage Pressure Ratio	Fan Stage Efficiency (%)	Rotor Temperature Ratio	IGV Pressure Ratio	IGV - Rotor Pressure Ratio	IGV - Rotor Efficiency (%)
0	0	194	1590	2455	1.132	80.0	1.043	1.000	1.131	79.4
0	10	194	1490	2490	1.135	78.2	1.044	1.001	1.135	78.6
0	20	192	1500	2395	1.134	79.8	1.045	1.001	1.136	80.3
0	30	184	1480	1950	1.116	67.8	1.046	1.001	1.136	78.0
0	40	168	1630	1180	1.070	36.8	1.050	1.000	1.140	72.0
0	50	143	1460	660	1.045	20.2	1.035	0.988	1.147	62.2
45	0	78	530	630	1.043	28.1	0.988	1.050	1.071	46.1
45	10	78	520	660	1.042	26.5	0.989	1.050	1.072	46.8
45	20	78	500	600	1.040	26.0	0.990	1.050	1.070	44.4
45	30	77	520	520	1.041	25.2	0.986	1.053	1.071	44.7
45	40*	71	520	480	1.043	24.5	0.981	1.062	1.074	43.1
45	40**	86	520	460	1.037	23.5	1.007	1.035	1.071	44.3
45	50*	66	510	390	1.039	18.3	0.974	1.068	1.083	40.9
45	50**	84	510	460	1.045	26.8	1.006	1.036	1.071	41.7
45	60	80	520	330	1.038	18.8	1.002	1.050	1.077	39.3
45	70	62	530	125	1.022	6.7	1.004	1.066	1.091	26.8
45	80	34	530	20	1.003	5.0	1.023	1.073	1.106	17.6
60	0	44	400	300	1.024	13.6	0.972	1.055	1.022	12.2
60	10	44	400	270	1.021	11.4	0.973	1.056	1.020	10.8
60	20	44	390	250	1.020	10.2	0.974	1.055	1.020	10.2
60	30	44	390	240	1.020	10.6	0.974	1.056	1.020	10.2
60	40	42	400	230	1.024	12.7	0.970	1.056	1.021	11.2
60	50	41	390	230	1.028	14.2	0.966	1.055	1.022	11.6
60	60	36	390	190	1.030	15.0	0.958	1.056	1.030	14.2
60	70	28	400	95	1.027	12.4	0.940	1.067	1.055	24.2
60	80	20	390	20	1.000	0.0	0.977	1.077	1.113	24.2

*Exit Vane Closing
**Exit Vane Opening

TABLE VII - CONTINUED

IGV Closure (deg)	DEGV Closure (deg)	Inlet Flow (lb/sec)	Shaft Horse-Power (hp)	Thrust (lb)	Fan Stage Pressure Ratio	Fan Stage Efficiency (%)	Rotor Temperature Ratio	IGV Pressure Ratio	IGV - Rotor Pressure Ratio	IGV - Rotor Efficiency (%)
70	0	24	480	55	1.017	5.2	1.020	1.052	0.992	0.0
70	10	23	500	30	1.010	3.4	1.022	1.050	0.991	0.0
70	20	23	470	38	1.010	3.4	1.020	1.052	0.992	0.0
70	30	22	470	50	1.012	4.2	1.018	1.052	0.995	0.0
70	40	22	480	60	1.016	5.6	1.014	1.054	1.000	0.0
70	50	21	480	60	1.022	8.1	1.011	1.054	1.004	1.4
70	60	18	490	58	1.032	11.0	1.010	1.057	1.012	4.3
70	70	14	490	25	1.030	8.6	0.999	1.074	1.040	10.7
70	80	8	440	0	1.000	0.0	1.019	1.106	1.136	21.5
80	0	8	580	0	1.002	0.8	1.038	1.047	1.007	1.3
80	10	8	600	0	1.005	0.9	1.034	1.049	1.005	1.0
80	20	8	560	8	1.005	1.0	1.032	1.048	1.005	0.8
80	30	7	590	8	1.007	1.4	1.028	1.050	1.006	1.1
80	40	8	570	15	1.008	2.0	1.024	1.048	1.008	1.9
80	50	8	550	10	1.015	3.6	1.021	1.052	1.012	2.9
80	60	7	540	13	1.028	6.4	1.022	1.053	1.020	4.7
80	70	8	530	18	1.028	6.2	1.025	1.060	1.043	9.4
80	80	14	490	15	1.000	0.0	1.045	1.095	1.115	13.3

UNCLASSIFIED

Security Classification

DOCUMENT CONTROL DATA - R & D

(Security classification of title, body of abstract and indexing annotation must be entered when the overall report is classified)

1. ORIGINATING ACTIVITY (Corporate author)	2a. REPORT SECURITY CLASSIFICATION
Pratt & Whitney Aircraft Division of United Aircraft Corporation West Palm Beach, Florida	Unclassified
	2b. GROUP

3. REPORT TITLE

CONVERTIBLE FAN/SHAFT ENGINE VARIABLE FAN GEOMETRY INVESTIGATION

4. DESCRIPTIVE NOTES (Type of report and inclusive dates)

Final Report

5. AUTHOR(S) (First name, middle initial, last name)

David L. Wright
Burton A. Jones

6. REPORT DATE	7a. TOTAL NO. OF PAGES	7b. NO. OF REFS
April 1970	120	8

8a. CONTRACT OR GRANT NO.	9a. ORIGINATOR'S REPORT NUMBER(S)
DAAJ02-69-C-0002	USAAVLABS Technical Report 70-28
b. PROJECT NO.	
c. Task 1G162203D14415	9b. OTHER REPORT NO(S) (Any other numbers that may be assigned this report)
d.	PWA FR-3567

10. DISTRIBUTION STATEMENT

This document is subject to special export controls, and each transmittal to foreign governments or foreign nationals may be made only with prior approval of U. S. Army Aviation Materiel Laboratories, Fort Eustis, Virginia 23604.

11. SUPPLEMENTARY NOTES	12. SPONSORING MILITARY ACTIVITY
	U.S. Army Aviation Materiel Laboratories Fort Eustis, Virginia

13. ABSTRACT

Preliminary design studies have shown that advanced VTOL aircraft performance can be enhanced when the aircraft are coupled with a turbofan engine having the ability to provide shaft power to the vertical lift rotor (convertible fan/shaft engine). The program reported herein was conducted to determine the feasibility of using variable fan inlet and duct exit guide vanes to effectively reduce fan horsepower and eliminate thrust during periods of vertical lift and hover. An exploratory test program was conducted in an existing 0.5 hub-tip ratio compressor research rig modified to simulate a high-bypass-ratio fan configuration. This fan configuration consisted of variable inlet and exit guide vanes, a fan rotor, and a simulated gas generator flowpath providing a 4.2:1 bypass ratio. The fan rotor was an existing moderate-speed rotor blade with a tip diameter of 43 inches, tip speed of 1150 fps, and design pressure ratio and flow of 1.35 and 285 lb/sec, respectively.

Results from the test program established the feasibility of using variable-geometry inlet and duct exit guide vanes to effectively reduce fan horsepower and thrust. Fan horsepower was reduced to 16 percent of the maximum (cruise) power absorbed by the fan, and fan thrust was reduced by 100 percent. The test results indicate that the potential exists for reducing fan horsepower to values of less than 10 percent of the cruise power. Inlet guide vane, rotor blade, and duct exit guide vane stresses were within safe operating limits over the test range of guide vane positions.

DD FORM 1 NOV 68 1473 REPLACES DD FORM 1473, 1 JAN 64, WHICH IS OBSOLETE FOR ARMY USE.

UNCLASSIFIED

Security Classification

14. KEY WORDS	LINK A		LINK B		LINK C	
	ROLE	WT	ROLE	WT	ROLE	WT
Convertible Fan/Shaft Engine						
Variable Geometry Inlet and Exit Guide Vanes						
Turbofan Power and Thrust Modulation						
VTOL Aircraft Propulsion Systems						